An investigation on the fretting wear and corrosion damage to the head neck interface of total hip replacement: A finite element modelling approach

by

Khosro Fallahnezhad

Thesis
Submitted to Flinders University
for the degree of

Doctor of Philosophy

College of Science and Engineering

23rd May 2018

Contents

List of Figures

List of Tables

Abstract

Over the past years, modular design of hip joint replacement has attracted an increasing interest due to its several advantages. However, the modular design of hip joint implant can result in fretting wear in the interface of the head-neck junction, especially in metallic cases. As hip implant is operating inside the corrosive environment of human body, electrochemical corrosion occurs in metallic interfaces which is usually in the form of crevice corrosion. Combination of mechanical fretting wear and electrochemical corrosion results in fretting corrosion (mechanically assisted corrosion). Metallic debris and ions detached from the interface of the head-neck junction are proven to have detrimental influences on body tissues which can ultimately results in revision surgeries with its associated major risks.

This PhD project aims to comprehensively investigate fretting wear and corrosion failure of the head-neck junction of hip joint replacement, using a computational approach. In the first phase of this project, a three dimensional Finite Element (FE) model was developed and verified to investigate the mechanical environment of the head-neck junction. The model was then used to investigate the assembling process of the head neck junction and parameters that can influence the strength of the junction. This model was further developed to investigate the behaviour of the junction subjected to loading of daily activities. In this investigation several mechanical parameters that can influence on the fretting wear process were evaluated and a range of contact pressure (0-350 MPa) and micro-motion (0-32 μm) was suggested that can be used to develop more realistic *in-vitro* tests and FE simulations of fretting wear process. In the second phase of the project, an adaptive FE model was developed to simulate fretting wear process in the CoCr/CoCr head-neck junction. This model was developed for both dry and simulated body fluid conditions. It was revealed that simulation of fretting wear in a dry condition is a major simplification that cannot provide reliable outcomes. The model with the presence of the body fluid was then used to investigate the influence of angular mismatch (±0.124°) and assembly force (2-5 kN) on fretting wear process and the volume of material loss over several millions of fretting cycles. It was found that junctions with distal angular

mismatch are more resistant against fretting wear. Moreover, results of this study revealed that although increasing the impaction force can enhance the strength of the junction, it can result in more damaging fretting wear process, in term of lost material. In the last phase of this project, for the first time, an adaptive FE model was developed to simulate fretting corrosion process. This model that was developed for a pin-on-disc geometry is able to quantify material loss caused by both fretting wear and electrochemical corrosion simultaneously it is also able to estimate the volume of the removed oxide layer, during the process of fretting corrosion.

The outcomes of this research provides a deep understanding about the performance of the head neck junction of modular hip replacement and different parameters that can play major roles in its failure. Moreover, the finite element model of fretting corrosion process that is presented in this thesis, can be a good platform to model this phenomena for different geometries and applications.

List of Publications

1. **Fallahnezhad, K**.; Farhoudi, H.; Oskouei, R.H.; Taylor, M. Influence of geometry and materials on the axial and torsional strength of the head–neck taper junction in modular hip replacements: A finite element study. *Journal of the Mechanical Behavior of Biomedical Materials* **2016**, *60*, 118-126.

   contributions: K**.** Fallahnezhad, H. Farhoudi, R.H. Oskouei and M. Taylor all contributed to the design of this study. K**.** Fallahnezhad developed the finite element model and extracted results. K**.** Fallahnezhad, H. Farhoudi, R.H. Oskouei and M. Taylor contributed to discussion of results. K**.** Fallahnezhad prepared the first draft of this paper. K**.** Fallahnezhad, R.H. Oskouei and M. Taylor contributed to prepare the final manuscript of the paper.

2. **Fallahnezhad, K**.; Farhoudi, H.; Oskouei, R.H.; Taylor, M. A finite element study on the mechanical response of the head-neck interface of hip implants under realistic forces and moments of daily activities: Part 2, *Journal of the Mechanical Behavior of Biomedical Materials* **2017**, *77*, 164-170.

   contributions: K**.** Fallahnezhad, H. Farhoudi, R.H. Oskouei and M. Taylor all contributed to the design of this study. K**.** Fallahnezhad developed the finite element model. H.Farhoudi developed the MATLAB code. K**.** Fallahnezhad and H. Farhoudi extracted results. K**.** Fallahnezhad, H. Farhoudi, R.H. Oskouei and M. Taylor contributed to discussion of results. K**.** Fallahnezhad prepared the first draft of this paper. K**.** Fallahnezhad, H. Farhoudi, R.H. Oskouei and M. Taylor contributed to prepare the final manuscript of the paper.

3. **Fallahnezhad, K**.; Oskouei, R.H.; Badnava, H.; Taylor, M. An adaptive finite element simulation of fretting wear damage at the head-neck taper junction of total hip replacement: The role of taper angle mismatch. *Journal of the Mechanical Behavior of Biomedical Materials* **2017**, *75*, 58-67.

   contributions: K**.** Fallahnezhad, R.H. Oskouei and M. Taylor contributed to the design of this study. K**.** Fallahnezhad developed the finite element model and extracted results. K**.** Fallahnezhad developed the UMESHMOTION code. H. Badnava contributed in developing the UMESHMOTION code. K**.** Fallahnezhad, R.H. Oskouei and M. Taylor contributed to discussion of results. K**.** Fallahnezhad prepared the first draft of this paper. K**.** Fallahnezhad, R.H. Oskouei and M. Taylor contributed to prepare the final manuscript of the paper.

4. **Fallahnezhad, K**.; Oskouei, R.H.; Taylor, M. Development of a fretting corrosion model for metallic interfaces using adaptive finite element analysis. *Finite Elements in*

Analysis and Design, in press (accepted on 14 May 2018) (DOI: https://doi.org/10.1016/j.finel.2018.05.004).

contributions: K**.** Fallahnezhad, R.H. Oskouei and M. Taylor all contributed to the design of this study. K**.** Fallahnezhad developed the finite element model and extracted results. K**.** Fallahnezhad developed the UMESHMOTION code. K**.** Fallahnezhad and R.H. Oskouei contributed to discussion of results. K**.** Fallahnezhad prepared the first draft of this paper. K**.** Fallahnezhad, R.H. Oskouei and M. Taylor contributed to prepare the final manuscript of the paper.

5. **Fallahnezhad, K**.; Oskouei, R.H.; Badnava, H.; Taylor, M. The influence of assembly force on the material loss at the head-neck junction of hip implants in physiological body fluid subjected to cyclic fretting wear. Manuscript being submitted to *Materials*.

   contributions: K**.** Fallahnezhad, R.H. Oskouei and M. Taylor contributed to the design of this study. K**.** Fallahnezhad developed the finite element model and extracted results. K**.** Fallahnezhad developed the UMESHMOTION code. H. Badnava contributed in developing the UMESHMOTION code. K**.** Fallahnezhad, R.H. Oskouei and M. Taylor contributed to discussion of results. K**.** Fallahnezhad prepared the first draft of this paper. K**.** Fallahnezhad, R.H. Oskouei and M. Taylor contributed to prepare the final manuscript of the paper.

6. Farhoudi, H.; **Fallahnezhad, K**.; Oskouei, R.H.; Taylor, M. A finite element study on the mechanical response of the head-neck interface of hip implants under realistic forces and moments of daily activities: Part 1, level walking. *Journal of the Mechanical Behavior of Biomedical Materials* **2017**, *75*, 470-476.

   contributions: K**.** Fallahnezhad, H. Farhoudi, R.H. Oskouei and M. Taylor all contributed to the design of this study. K**.** Fallahnezhad developed the finite element model. H. Farhoudi developed the MATLAB code. K**.** Fallahnezhad and H. Farhoudi extracted results. K**.** Fallahnezhad, H. Farhoudi, R.H. Oskouei and M. Taylor contributed to discussion of results. H. Farhoudi prepared the first draft of this paper. K**.** Fallahnezhad, H. Farhoudi, R.H. Oskouei and M. Taylor contributed to prepare the final manuscript of the paper.

7. **Fallahnezhad, K.;** Badnava, H.; Oskouei, R.H.; Taylor, M. *The influence of assembly force on the material loss at the head-neck junction of hip implants in physiological body fluid subjected to cyclic fretting wear*, XXVI Congress of the International Society of Biomechanics, Brisbance, Australia, July 2017.

   contributions: K**.** Fallahnezhad, R.H. Oskouei and M. Taylor contributed to the design of this study. K**.** Fallahnezhad developed the finite element model and extracted results. K**.** Fallahnezhad developed the UMESHMOTION code. H. Badnava contributed in developing the UMESHMOTION code. K**.** Fallahnezhad, R.H. Oskouei and M. Taylor contributed to discussion of results. K**.** Fallahnezhad prepared the first draft of this paper. K**.** Fallahnezhad, R.H. Oskouei and M. Taylor contributed to prepare the final manuscript of the paper.

8. **Fallahnezhad, K**.; Farhoudi, H.; Oskouei, R.H.; Taylor, M. *Development of a fretting wear model for the head-neck junction of hip implants in a simulated physiological body fluid*, 3rd International Conference on BioTribology (ICoBT 2016), London, England, Sep 2016.

   contributions: K**.** Fallahnezhad, H. Farhoudi, R.H. Oskouei and M. Taylor all contributed to the design of this study. K**.** Fallahnezhad developed the finite element model and extracted results. K**.** Fallahnezhad developed the UMESHMOTION code. K**.** Fallahnezhad, R.H. Oskouei and M. Taylor contributed to discussion of results. K**.** Fallahnezhad prepared the first draft of this paper. K**.** Fallahnezhad, H. Farhoudi, R.H. Oskouei and M. Taylor contributed to prepare the final manuscript of the paper.

9. **Fallahnezhad, K**.; Farhoudi, H.; Oskouei, R.H.; Taylor, M. *A three dimensional finite element model of the head-neck junction of a modular total hip arthroplasty*, Australian and New Zealand Orthopaedic Research Society (ANZORS), 20th Annual Scientific Meeting, Adelaide, Australia, Sep 2014; p 139.

   contributions: K**.** Fallahnezhad, H. Farhoudi, R.H. Oskouei and M. Taylor all contributed to the design of this study. K**.** Fallahnezhad developed the finite element model and extracted results. K**.** Fallahnezhad, H. Farhoudi, R.H. Oskouei and M. Taylor contributed to discussion of results. K**.** Fallahnezhad prepared the first draft of this paper. K**.** Fallahnezhad, H. Farhoudi, R.H. Oskouei and M. Taylor contributed to prepare the final manuscript of the paper.

All co-authors granted permission for the candidate to include the publications in the thesis.

Declaration

I certify that this thesis does not incorporate without acknowledgment any material previously submitted for a degree or diploma in any university; and that to the best of my knowledge and belief it does not contain any material previously published or written by another person except where due reference is made in the text.

Full Name: Khosro Fallahnezhad

Signed:

Date: 23/10/2017

Acknowledgment

I would like to express my deepest appreciation to my principle supervisor, Dr Reza Oskouei, who patiently helped, supervised and supported me over the course of my PhD. This work could not have been possible without his guidance and persistent help.

I would like to thank my co-supervisor, Professor Mark Taylor, whose deep knowledge in biomechanics and computational modelling enhanced this work's quality.

I thank my colleagues, Hamid and Hojjat, who have always been ready to help me at different stages of this work.

I also acknowledge the support for my PhD received from the Australian Government Research Training Program Scholarship.

A special thanks to my family. Words cannot express how grateful I am to my mother and father for all of the sacrifices that they have made for me. In the end, I would like to appreciate my beloved wife, Elahe, who spent sleepless nights with me, and was always my support in moments when there was no one to answer my doubts.

Introduction

Previous studies on modular total hip replacements have identified the occurrence of fretting corrosion (mechanically assisted corrosion) in the head-neck taper junction of hip joint implants. This phenomenon can generate metal debris that is proven to have detrimental effects on various body tissues such as the spleen, bones and liver. To date, many retrieval studies, *in vitro* tests, and numerical studies have been developed to understand the occurrence and intensity of the fretting corrosion damage to the head and neck materials. However, there are still some gaps in this research area which require more investigation. This PhD project aims to investigate different aspects of the mechanical parameters that can influence the fretting wear damage of the head-neck junction of total hip replacements.

In Chapter one: A comprehensive review on the previous research in this field is provided. In the first part of this chapter, the history of hip implants, including several proposed designs and materials, which have been used to produce hip implants, is presented. Moreover, the advantages and complications of the modular design, as the most pragmatic design that is being widely used, are mentioned. In the second part, the fretting corrosion damage in the head-neck junction is reviewed. The different aspects of this damage, including its previously investigated causes and influences on the head-neck junction operation and its detrimental effects on tissues, are reviewed. The third part reviews studies that have been developed on the assembling process of the head-neck junction. The chapter's fourth part is dedicated to wear, nature of fretting wear, the mechanics of fretting wear, and the research that has been developed in this field. The fifth part provides a literature review of the finite element studies developed in this area, including different on-cycle and adaptive models. In the last part, this area's research gaps, which still need more investigation, are mentioned.

In Chapter two: a three-dimensional (3D) explicit FE model of an isolated femoral head-neck junction was developed to simulate the real geometry of the head and neck components with a non-linear frictional contact and elastic-plastic properties of the mating materials. The FE model was verified by previously reported experimental assembling and disassembling tests. The model was then used to investigate the mechanics of the head-neck junction in order to understand which parameters contribute to the axial and torsional strength of the interface.

In Chapter three: the mechanical behaviour of the head-neck taper junction, particularly a CoCr/CoCr junction with a 12/14 taper design and a proximal mismatch angle of 0.024°, which is subjected to mechanical loads of common daily activities, is evaluated. To this end, the three-dimensional model developed in the second chapter is used. A range of contact stresses and relative micro-motions is also determined, which may be accordingly used in relevant *in vitro* tests to represent a wide range of routine activities for this type of taper junction.

In Chapter four: an adaptive finite element simulation is developed, to predict fretting wear in the head-neck taper junction of a hip joint implant, through a two-dimensional (2D) model based on Archard's Wear Equation. This model represents the most critical section of the head-neck junction, which was identified from the 3D model of the whole junction (Chapter three), subjected to one cycle of level gait loading. To model the fretting wear, a FORTRAN code is developed that can control the position of the surface nodes through the ABAQUS UMESHMOTION subroutine, within an adaptive meshing constraint. To reduce the computational cost, an adaptive wear simulation was used, which assumes that the wear rate remains constant during a pre-determined number of cycles (ΔN). A PYTHON code together with a MATLAB code are developed to compute the lost material in the form of worn area from the contacting surfaces at various numbers of cycles of walking activity, as well as the depth of wear over the neck length for each case. The model was used to explore the influence of the junction environment (dry and phosphate buffered solution (PBS) conditions) with comparing the fretting wear behaviour of the head-neck junction in both conditions.

In Chapter five: The 2D model developed in the previous chapter is used to investigate the effect of angular mismatch between the head and neck components on the material loss and fretting wear process over four million gait cycles of walking. Different cases with distal and proximal angular mismatches, and the sample with perfect contact, are investigated for which the variation of the contact pressure, micromotion, contact length and the wear profile are presented. Moreover, the graph of material loss versus number of cycles is presented to track the magnitude of the material loss over the fretting wear process. To develop more realistic simulations and avoid the major simplification of the dry condition, the fretting wear simulations of the head-neck junction for all cases are analysed only for the PBS condition.

In Chapter six: The main research objective is to evaluate the effect of assembly force on the material loss and fretting wear process, using the adaptive FE model developed in Chapter four. The 2D fretting wear model of the CoCr/CoCr taper junction is assembled with four different assembly forces of 2000 N, 3000 N, 4000 N, and 5000 N. A PYTHON code and a MATLAB code are developed to report the contact pressures and relative micro-motions at the contact interface, and to find the material loss in the form of worn area from the surface, at various cycles (up to 1,025,000 cycles) of normal walking gait loading.

In Chapter seven: An adaptive finite element model is successfully developed to simulate fretting corrosion at metallic interfaces. Archard's Wear Equation and a previously established electrochemical equation are simultaneously employed. This code's algorithm is able to determine the volume of passive oxide layers removed from the interface and/or re-generated onto the surface and material loss caused by both fretting wear and corrosion. The model is then used to simulate the fretting corrosion process for a CoCr/CoCr interface under a varying profile of fretting sliding and normal stresses of 250 and 500 MPa. This model can be a good platform for finite element modelling of fretting corrosion in various applications and future studies to further investigate surface damage to materials in fretting corrosion situations.

Chapter 1 Literature Review

1.1 Hip joint anatomy, biomechanics and diseases

The hip joint is a synovial joint made of a femoral head (ball) and the acetabulum (socket). The axial skeleton is connected to the lower extremity by the hip joint and therefore, the hip joint can be considered as the joint of the femur with the pelvis. Figure 1.1 demonstrates the anatomy of the hip joint.

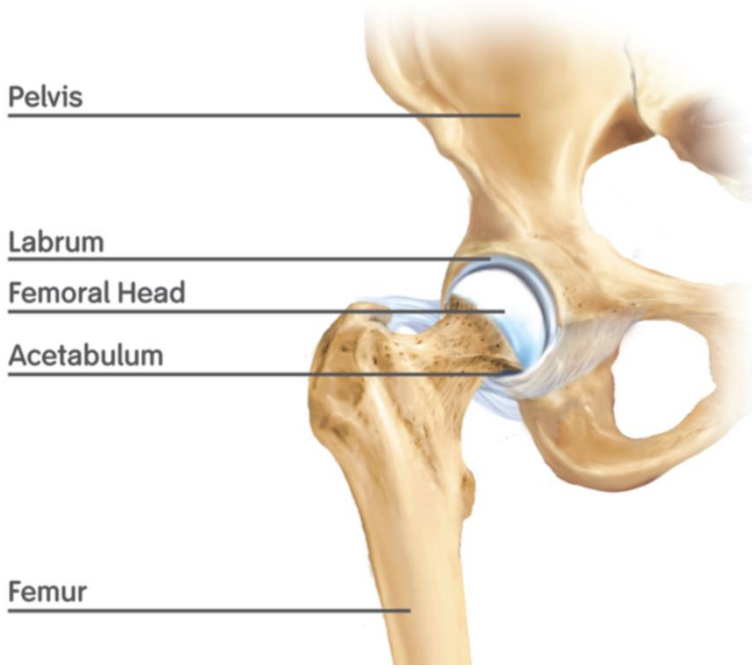

Figure 1.1- Anatomy of hip joint (Smith & Nephew Education and Evidence).

Some of the following causes of hip disease are mentioned below:

1. Arthritis;
   - Osteoarthritis, which is the most common form of arthritis
   - Inflammatory arthritis (e.g. rheumatoid and ankylosing spondylitis)
2. Bone fracture;
3. Slipped capital femoral epiphysis, which occurs mostly in teens;
4. Abnormal developmental conditions (e.g. hip dysplasia);

5. Soft tissue pain; and
6. Perthes disease, which is the lack of blood supply around the femur head and can cause to cells die.

The main cause of primary total hip replacement is osteoarthritis. According to National Joint Replacement Registry's 2017 annual report, osteoarthritis has been the reason of 88.8% of primary total hip replacement in Australia.

Osteoarthritis is when the degeneration of the joint cartilage causes changes and damage to the bones underlying the joint. In this disease, the cartilage becomes stiff and brittle (Loeser 2006), and in some cases it breaks and floats within the hip joint's synovial fluid, which in turn can result in inflammation. In some cases, the breakdown of cartilage is so serious that it cannot cover two contacted bones anymore. It is widely accepted that the major reason of osteoarthritis is cellular change, which can cause cartilage to lose its elasticity (Loeser 2006, Goldring and Goldring 2010). Apart from the hip joint, even the spine, fingers, toes and shoulders can be affected by osteoarthritis (Figure 1.2).

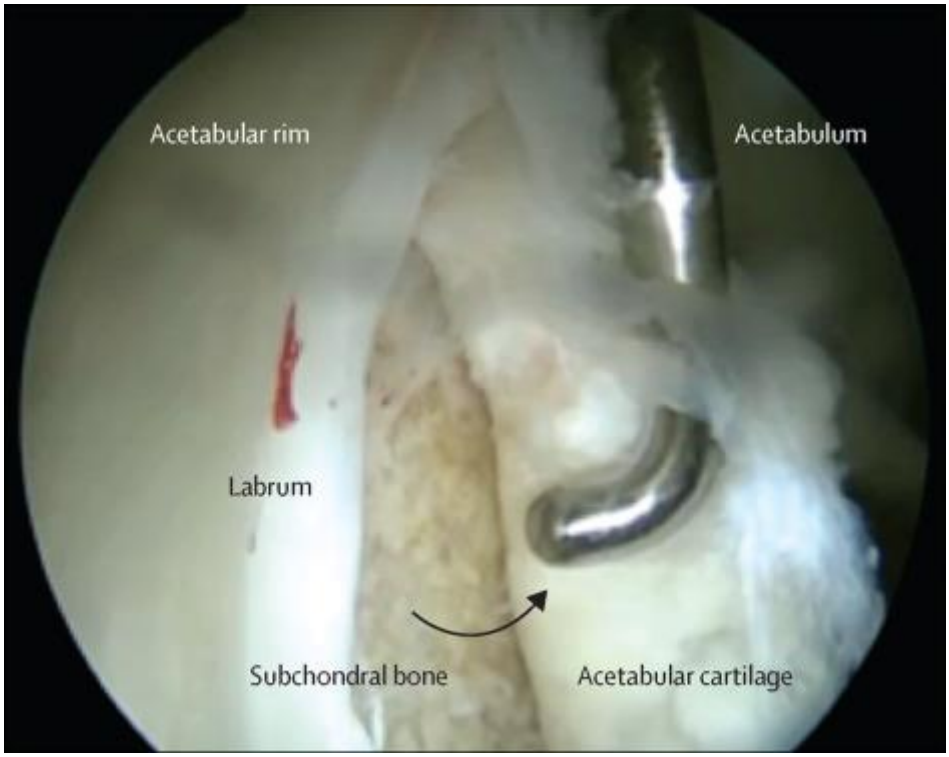

Figure 1.2- The acetabular cartilage delamination leading to the development of osteoarthritis (Glyn-Jones, Palmer et al. 2015).

There is no effective pharmacological treatment available for the different forms of arthritis. However, there are some non-pharmacological options, such as different exercises that are proven to greatly influence the treatment and prevention of arthritis. Till date, the best option for people who suffer from end-stage osteoarthritis is hip joint replacement surgery.

To investigate the mechanics of hip joint implant, it is required to understand the loading structure pattern that is being applied to hip joint during daily activities. Figure 1.3 demonstrates the loading pattern, which is being applied to the hip joint. As can be seen in this figure, the two main forces that are being applied to the hip joint are body weight force and muscle force. This figure also shows the resultant force and the mathematical relation between these forces according to their angles.

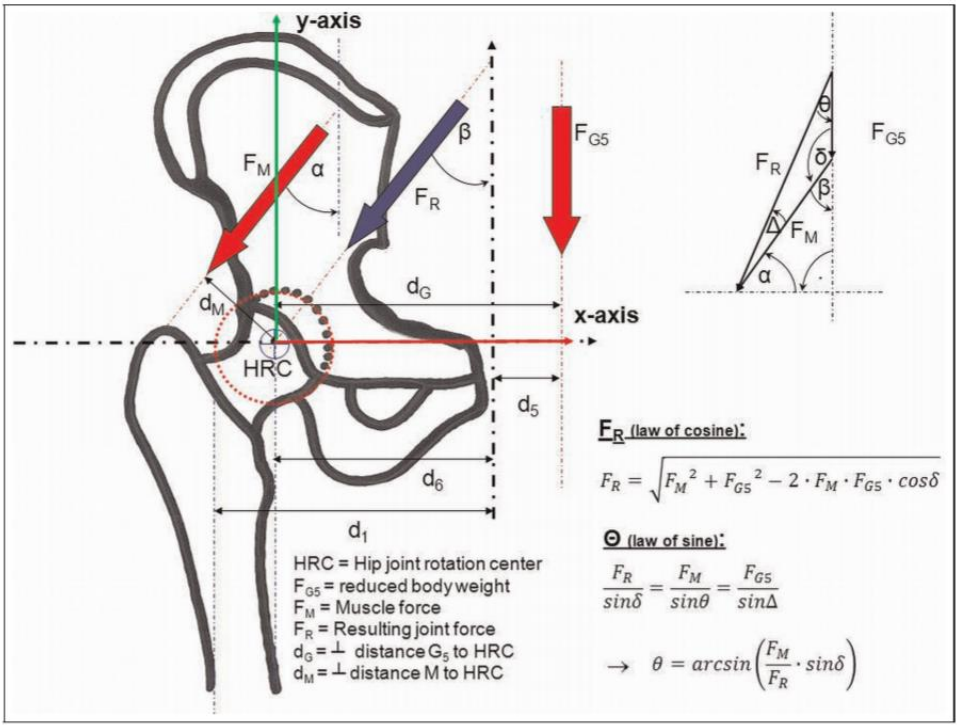

Figure 1.3- Loading structure of the hip (Eschweiler, Fieten et al. 2012)

1.2 History of hip joint implants

Over the past 100 years, operative procedure history shows dramatic progression of operation, together with the progress of materials and methods, which have contributed to its development especially in the case of hip joint operations. Knowledge of this history not only helps in better understanding total hip replacement (THR) (Figure 1.4), but also illustrates the reason behind the different designs of hip joint implants, different materials from which hip implants are made, and the blind points of these designs and materials (Knight, Aujla et al. 2011).

For the first time, in 1891 Professor Themistocles Glück implemented ivory as the femoral heads for patients affected by tuberculosis (Wessinghage 1991). The results of these attempts were published in the 10th International Medical Conference. Afterwards, till the early 20th century, different surgeons experimented with interpositional arthroplasty. Various tissues such as pig bladders submucosa were placed between articulating hip surfaces of the arthritic hip (Learmonth, Young et al.). In 1925, Marius Smith-Petersen created and implemented the first glass hip implant (Charnley 1961). Although glass is a bio compatible material, it wasn't strong enough against the great force and shattered. George McKee, a surgeon from England, used metal-on metal prosthesis, in 1953 (Brown, Davies et al. 2002). He started his work by using a modified version of Thompson's stem. However, he implemented a cobalt-chrome socket for the acetabulum. This method has had a quite high survival rate of 74% for 28 years. It should be mentioned that some local effects, caused by metal particles, was reported in some retrieval surgeries in 1970. In 1960, surgeon John Charnley (father of the modern THR) designed his prostheses similar to those that are being used today (Charnley 1961). It contained three parts: acrylic bone cement, a polyethylene acetabular component, and a metal femoral stem [2].

It was since the 1980s that hip joint implants with modular design of the femoral component gradually turned out to be popular (John Cooper, Della Valle et al. 2012) (Figure 1.4). Modularity at the head-neck junction of THR implants provides intraoperative flexibility, the possibility to use different material combinations and femoral head diameters. Additionally, by means of modular design, subsequent revision can be simplified by retaining the stem and performing head substitution (John Cooper, Della Valle et al. 2012, Srinivasan, Jung et al. 2012, Dyrkacz, Brandt et al. 2013). More importantly, a modular design gives the surgeon the flexibility to intra-operatively adjust the femoral head's position, allows them to achieve equal

leg length and position of the hip joint centre. Gradually, the tendency of using a femoral hip-stem with lower stiffness (close to the stiffness of bone) has increased. Accordingly, the use of titanium alloys (Ti6Al4V, ASTM F-136-79) instead of cobalt-chrome materials (HS 21, ASTM F-75) grew.

Figure 1.4- Modular design of hip joint implant

However, there were still concerns about titanium stems used in cement applications, due to difference of stiffness and module of elasticity between titanium and cement. The first generation of head-stem implants, which were made of titanium, suffered from more burnishing, scratching, and loss of sphericity compared with the cobalt-chrome one (Collire, Surprenant et al. 1991). Hence, in mid 1980s, implants with variable lengths and materials of stems and separate spherical heads were proposed as a design that could be mated during the surgery.

1.2.1 Complications of modular design

It appeared that using the titanium stem and a cobalt-chrome head is the most appropriate solution for biological applications (Knight, Aujla et al. 2011). The titanium alloy stem had the most suitable stiffness with quite a good agreement with bone, and the cobalt-chrome head was resistant enough against the wear. However, one major concern was raised for using modular head-neck junctions with metal-on-metal combinations, especially for combinations of different materials, and it was the potential of fretting corrosion. The taper design for the head-neck junction is widely being used to provide a firm and reliable connection. Due to the taper design and manufacturing tolerances, there is always an angular mismatch between the head and neck components (Bisseling, Tan et al. 2013). Depending on each component's taper angle, such an angular mismatch can cause the head-neck junction to have its main contact at the bottom or top of the trunnion, known as distal and proximal contacts, respectively (Figure 1.5). However, the fluid can still penetrate inside the junction and cause corrosion (Figure 1.6).

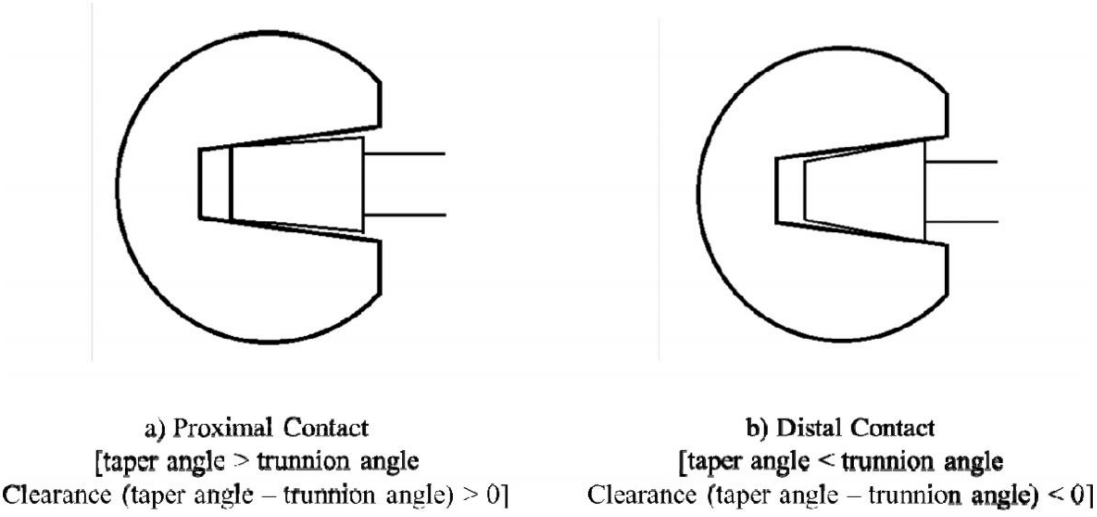

Figure 1.5- Schematic diagram showing proximal and distal contact in head-neck junction (Kocagöz, Underwood et al. 2013)

There are several taper junction designs available in the market (in terms of size and geometry). 11/13 and 12/14 are the most popular designs that are reported in different studies to have various taper angles in the range of 4°–6°. To date, previous studies report that there is no established relation between fretting corrosion and taper angle. Over the past few years, the 14mm/16mm trunnions has been replaced by 12mm/14mm ones. The main reason for such a

trend is that smaller sizes of trunnion (neck) cross section can be designed with a smaller length, which can, in turn, enhance the range of the motion.

Several defects and damages can cause the revision of a primary modular hip replacement. Statistics show that the main reasons for revision are prosthesis dislocation, infection, loosening/lysis, and fracture with the percentage of 21.6%, 17.7%, 25.6% and 19.5%, respectively (The Australian Orthopaedic Association National Joint Replacement Registry).

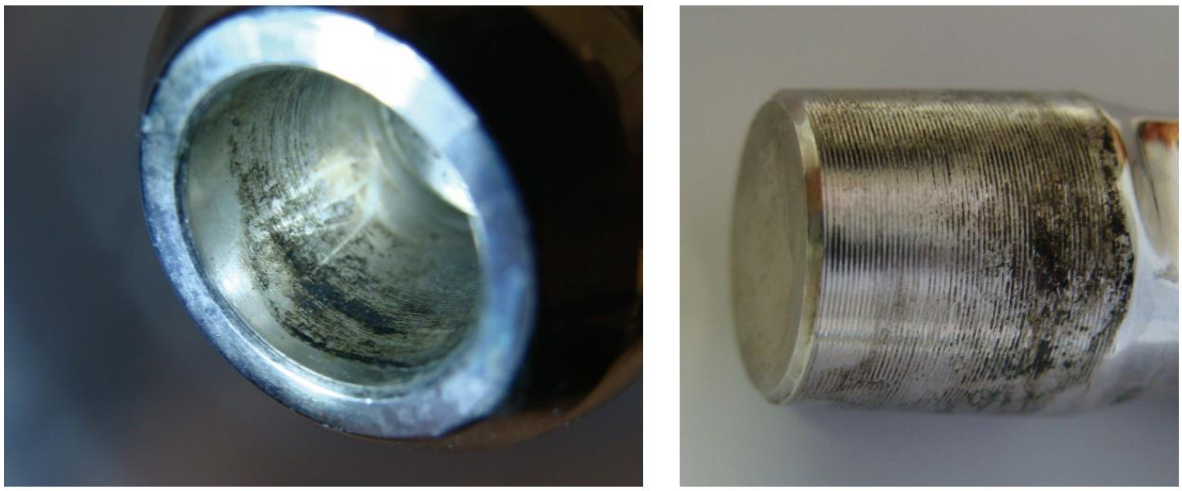

Figure 1.6- Occurrence of fretting corrosion in head and neck (Hussenbocus, Kosuge et al. 2015)

1.3 Fretting corrosion in THR

Despite several advantages, the modularity of the femoral component, particularly the metallic head-neck junctions, can potentially result in fretting wear, which can occur when two contacting metallic components are subjected to tangential oscillatory movements (Jauch, Huber et al. 2011). Given the presence of a corrosive medium all around the implant, the shear stresses induced under fretting conditions may disrupt the metal's passive layer (Figure 1.7) (Mathew, Srinivasa Pai et al. 2009, Zhu, Cai et al. 2009), and thus, accelerate corrosion at the head-neck interface (Rodrigues, Urban et al. 2009). This combined failure mechanism caused by a complex interaction between fretting wear and corrosion is known as 'fretting-corrosion'

and/or ‘mechanically assisted crevice corrosion’ in orthopaedic hip joint implants (Gill, Webb et al. 2012, Swaminathan and Gilbert 2012, Higgs, Hanzlik et al. 2013).

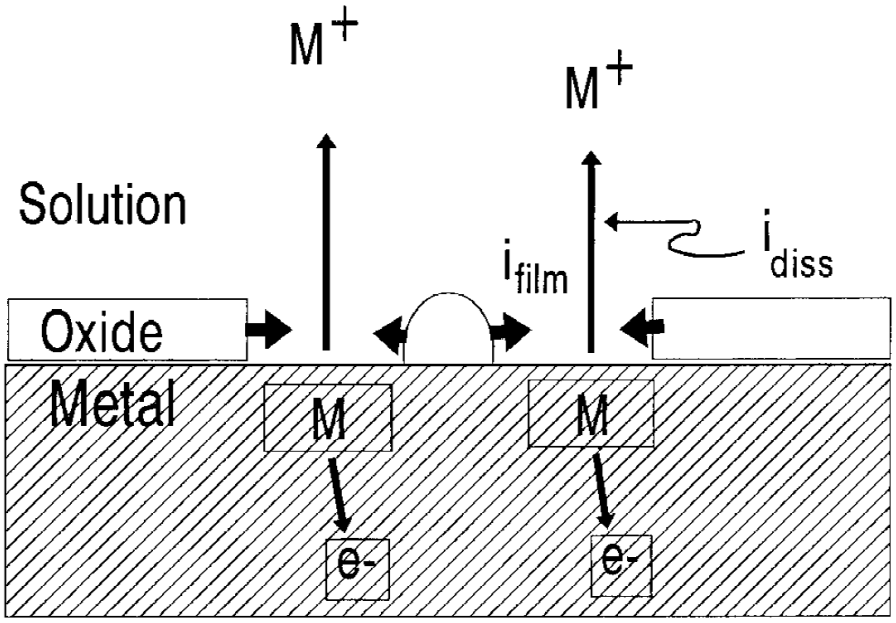

Figure 1.7- Disruption of metallic oxide layer and the process of passive layer reformation and metallic dissolution (Goldberg and Gilbert 1997)

Several retrieval studies have proven the presence and damaging effects of fretting corrosion in the head-neck junction of a THR. Urban and his colleagues conducted a retrieval study of 269 implants to investigate fretting and corrosion damage in two different combinations of head-neck junctions (Hussenbocus, Kosuge et al. 2015). They reported that 38% of CoCr head-titanium stem couples and 21% of CoCr head-CoCr stem couples were damaged because of fretting and corrosion. In a similar research, Goldberg and his colleagues conducted a multi-centre retrieval study of THRs. They investigated the effect of different parameters such as material combination, flexural rigidity, metallurgic condition, neck moment arm head, neck length, and time of implantation on fretting and corrosion of head-neck junctions. Different levels of damage were observed in 28% of the heads of similar alloy couples, and 42% of the heads of mixed alloy couples. They also reported that the fretting and corrosion damage levels were higher in heads compared to necks (Goldberg, Gilbert et al. 2002). Fretting-corrosion has been known to contribute to a degradation process, which reduces the integrity of the implant structure and releases products whose reaction can be harmful when in contact with organic tissues (Sansone, Pagani et al. 2013).

Hydroxides and oxides are the two main products of metal degradation that are mostly found in synovial tissues. Compared with polyethylene particles, metal particles are smaller and the number of them is much more than the polyethylene ones (about 13500 times) (Cobb and Schmalzreid 2006). Smaller particle sizes can cause a larger surface of tissues to be affected by the particles (Figure 1.8). In other words, by decreasing the size, the biological activity per given mass increases (Billi and Campbell 2010). Hence, they can easily affect different tissues such as bones, the spleen and liver (Urban, Jacobs et al. 2000) (Figure 1.8). Additionally, metal ions may enter the blood and affect the erythrocytes. In this way, they may also be transported through the body, which may cause immunological effects, as they are genotoxic and cytotoxic (Doorn, Campbell et al. 1998). These metal particles can also negatively affect cells in different ways. They may pass the cell plasma membrane by diffusion or endocytosis. Inside the cells, these particles may oxidatively attack, which can damage the cells body and also produce free radicals. Moreover, the oxygen which is reacted from Cr, Ni, Co and Ti combinations can damage the proteins, lipids and nucleus. Walter et al. (Walter, Marel et al. 2008) investigated the chromium and cobalt ions levels in 29 patients after unilateral hip resurfacing with a 54mm sized femoral Birmingham Hip Resurfacing Prosthesis. They measured ion levels in whole blood, red cells, serum, and plasma in patients. They concluded that low amounts of Cr and Co are related to red blood cells, while most of them are associated with serum/plasma. They also suggest that most of the material loss is because of the normal wearing rather than corrosion. Swaminathan et al. (Swaminathan and Gilbert 2012) have developed an integrated systematic method for the investigation of fretting corrosion for metal-on-metal contacts. They have not only developed a test system to investigate the effect of different elements on fretting corrosion, but also proposed a model in which they tried to consider all of the mechanical and electrochemical parameters that contribute in fretting corrosion damage. Compared with the other combinations, it was understood that, to generate the highest fretting corrosion currents in Ti6Al4V/Ti6Al4V couples, the lowest amount of work was needed. Dimah et al. (Dimah, Devesa Albeza et al. 2012) studied corrosion and tribocorrosion behaviours of titanium alloys under sliding conditions in both PBS and PBS–BSA conditions. They used *ex situ* surface characterisation and tribo-electrochemical methods. They found that the alloy's chemical composition and microstructure mainly affect the wear accelerated corrosion. They found that

increasing the rest time between sliding cycles causes the growing of passive layer films during the pause period, which can result in increasing the wear coefficient.

Figure 1.8- Corrosion at the head-neck taper as a cause for adverse local tissue reactions after total hip arthroplasty (John Cooper, Della Valle et al. 2012)

One of the important parameters that helps implants resist corrosion is a passivation layer (Balamurugan, Rajeswari et al. 2008). Passivation layer dynamics is one of the most important concepts that contributes to different types of corrosion. A passive layer can be produced as an *in vivo* process or due to surface treatment. This layer protects implants from different kinds of corrosion by protecting the metal from direct exposure with the electrochemical environment. In the case of crevice corrosion, different parameters such as low PH levels, chloride ions and oxygen tension accelerates the solubility of the metal oxide film. Moreover, the presence of fretting mechanically destructs the passivation layer, which leads to the predomination of crevice corrosion. Some studies have been developed to investigate different parameters' effects on the delamination of the passivation layer in head-neck junction (Sivakumar, Kumar et al. 2011, Jauch, Coles et al. 2014).

Jauch et al. (2014) have developed an experimental set-up that investigates the minimum amount of torque required to remove the passive layer in a head-neck junction in different assembly forces and axial loads. They determined the torque's effect on the taper strength by means of the pull-of force. They concluded that tapers that were assembled with a higher assembly force needed larger torque to remove the passivation layer. Additionally, they found

that axial force had no effect on the fretting behaviour of the junction. Sivakumar et al. (2011) investigated the fretting corrosion behaviour of Ti-6Al-4V alloy in a saliva solution containing different amounts of fluoride ions. They evaluated the change in free corrosion potential (FCP) as a function of time. Starting the fretting caused the damage of the passive film, which resulted in a cathodic shift in FCP. When the fretting was stopped, the repassivation process of Ti-6Al-4V instantly started only in the saliva solution. However, the negative effect of fluoride ions on passive film formation caused the zones damaged by fretting to not be able to be repassived instantly. They finally concluded that the fretting corrosion behaviour of Ti-6Al-4V strongly depended on the fluoride ion concentration.

As mentioned before, previous studies on modular THRs have identified the occurrence of fretting wear in the head-neck taper junction of hip joint implants. This phenomenon can generate metal debris that is proven to have detrimental effects on various body tissues such as the spleen, bones and liver (Doorn, Campbell et al. 1998, Urban, Jacobs et al. 2000, Walter, Marel et al. 2008). Hence, to investigate the process of fretting wear in the head-neck junction of hip joint implant, it is essential to have a deep understanding of the nature of fretting wear, mechanics of fretting wear, and research that has been developed in this area.

1.4 Fretting wear

By definition, fretting is a small amplitude oscillatory motion between two solid surfaces that are in contact by means of a load (Godfrey and Bisson 1952). Fretting consequently produces debris particles and grooves and pits on surfaces. Fretting frequently occurs in mechanically fastened joints that are subjected to fluctuating loads (Mitchell 1983). Machine components are another source of fretting problems. For example, the contact between hubs or shrink and press-fits junctions, like what we have in a head-neck junction of the hip joint implant, are some cases where fretting may occur. Fretting is also an important concern to the aeroengine industry because many assemblies are under cyclic loads and therefore, can be damaged by fretting (Heinz 1989). Accordingly, a lot of studies have been developed on fretting and fretting wear. Here, the study has tried to review the literature related to fretting and fretting wear.

By the end of the 20th century, further insight into the fretting process was developed. Vingsbo et al. (Vingsbo and Söderberg 1988) developed a concept of fretting maps to display the effects of different parameters such as load, frequency, amplitude and contact geometry. Godet and his colleagues proposed a concept of third-body tribology to address the effects of debris on fretting. Berthier and his colleagues proposed a model in which displacement and velocity change between different areas of contact surfaces with different elastic deformation, rupture and debris motions. Additionally, many studies have been developed to propose analytical and numerical solutions to fretting contact problems (Johnson 1985, Hills and Nowell 1994).

In term of experimental efforts, many studies have been developed to investigate the different aspects of wear and fretting wear. For the first time in 1927, Tomlison designed a fretting test machine. In his design, the configuration was set up to produce small amplitude rotational movements. He concluded that the observed damage was because of relative motion or slip between the contacting surfaces. Waterhouse et al. (Waterhouse 1972) suggested that the most important parameters of fretting wear, which distinguish it from other forms of wear are: stroke, which is the amplitude of relative displacement between two contacting bodies, restricted opportunity for the wear products to scape, and the contacting area's relative velocity that should be much lower during fretting than during sliding wear. Uhlig et al. (Uhling 1954) believed that fretting wear consists of two main terms where the first one is chemical based and the other is a mechanical process. Waterhouse and Taylor (Waterhouse and Taylor 1974) suggested that the delamination process effectively contributes in the material removal in the next stages of fretting. The effects of various parameters and variables on the process of fretting wear were also investigated. Collins et al. (Collin and Macro 1964) reported that there are up to fifty parameters that can affect fretting wear. First, contact conditions such as loads, slip amplitude, frequency, duration, and geometry. Second, environmental conditions such as temperature, humidity, and lubricant. Third, material properties and behaviour, such as hardness, strength, fatigue, ductility, and so on. Hence, the preventive methods, which can be taken to reduce or to eliminate damage due to fretting wear, are diverse. Fretting wear can be suppressed by geometry modification of components and changing the contacting materials (Waterhouse 1992). Using the appropriate lubricant is the other solution to reduce the fretting wear (Sato, Shima et al. 1988). Additionally, surface treatments and coating are the other possible solutions to fretting damage (Bill 1978, Harris, Overs et al. 1985).

Several studies have been developed to propose wear and fretting wear models. For this purpose, it is very important to deeply understand mechanisms and the mechanics of wear and fretting wear.

So far, it is generally accepted that wear mechanisms, such as adhesion, abrasion, fatigue and corrosion, can act in conjunction with one another to damage the surfaces. The relative influence of different wear mechanisms may even change as the fretting process continues. The fretting wear mechanism occurs in three stages as a function of time (Hurricks 1970, Waterhouse 1992):

- *The initial stage:* In the first thousand cycles of metal-on-metal contact, the major mechanism is metal transfer and adhesion, which results in local welding, roughening of the surface and high friction.
- *Debris generation:* The oxidised debris begins to accumulate at the interface and the metal-on-metal contact and coefficient of friction decrease. If the oxidised particles are harder than the surface metal, the abrasive action begins.
- *The steady state:* The coefficient of friction becomes more or less constant. The abrasive action of wear particles is decreased by the formation of compacted debris beds.

There are some important parameters that affect fretting wear:

1- *Amplitude of displacement:* It is the maximum relative displacement which differs from the actual slip of the contact interface. For the first time, Waterhouse (Waterhouse 1992) developed some experimental tests to define the borders between wear and fretting wear. They concluded that the value of the wear rate is insignificant when the amplitude is below 10 µm. On the other hand, when the amplitude is more than 100 µm it is quite above the fretting limit, and such a process should be considered as a reciprocating wear sliding. In contrast, some researchers suggested that the upper limit of the fretting wear stroke is about 300 µm (Soderberg and Vingsbo 1987, Xushou, Chuenhe et al. 1989). This difference seems to be a result of the different parameters such as material properties, frequency and normal load.

2- *Normal force:* Some researchers such as Wright, Feng et al. and Reed et al. (Feng and Uhilg 1954, Glascott, Stott et al. 1984) suggested that in a constant value of slip amplitude, the wear rate is linear depending upon the applied normal force. However, Waterhouse (Watrehouse 1985) found that the effect of the normal force should be more complicated than just a linear behaviour. Actually, he concluded that small change in the normal load can considerably affect the mode of fretting. Additionally, Iwabuchi (Iwabuchi 1991) investigated the change of the wear volume with and without considering the contact surface particles. He suggested that when there are no particles, load increasing causes the wear rate to increase. When particles exist on the surface area, the effect of the normal force is different. In this condition, when the normal force is gradually increased, the wear damage increases due to the higher abrasion at higher loads. If the load is further increased, there will be a kind of rapid compaction and agglomeration of the particles, and will reduce the wear rate.

3- *Contact geometry:* Contact geometry can affect the dimension of the real contact area and the amount and positions of the stress concentration. The other effect of the surface geometry is related to the trapping and escape of the wear debris. Waterhouse argues that cases such as spheres on flat, or crossed cylinders have more of an ability to push out the debris.

4- *Frequency:* Soderberg et al. investigated the influence of the frequency on fretting damages. They suggested that in the partial slip situation, the increase in the interfacial strain rate at high frequencies causes an increase in corrosion and fatigue damage. However, in the total slip condition, there is no significant influence. On the other hand, Berthier et al. (Berthier, Vincent et al. 1989) argued that the effect of the frequency is highly dependent on the type of materials, third body formed, and also dynamic environment.

Fretting contact mechanics is dependent on stresses and deformation under fretting conditions. There are two important features in any fretting conditions: first, a cyclic tangential force and second, slip between the contacting surfaces. In such conditions, the following two general cases can occur:

- Gross slip in which the tangential force is equal to the limitation frictional value ($T = \mu P$).
- Partial slip in which the tangential force is less than the limiting frictional force ($T < \mu P$) (Figure 1.9).

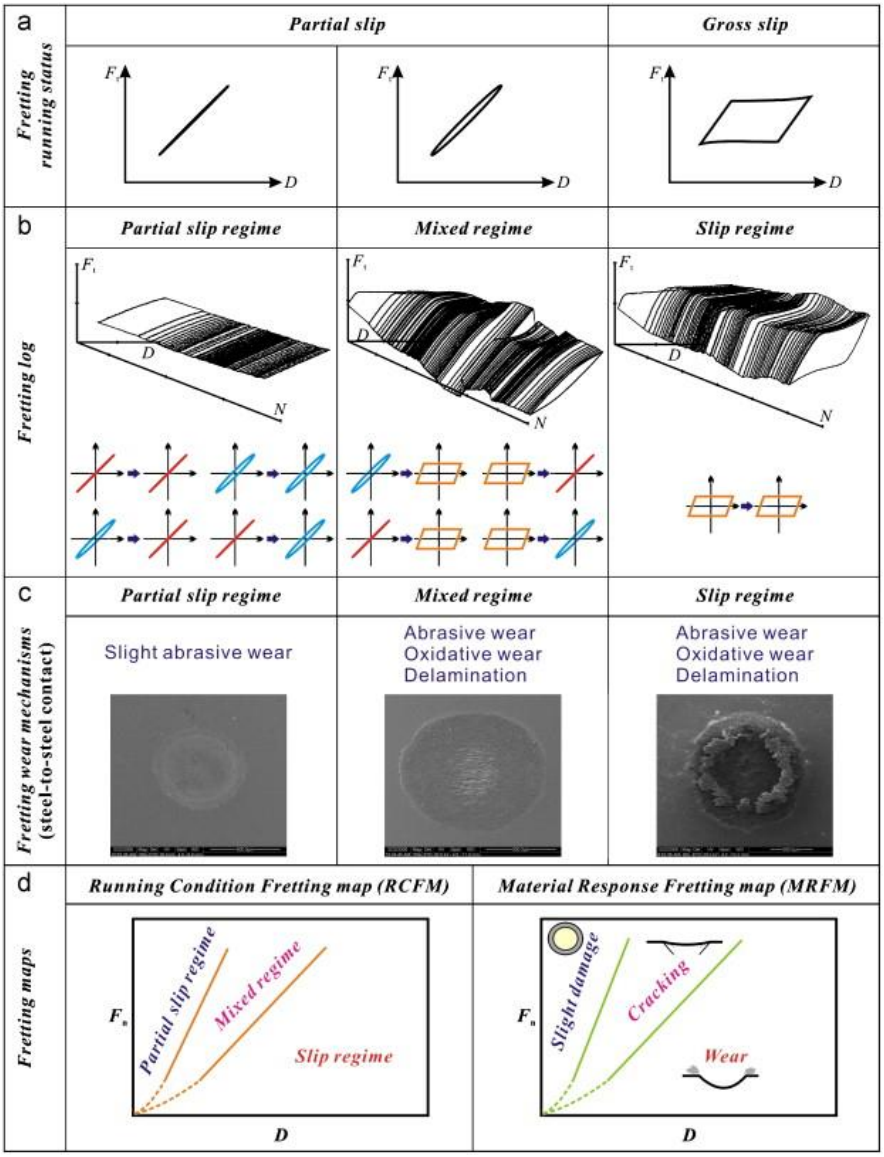

Figure 1.9- Outline for tangential wear: medium carbon steel flat against 52100 bearing steel ball (Zhu and Zhou 2011).

Sackfield et al. (Sackfield and Hills 1983) studied the contact mechanics of a cylinder sliding in a direction perpendicular to its axis. Using Hertzian theory, they proposed formulations that computed the width of the contact area and contact pressure (Figure 1.10).

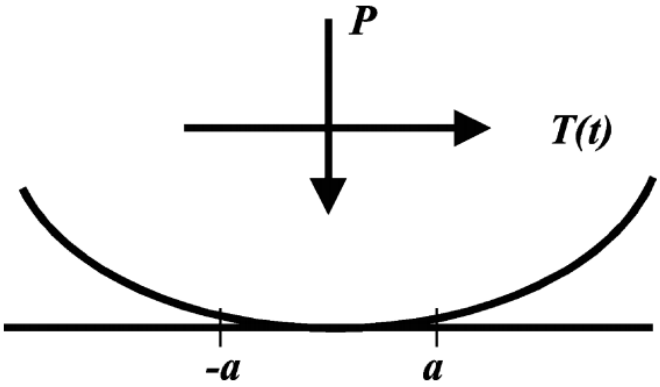

Figure 1.10- Fretting wear contact (McColl, Ding et al. 2004)

$$a = \left[\frac{4PR}{\pi E^*}\right]^{1/2} \tag{1.1}$$

$$P_0 = \left[\frac{PE^*}{\pi R}\right]^{1/2} \tag{1.2}$$

Where, in these equations, a is half the contact area width, P is the applied normal load, E^* is the composite modulus of the two contacting bodies, P_0 is the maximum contact pressure, and R is the relative curvature.

Cattaneo and Mindlin have proposed a solution for the partial slip. They assumed that the shear traction at any point on the interface cannot be higher than the limiting friction. They considered that the interface is divided into two areas, a circular region ($r \leq c$), in which the surfaces are stuck together, and an annular region($c \leq r \leq a$) where the slip occurs. For these two areas they have proposed two different equations for the shear traction. The extent of the central stick zone c is given by:

$$c \,/\, a = [1 - T/(\mu P)]^{1/2} \tag{1.3}$$

In the area where the surfaces slip($c \leq r \leq a$), the shear traction given by:

$$q(r) = \frac{3\mu P}{2\pi a^2}\left[1 - \frac{r^2}{a^2}\right]^{1/2} \quad (1.4)$$

In the stuck area ($r \leq c$) the shear traction is given by:

$$q(r) = \frac{3\mu P}{2\pi a^2}\left\{\left[1 - \frac{r^2}{a^2}\right]^{1/2} - \frac{c}{a}\left[1 - \frac{r^2}{a^2}\right]^{1/2}\right\} \quad (1.5)$$

It should be considered that analytical solutions can only be obtained for very limited cases of contact problems. Therefore, many numerical methods have been developed to investigate more complicated load structures and geometries. Nowell et al. (Johnson and Johnson 1987) proposed a numerical method based on integral equation to analyse some contact arrangements. Additionally, some analytical contact studies have been developed based on the simplified constitutive plasticity models. They have been mostly based on the perfectly plastic theories and/or kinematic strain hardening (Ponter, Hearle et al. 1985, Johnson 1995, Kapoor 1997). But there are two problems in using these kinds of models for investigating fretting. The admitted limitation of these theories is that they cannot calculate the magnitude of the strain in each cycle. Moreover, since the loading considered is far greater than the experienced in a typical fretting situation, they cannot appropriately analyse the fretting problems.

1.4.1 Modelling

Wear is a dynamic process that is a combination of surface and material properties, operating conditions, stresses and geometry. Three important wear models have been proposed to describe the wearing behaviour.

Barwell et al. (Barwell 1958) proposed wear equations in an empirical type that was directly taken from experimental tests. They proposed three equations in which the wear rate was defined as functions of time. They suggested that wear rate can be computed by one of these three equations.

$$V = \frac{\beta_1}{\alpha_1}\{1 - \exp(-\alpha_1 t)\} \tag{1.6}$$

$$V = \alpha_1 t \tag{1.7}$$

$$V = \beta_1 \exp(\alpha_1 t) \tag{1.8}$$

Where V is the wear rate volume, α_1 is a material constant, t is time and β is a surface parameter. Although these equations are limited to the range for which tests are conducted, the accuracy of these experimental tests is more than analytical models (Meng and Ludema 1995).

Archard (Archard 1953) proposed a wear model based on contact mechanics. He defines wear volume as a function of sliding distance and normal force. Oqvist developed a numerical model to simulate a reciprocating contact condition between a cylinder and flat made of steel (Barwell 1958). Having the ability of being localised, Archard's model has been used in different analytical and computational models. Based on Archard's equation a stepwise procedure was used to calculate the properties of contact. Johansson (Johansson 1994) proposed a finite element model to compute the wear rate. He developed a contact algorithm in which he used Archard's equation where the contact pressure was in relation with geometry changes. In his algorithm, Archard's model can be expressed as:

$$dh = kpdS \tag{1.9}$$

Where dh is wear depth increment, k is wear coefficient, p is contact pressure and dS is slip distance increment.

Goryacheva et al. (Goryacheva, Rajeev et al. 2000) developed a numerical model based on Archard's model to simulate the partial slip condition for a two-dimensional case.

McColl et al. (McColl, Ding et al. 2004), proposed a finite element model to simulate fretting wear in a pin-on-disc set up, based on Archard's equation. They performed a cylinder-on-flat test and the material was a high-strength steel alloy (Figure 1.11). They compared the surface profiles, caused by fretting wear, in the FE model and experimental tests with each other, and validated their model quite accurately. They conducted wear tests for different normal loads of 185 N, 500 N, 1670 N and the amplitude of sliding for all cases was 50 µm. To verify their model, they conducted several experimental tests, for different numbers of fretting cycles (Figure 1.12).

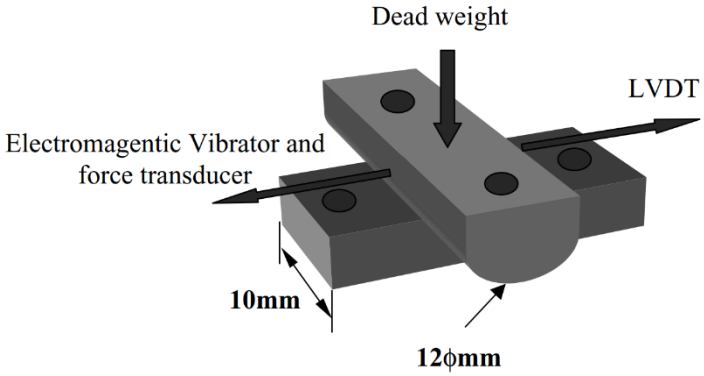

Figure 1.11- Schematic figure of the test design (McColl, Ding et al. 2004)

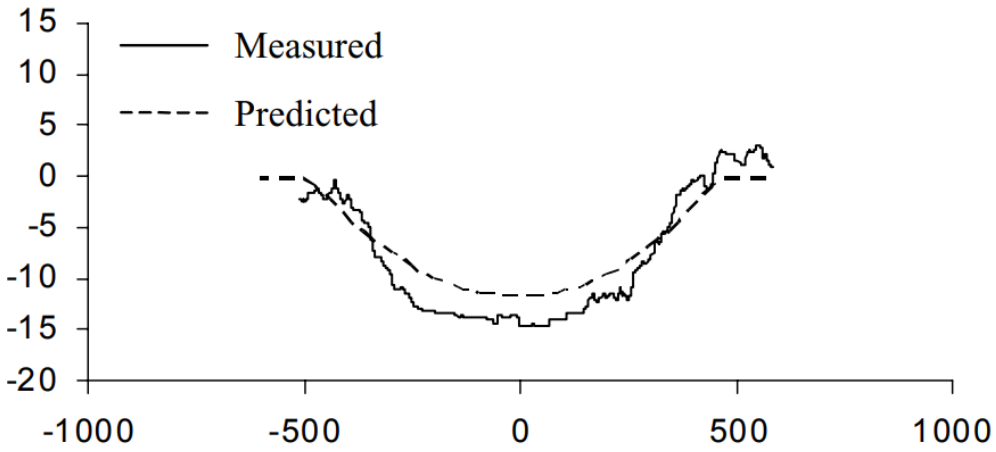

Figure 1.12- Comparison of FE results and experimental results for damaged surface at 1670 N normal load (McColl, Ding et al. 2004)

They also presented the variation of contact pressure during the process of fretting wear, which can also provide the contact length variation (Figure 1.13).

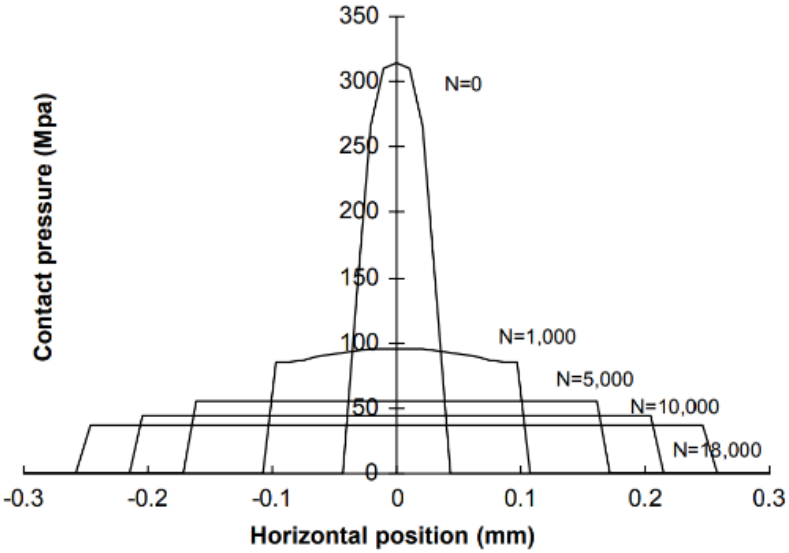

Figure 1.13- Variation of contact pressure with increasing number of fretting wear cycles under 185 N normal load (McColl, Ding et al. 2004)

Their results revealed that in the first 1000 wear cycles, the variation rate of contact stress and contact width is more significant compared to rest of the test. Where, in the first 1000 cycles, the contact width increased by about 100% and the peak contact pressure decreased by 40%.

There are also some other fretting wear models based on the energy approach or elastic-plastic shakedown response of materials (Fouvry, Kapsa et al. 1996, Fouvry 2001). In this model, the volumetric wear is related to the accumulated activation energy caused by traction force and energy wear coefficient, which is a material property.

Recently, very limited studies, on the subject of hip joint implants, have developed adaptive finite element models (adaptive finite element methods control mesh design during the process of solution to provide more accurate results) to simulate the fretting wear process in the head-neck junction.

1.5 Assembling process in the head-neck junction

The potential of the occurrence of fretting depends on the strength of the head-neck junction (junction's resistance to relative motion) achieved during the assembly process, as well as the

complex loads applied during daily activities (Mroczkowski, Hertzler et al. 2006). The ability of the taper junction to resist torsional loads is more important/just as important as the ability to resist axially applied forces (Jauch, Coles et al. 2014, Farhoudi, Oskouei et al. 2015). Hence, the strength of the head-neck junction and the different parameters, which can contribute in the junction strength, have been investigated in some previous studies. Pennock et al. (Pennock, Schmidt et al. 2002) have investigated the effect of varying impaction force, repeated impactions, and fluid contamination on the disassembly strength of Morse-type tapers. They used different impactions (applied using a 1.4 kg drop hammer) to assemble the head-neck junction and a uniaxial pull-off load was applied to disassemble the junction. They concluded that there was a linear relationship between the taper junction assembly force and the disassembly load (Figure 1.14). This study revealed that different parameters, such as surface roughness, taper mismatch, and taper angle, play an important role in the head-neck junction's strength. However, there are several variables that can be controlled by a surgeon, such as the number of impactions and whether the junction is wet or dry (Figure 1.15), which can influence the junction's strength.

Lieberman et al. (Lieberman, Rimnac et al. 1994) analysed the head-neck taper interface in forty-eight implants with three different designs of retrieved hip prostheses. In cases where the femoral head was still assembled to the stem, they performed pull-off testing to measure the disassembling force. They concluded that the improvement of the head-neck mating surfaces' tolerance can increase the taper junction's strength. This strength, by decreasing the micro-motion and fluid at the taper interface, can result in preventing corrosion.

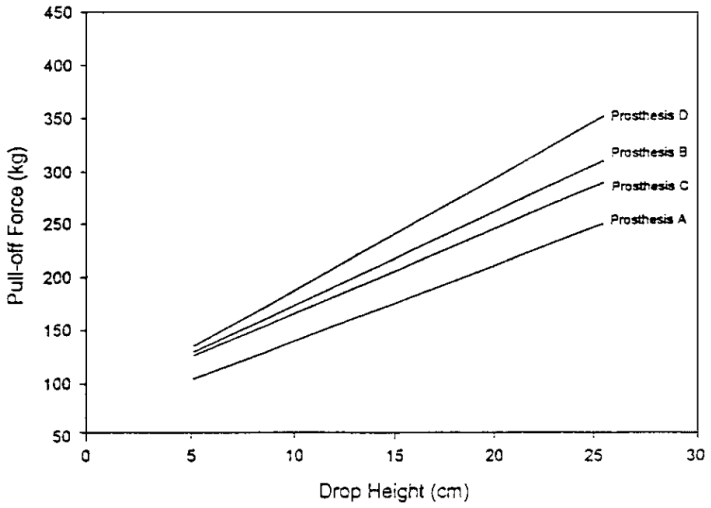

Figure 1.14- Pull-off force versus drop height for four cases (Pennock, Schmidt et al. 2002)

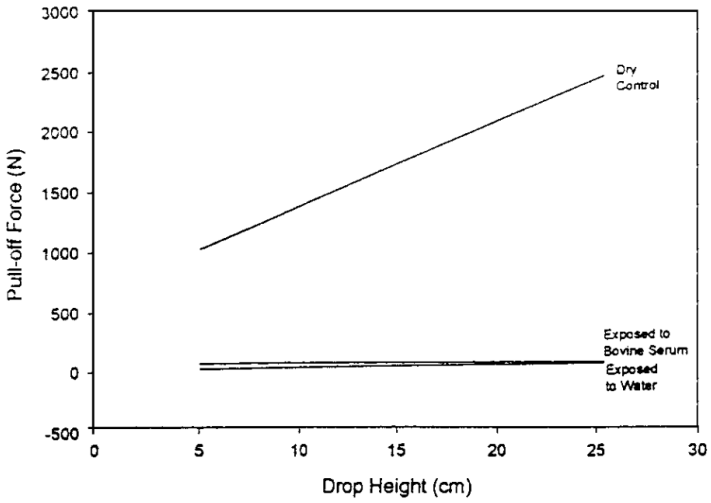

Figure 1.15- Data show the effect of wet versus dry assembly conditions on the strength of taper (Pennock, Schmidt et al. 2002)

Jauch et al. [31] investigated the influence of material coupling and assembly condition on the magnitude of micro-motion, at the interface of a modular hip junction for the two combinations of CoCr head-Ti neck and CoCr head-CoCr neck. They found that using a titanium neck and contaminated interference increases the micro-motion between the head and neck, which can result in increasing the risk of fretting and corrosion. Figure 1.16 shows that the magnitude of micro-motion in the case with the Ti neck is 50% more than that in the case with the CoCr

neck, in clean conditions. Moreover, the micro-motion of the junction with the Ti neck in the contaminated condition is 116% more than when it is assembled in the clean condition.

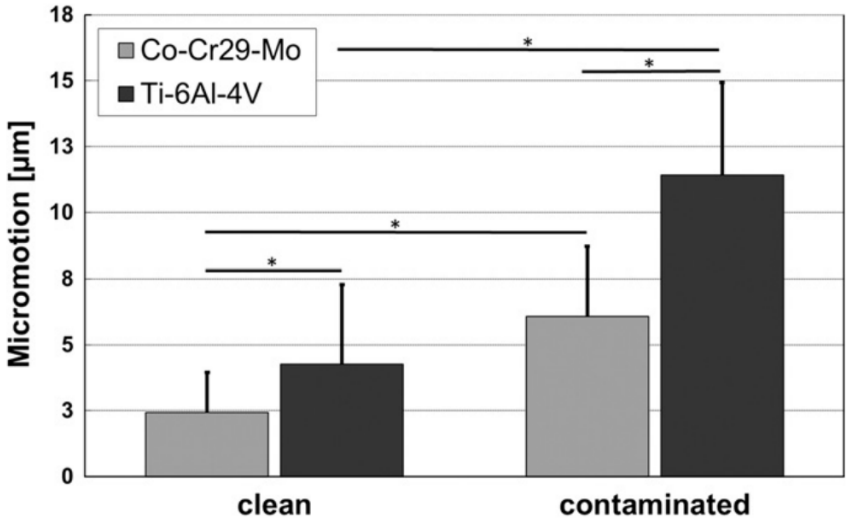

Figure 1.16- Relative micro-motion in the head-neck junction for cases with different material coupling and assembly conditions (Jauch, Huber et al. 2011)

Rehmer et al. (Rehmer, Bishop et al. 2012) experimentally investigated the influence of assembly process and material combination on the torsional and axial strength of the head-neck junction for three combinations of CoCr head-Ti neck, CoCr head-CoCr neck and Ceramic head-Ti neck. The mismatched angles reported for each combination in their study was 0.024° for CoCr-CoCr, 0.015° for Ti-CoCr, and 0.043 for Ti-Ceramic. Each case was subjected to different assembling processes. A different number of impactions applied by rubber and metallic hammers were used to assemble the junctions. For each case, a uniaxial pull-off force and twist-off moment were applied to disassemble the junctions. Figure 1.17 shows the pull-off force versus assembly force for CoCr-CoCr junction. Figure 1.18 demonstrates the turn-off moment versus assembly force for different specimen.

Moreover, a quasi-static push-on force was also applied to assemble each junction sample. In line with the results, they suggested that a sufficient head-taper junction can be achieved by minimal impaction forces of 4 kN. Additionally, because the CoCr head-CoCr neck combination has a lower strength against torsional moments, more attention should be paid to the assembly of CoCr heads on CoCr tapers.

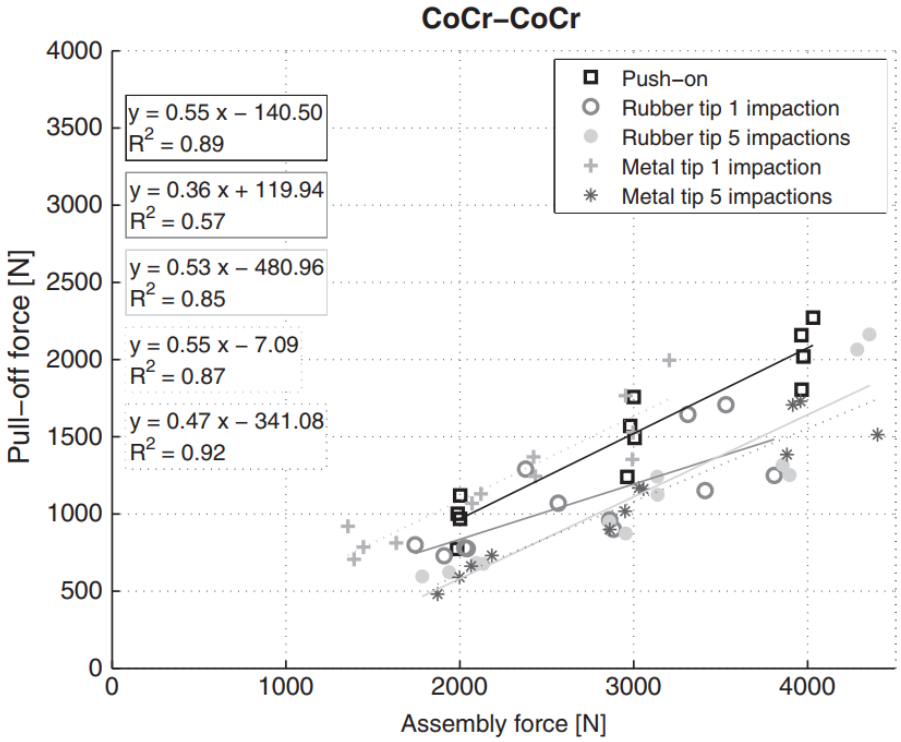

Figure 1.17- Pull-off force versus assembly force for CoCr-CoCr junction (Rehmer, Bishop et al. 2012)

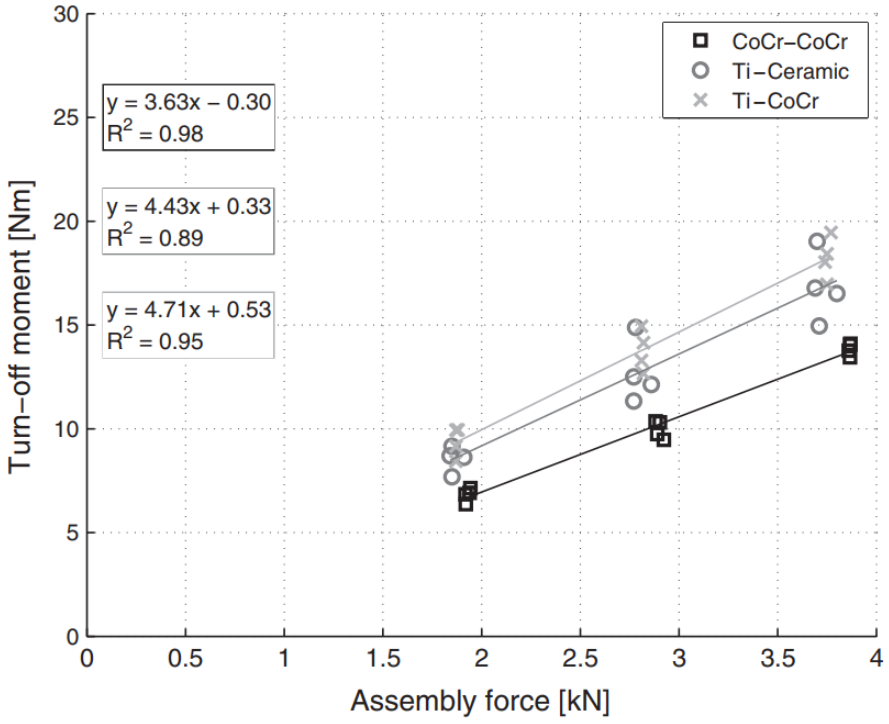

Figure 1.18- Turn-off moment versus assembly force for different material combinations (Rehmer, Bishop et al. 2012)

However, they didn't discuss the importance and role of the different parameters that contribute to the strength of the head-neck junction. Moreover, the reason behind different torsional strengths in junctions with a Ti neck and a CoCr neck wasn't disclosed. It seems that there still is a lack of investigation about the effects of different parameters on axial and torsional strengths of the head-neck junctions in hip joint implants.

Despite there being several studies, which have been developed to investigate different aspects of the assembling process and different parameters that can influence it, there is still a need to determine the influence of assembling process on the head-neck junction's mechanical environment. The assembling process can directly affect the junction's mechanical properties, such as contact stress, relative micro-motion and contact length, which can accordingly influence the fretting wear process in the head-neck junction.

1.6 Finite element modelling of head-neck junctions

Generally, finite element models, which have been proposed for the head-neck junction of hip replacement, can be divided into two categories. The first kind of model aims to investigate the mechanical behaviour of the junction subjected to just one cycle of loading. These models try to investigate the influence of parameters such as assembly and gait loads, mismatched angles, material combination and geometry parameters on the junction's mechanical responses. These types of simulations usually do not consider the influence of the cyclic nature of fretting wear. Recently, the finite element method has been used to predict the amount of material loss in the taper junction as a result of fretting wear over a few million cycles of loading. These types of FE models try to consider the influence of the cyclic nature of fretting wear on the surface damage of the head-neck junction interface, using adaptive finite element models. This section reviews the latest FE models developed for both mechanical behaviour and fretting wear at the head-neck junction.

1.6.1 Mechanics of head-neck junction

To better understand the potential fretting environment of the head-neck junction, there is a need to determine stress, strain and displacement distributions, particularly shear stresses and relative interface micro-motions. Due to the complex geometry, frictional contact, and complicated nature of mechanical loadings (assembly load, and loads of physical activities), finite element (FE) modelling is a convenient and effective method to interrogate the mechanical environment. In the area of modular taper junctions of hip implants, several finite element simulations have been developed to evaluate the mechanical responses of the contacting components. Chu et al. (Chu, Elias et al. 2000) developed an FE model to investigate a taper junction subjected to gait load levels. They concentrated on relative micro-motions and stress distribution. However, they neglected the angular mismatch in the junction and assumed that there is a perfect fit at the cone-sleeve interface.

Dyrkacz et al. (Dyrkacz, Brandt et al. 2015) developed an FE model to investigate the parameters that contribute to the magnitude of the relative micro-motion at the head-neck junction interface. The process of their simulation included assembling parts, applying 3300 N of compression load and 100 N of tension load, which were applied with 30° of uniaxial direction (Figure 1.19).

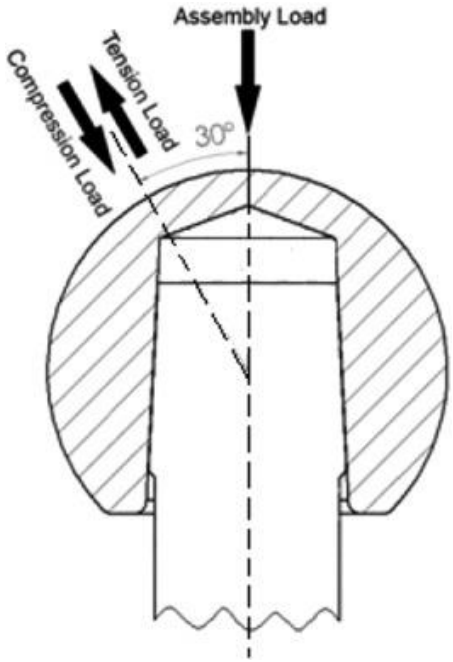

Figure 1.19- Schematic figure of Dyrkacz et al.'s (Dyrkacz, Brandt et al. 2015) model

The micro-motion of the head's centre was measured and presented for different cases of head size, taper size, assembly force angle of loading and distance between centres of head and neck (Figure 1.20).

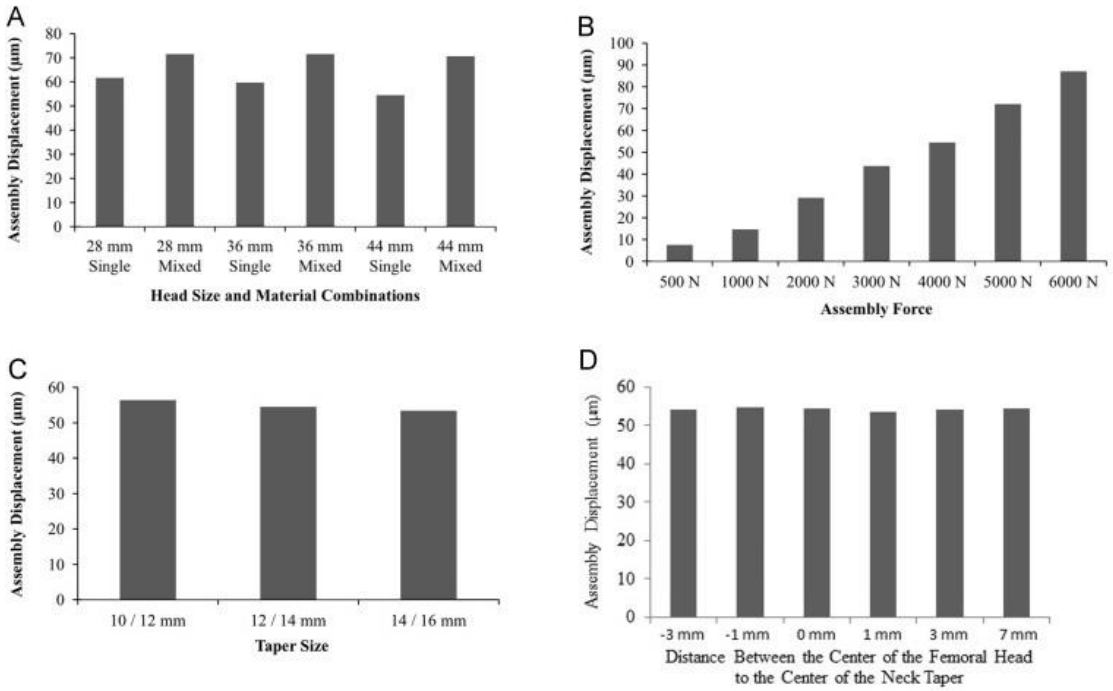

Figure 1.20- Micro-motion of the head for (a) different head size and material combinations (b) different assembly force (c) different taper sizes (d) different distance between centres of head and neck (Dyrkacz, Brandt et al. 2015)

Their results showed that increasing the head size, assembly force and taper size can increase the relative micro-motion. Additionally, they concluded that the relative micro-motion of the mixed alloy material combination is more than that of combinations in which the head and neck are made of one alloy (Dyrkacz, Brandt et al.).

One of the most critical parameters, which effectively contributes in mechanical properties of the head-neck junction, is the mismatch angle of taper junction components. This parameter especially affects the contact behaviour of the junction (Langton, Sidaginamale et al. 2012). Kassim Abdullah (2010) developed a non-linear finite element model to investigate relative motion in a modular head-neck junction. It was concluded that parameters such as assembly load, friction and angular mismatch have significant effects on the micro-motion between the

head and neck under gait loading. It was shown that, by increasing the assembly load from 0 to 5500 N, the maximum magnitude of the maximum micro-motion decreases from 28 µm to 16 µm. Moreover, the magnitude of maximum micro-motion for a case with no angular mismatch was more than 40 µm, while this magnitude is less than 30 µm for cases with positive or negative angular mismatch. Donaldson et al. (Donaldson, Coburn et al. 2014) performed a stochastic finite element simulation on the head-neck junction for which 400 unique models were assessed using realistic variations of design variables, material properties and loading parameters to predict the fretting work (frictional work which is done over gait cycles). The fretting work was correlated with only three parameters: angular mismatch, centre offset and body weight. For verifying the model, they applied an axial impaction load at 45º off-axis to two sets of taper-trunnion pairs and measured the micro-motions. But, the specimens were made of 6061 aluminium at a 3:1 size scale. Since the FE model included different materials (CoCr head and Ti neck), and dimensions with respect to the verification experiments, the fretting prediction results may not be completely reliable.

Bitter et al. (Bitter, Khan et al. 2017) developed a combined experimental and finite element study to analyse the influence of assembly load on the fretting wear mechanism in total hip replacement. They developed their model for assembly forces of 2 kN, 4 kN, and 15 kN. They reported a drop in the fretting wear as the assembly forces increased. In their results, although they reported the pattern of the wear, they did not calculate the material loss volume. They also developed a one cycle FE model for three daily activities. According to the modified version of Archard's equation, they used contact pressure and relative micro-motion to produce a wear score parameter. However, their model was not able to track the fretting wear process, over the several cycles of sliding. They concluded that wear is more affected by relative micro-motion compared to contact pressure (Figure 1.21).

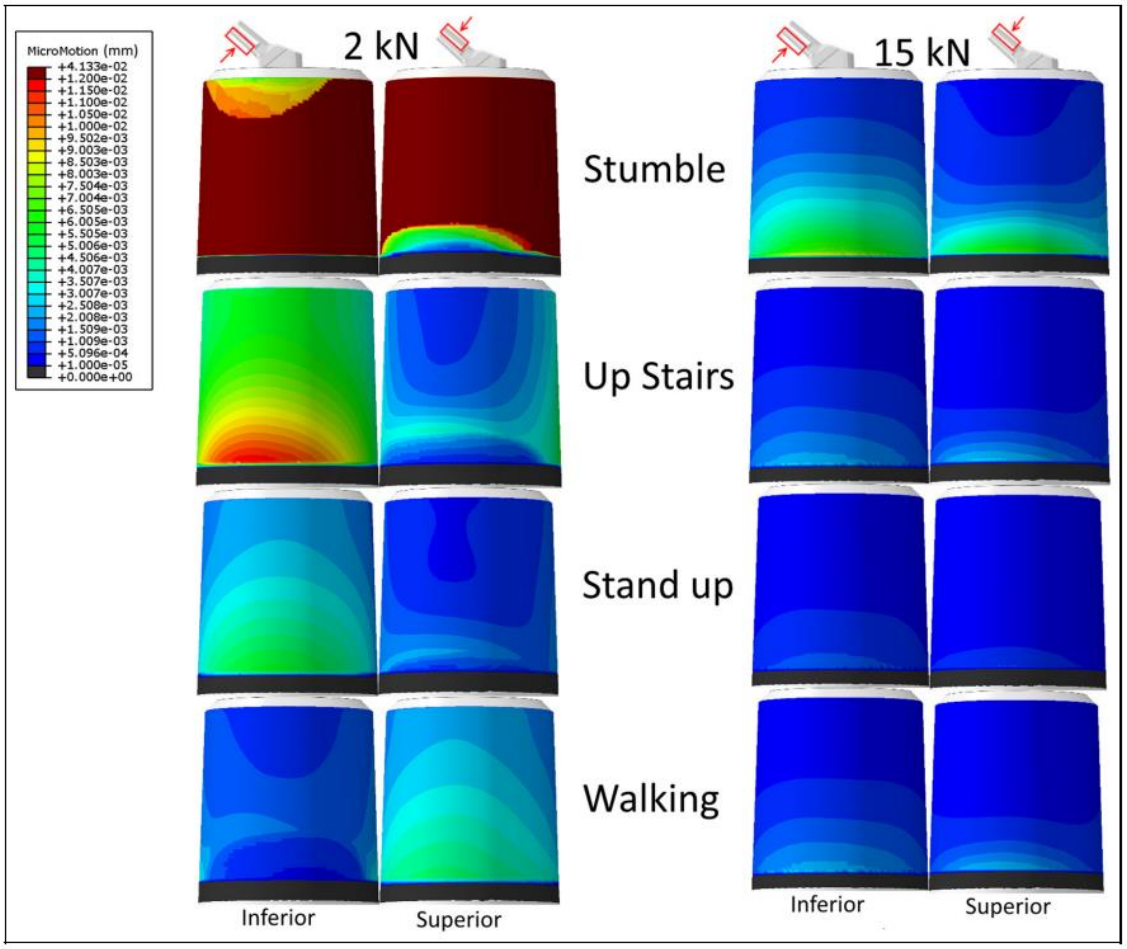

Figure 1.21- Micro-motion FE contour for different activities (Bitter, Khan et al. 2017)

A literature survey confirms that FE simulations of the head-neck junction require further improvements to approach real situations and achieve a realistic mechanical behaviour. These studies were limited to exploring the contact mechanics of the junction subjected to a single gait loading cycle.

1.6.2 Finite element models for fretting wear

As mentioned before, adaptive FE models have been recently used to simulate the fretting wear process of the head-neck junction.

Zhang et al. (Zhang, Harrison et al. 2013) developed a 2D axisymmetric model of the head-neck junction to predict wear in high cyclic gait loading. They applied a uniaxial cyclic load to simulate the gait loading. The material combinations were a CoCr head with a direct metal laser sintering (DMLS) Ti-6Al-4V neck and a CoCr head with a forged Ti-6Al-4V neck. DMLS Ti-6Al-4V was found to be more resistant to fretting wear. They provided the graphs of contact pressure, wear depth and slip versus number of cycles for each case. However, their model was a uniaxial model and therefore, the cyclic load had only a uniaxial component (Figure 1.22).

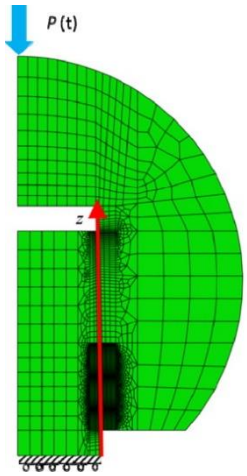

Figure 1.22- The axisymmetric fretting wear model (Zhang, Harrison et al. 2013)

English et al. (English, Ashkanfar et al. 2015) developed an FE model to estimate the amount of material loss and contact pressure at a head-neck junction subjected to several million cycles of a walking gait loading. They used a CoCr head and titanium neck combination with a perfect contact between the head and neck. In their model, an energy based equation of wear was used to quantify the material loss volume. In this equation, wear is dependent on dissipated energy, over the process of fretting wear and the energy wear coefficient which is a material property. In this study, the head-neck junction was first assembled with a 4 kN impaction force and then was subjected to several million cycles of walking gait loading. To verify this model, they used an observation method to compare the results of their simulation with the retrieved prostheses (Figure 1.23). They also presented the graph of the wear depth versus number of cycles.

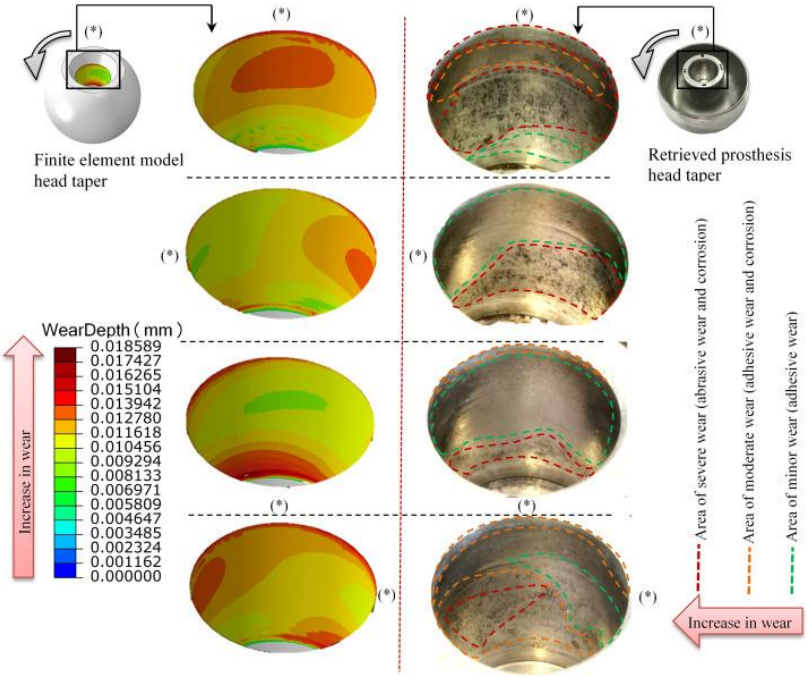

Figure 1.23- Observation method used by English et al. (English, Ashkanfar et al. 2015) to verify their simulation method

In another work, (English, Ashkanfar et al. 2016) investigated the effect of assembly force on the wear behaviour. To this end they used the FE model developed in their previous work to investigate the effect of the assembly force on material loss. They developed a simulation for each case of assembly and, for every case, the diagram of volumetric wear rate versus number of cycles was reported (Figure 1.24). It was reported that with increasing the impaction force to at least 4 kN, a significant reduction in the amount of wear debris can be achieved. They suggested that increasing the impaction force up to 4 kN provides the best condition of assembly regarding reducing the material loss caused by fretting wear.

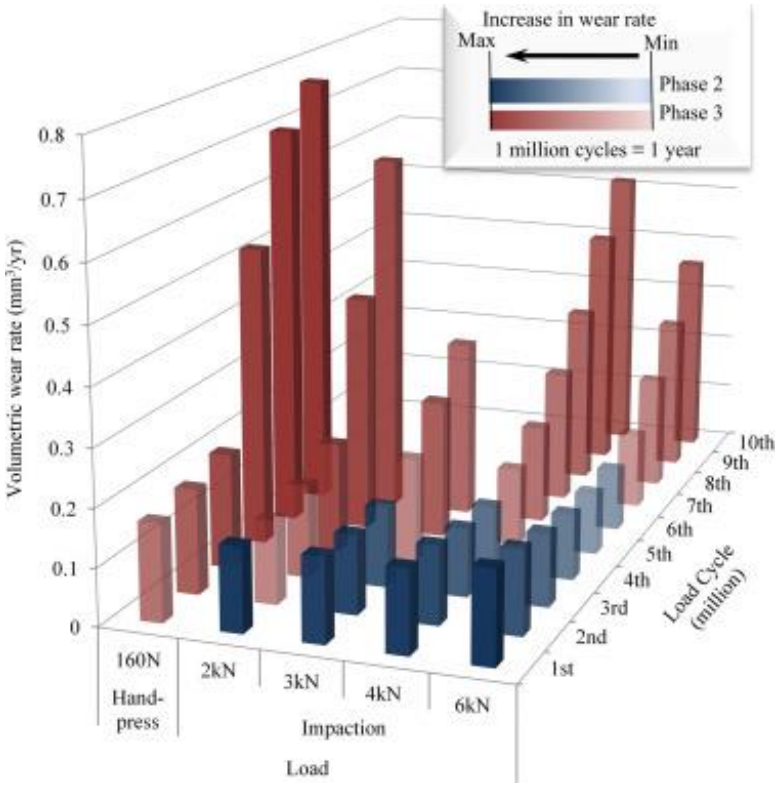

Figure 1.24- Volumetric wear rate with respect to assembly load (English, Ashkanfar et al. 2016)

Ashkanfar et al. (Ashkanfar, Langton et al. 2017) also investigated the influence of the micro-grooved trunnion stem surface finish on the fretting wear process in head-neck junction. To this end, they developed an FE simulation for two femoral stem models, one with machined micro-grooves and the other with a smooth trunnion surface finish, both coupled with a 36mm diameter CoCr femoral head with a smooth tapered surface finish. For both models they presented the graph of volumetric wear rate versus number of cycles (Figure 1.25). They concluded that the smooth interface provides better performance, regarding the reduction of material loss.

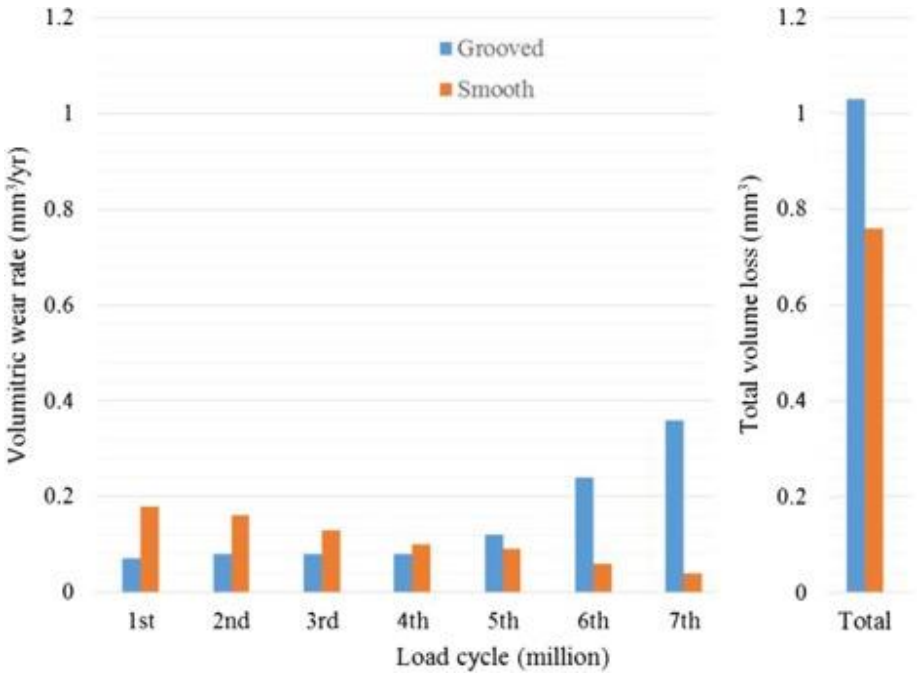

Figure 1.25- The graph of volumetric wear rate versus number of cycles (Ashkanfar, Langton et al. 2017)

1.7 Research gap

As mentioned before, due to exposing implants for long durations to cyclic loading of daily activities, material loss related factors, complexity of the junction geometry and mechanical loads, it is very hard and expensive to study the fretting wear mechanism through *in vitro* tests. Hence, finite element (FE) simulations appear to be more convenient and practical methods for studying fretting wear and material loss in hip implants' modular junctions.

Regardless of there being different FE studies, which have been developed to investigate the head-neck junction's mechanics, there is still a need to determine the junction's mechanical parameters, such as relative micro-motion, contact pressure, shear stress, fretting work and contact length. This can be further used to develop more realistic *in vitro* tests and FE simulations of fretting wear.

To date, the adaptive models were able to estimate the volume of the material loss caused by mechanical fretting wear. However, the material combinations used in the previous models

included CoCr for the head and titanium for the neck. More importantly, all the simulations that have been developed to date are based on the material properties (such as wear coefficient and friction coefficient) obtained in a dry condition, while implants work inside the corrosive environment of the human body. Also, mismatched angles at the junction has often been neglected in previous finite element studies, despite its important effect on the interface's mechanics, and thus, potentially on the fretting wear.

It is widely accepted that the damage of the head-neck junction of THR is a combination of mechanical fretting wear and electrochemical corrosion, known as mechanically assisted corrosion (fretting corrosion). A literature review confirms that, to date, no finite element model has been developed to simulate the fretting corrosion phenomenon in contacting surfaces of metallic materials, under fretting wear loading and in a corrosive environment where passivation and repassivation repeatedly occur. Therefore, the development of a new model, with both fretting wear and electrochemical corrosion phenomena, for metallic interfaces even for a simple geometry (e.g. pin-on-disc) is currently importantly needed to establish a model for the interrelated processes of fretting and corrosion, which can be used for real geometry and applications, like taper junctions.

1.8 Research objectives

- Developing a reliable three-dimensional finite element model that is able to simulate the mechanical behaviour of the head-neck junction.
- Mechanical response of the head-neck junction subjected to the loading of daily activities.
- Defining the most critical section of the junction and its corresponding loads, which can be used to develop a two-dimensional fretting wear model.
- Developing a two-dimensional adaptive finite element model to simulate the fretting wear process of the head-neck junction in a simulated physiological body fluid.
- Using the adaptive new FE model to investigate the influence of mismatched angles and assembly force on material loss.
- Developing a new FE fretting corrosion model which is able to simulate mechanically assisted corrosion of metallic interfaces.

Chapter 2 Three dimensional finite element model of the head-neck junction

This chapter is based on the following publication:

Fallahnezhad, K.; Farhoudi, H.; Oskouei, R.H.; Taylor, M. Influence of geometry and materials on the axial and torsional strength of the head–neck taper junction in modular hip replacements: A finite element study. *Journal of the Mechanical Behavior of Biomedical Materials* **2016**, *60*, 118-126.

2.1 Overview

In this chapter, a three dimensional explicit FE model of an isolated femoral head–neck junction was developed to simulate the real geometry of the head and neck components with a non-linear frictional contact and elastic-plastic properties of the mating materials. The FE model was verified by experimental assembling and disassembling tests conducted by Rehmer et al (Rehmer, Bishop et al. 2012). Two further combinations of CoCr head-Ti neck and CoCr head-CoCr neck were investigated in this study with the same geometries of the models that were used in Rehmer's tests (Rehmer, Bishop et al. 2012), but with different mismatch angles. In this chapter, the model was then used to investigate the mechanics of the head-neck junction in order to understand which parameters contribute to the axial and torsional strength of the interface.

2.2 Materials and methods

A three dimensional (3D) finite element model of an isolated head–neck junction was generated using ABAQUS 6.13 (Figure 2.1). In order to verify the model, a set of experimental test results on assembling and disassembling of the head and neck components was replicated (Rehmer, Bishop et al. 2012). A 12/14 taper was modelled and two material combinations were simulated: CoCr head/Ti neck, and CoCr head/CoCr neck. Table 2. 1 presents the angles and mismatch angles for the material combinations.

The experimental assembly process was replicated, where three different assembly loads were used to assemble the head-neck junction. These loads were applied at a rate of 500 N/s. The disassembly processes were also replicated to assess the pull-off force and the twist-off moment. For the pull-off test, the neck was displaced at a rate of 0.008 mm/s and the resulting reaction force was determined. For the twist-off test, the neck was rotated (with zero axial load) at a rotation rate of 0.1 °/s and the resultant moments were determined. The peak pull-off force and peak twist-off moment were then recorded to compare with the experimental tests. In the model, the external surface of the head was constrained in all directions and the bottom face of the neck was subjected to the loads and torques.

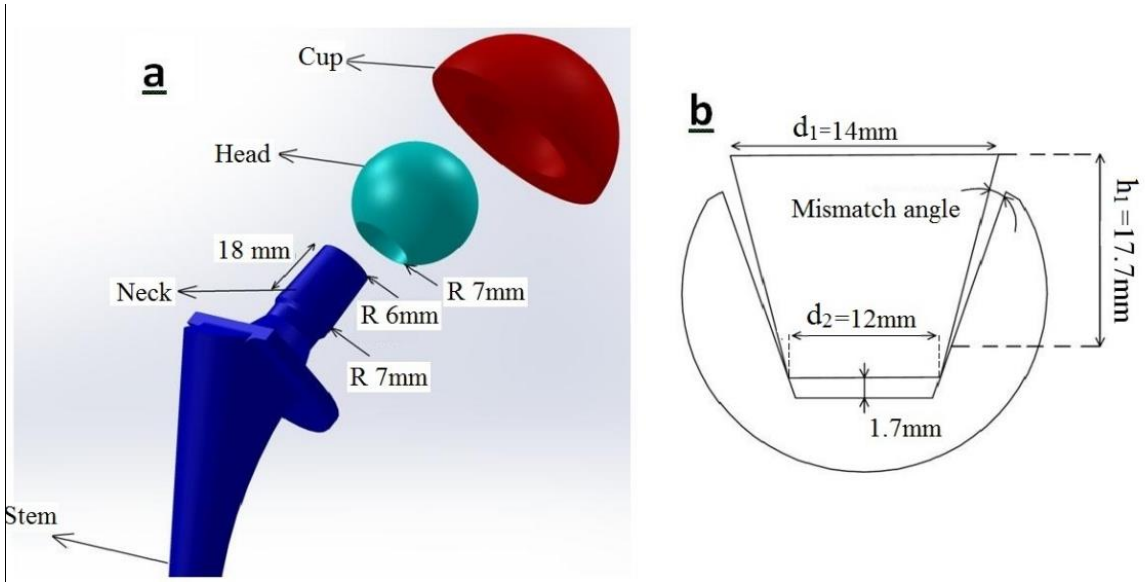

Figure 2.1– (a) Modular hip joint implant components; and (b) Geometry and dimensions of the head-neck junction used in the FE model.

Table 2.1. Angles of the head and neck components and their mismatch angles (Rehmer, Bishop et al. 2012).

Components	Angle [º]
CoCr neck	2.834
Titanium neck	2.843
CoCr head	2.858

Combinations (head/neck)	Mismatch Angle [º]
CoCr/CoCr	0.024
CoCr/Ti	0.015

An explicit (dynamic) FE analysis was utilised in the simulation using ABAQUS/Explicit. The explicit analysis was preferred because implicit methods require an extra computation for every time step; thus, they need larger time steps to implement. A “fixed mass-scaling” method was used to decrease the solution time. Mass-scaling must be used carefully to ensure that the inertia forces do not dominate and change the solution. To avoid this, kinetic energy was monitored

during the solution to ensure that the ratio of the kinetic energy to internal energy was always less than 10% (Documentation).

Contact was implemented between the femoral head and neck using a finite sliding formulation; and a surface-to-surface discretization method was used to apply this formulation. To represent the contact pressure, a Lagrange multiplier formulation was implemented. It is noted that the friction coefficient may not be constant and can vary in the junction under cyclic loading during its operation (Zhang, Harrison et al. 2013, Zhang, Harrison et al. 2014). However, as a simplification, friction coefficients were considered to be constant during the loading process. This was found to be an appropriate assumption for this study because of a good agreement achieved between the simulation and experimental results. A friction coefficient of 0.3 was applied between the Ti neck and CoCr head; and, CoCr neck CoCr head using a penalty method (Swaminathan and Gilbert 2012, Donaldson, Coburn et al. 2014).

Models were meshed with quadratic tetrahedral elements (C3D10M in ABAQUS) (Figure 2.2). The size of the elements was refined several times in order to obtain a converged solution. Accordingly, the size of the elements in contact surfaces was defined to be 0.15 mm. An elastic-plastic material model was used for CoCr properties (ISO 5238-12) with a Young's modulus of 210 GPa , Poisson's ratio of 0.3, yield stress of 910 GPa, tensile ultimate stress of 1350 GPa and tensile elongation of 15% (Davis 2000).

For the titanium alloy, an elastic-plastic material model (ISO 5832-3) was used to cover plasticity of the material in the model. A Young's modulus of 103 GPa, Poisson's ratio of 0.3, yield stress of 900 GPa, tensile ultimate strength of 959 MPa and tensile elongation of 15.1% were used for the titanium model. Considering the mentioned mechanical parameters, the stress-strain behaviour of these alloys was considered to be elastic-linear plastic. The following parameters were assessed: pull-off force; twist-off moment; contact length (CL) which represents the level of interaction between the head and neck components after assembly and contact pressure.

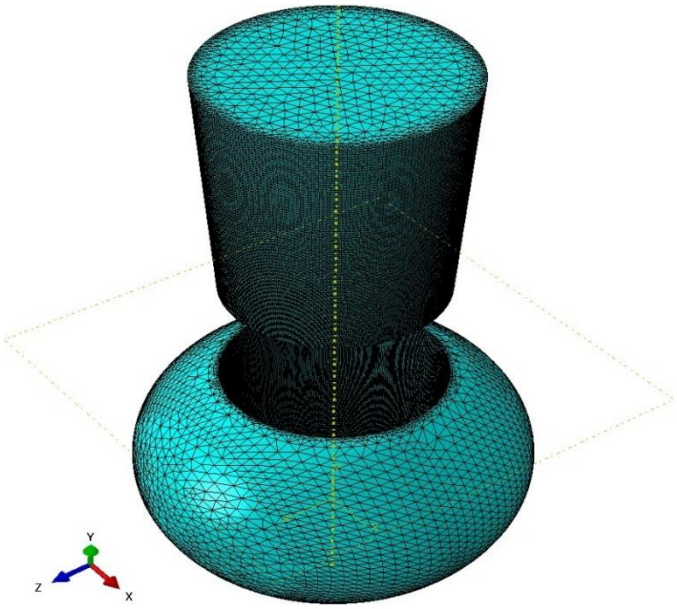

Figure 2.2– Meshing structure in the head and neck models.

2.3 Results

2.3.1 Verification of finite element simulations

The numerical results were compared with the experimental results of the same head-neck combinations under the same assembly loads reported by Rehmer et al. (Rehmer, Bishop et al. 2012) (Figure 2.3). An increasing linear trend was seen for both the pull-off and twist-off loads versus the assembly loads. In general, the higher assembly load, the greater pull-off and twist-off in both the CoCr and Ti head-neck combinations. The pull-off force was found to be similar in both CoCr/Ti and CoCr/CoCr under the same assembly loads (Figures 2.3a and 2.3c); whereas, twist-off moments in CoCr/Ti was longer than that of in CoCr/CoCr by approximately 36%.

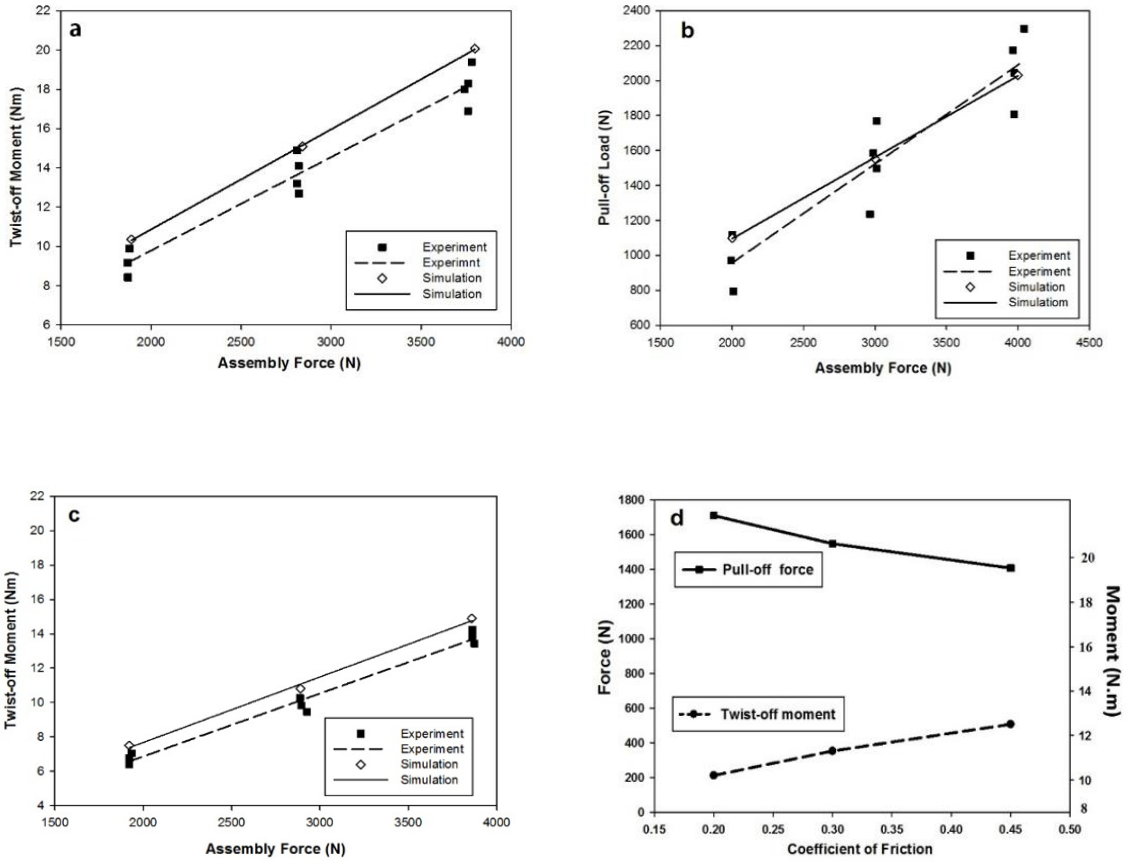

Figure 2.3– Comparison of simulation and experimental results: (a) Pull-off load in CoCr head/Ti neck junction, (b) Twist-off moment in CoCr head/Ti neck junction, (c) Pull-off load in CoCr head/CoCr neck junction, (d) Twist-off moment in CoCr head/CoCr neck junction (experimental data points were from (Rehmer, Bishop et al. 2012)).

The simulation results were found in good agreement with the experimental results for both pull-off and twist-off loads in different material combinations. The Mean Absolute Error (MAE) was determined for different cases to be between 4% and 10%. The best agreement was found for the pull-off loads in the CoCr/CoCr junction (Figure 2.3c). Also, both twist-off graphs suggest that the FE simulations tend to over-predict the twist-off moment. Given a considerable range in the experimental pull-off forces and twist-off moments under the same assembly loads, the FE predictions with their calculated MAEs were found to be in close agreement. Furthermore, to more clarification of coefficient of friction effect on simulation results, the pull-off force and twist-off moment were simulated for one case with assembling load of 3000 N, CoCr/CoCr material combinations and three friction coefficient of 0.2, 0.3 and 0.45 which is demonstrated in Figure 2.4 of appendix. With changing the coefficient of friction from 0.30 to 0.20, the pull-off force increased by 10.4% and the twist-off moment decreased

by 10.6%. With changing friction coefficient from 0.30 to 0.45, the pull-off force reduced by 9.1% and the twist-off moment increased by 10.6%.

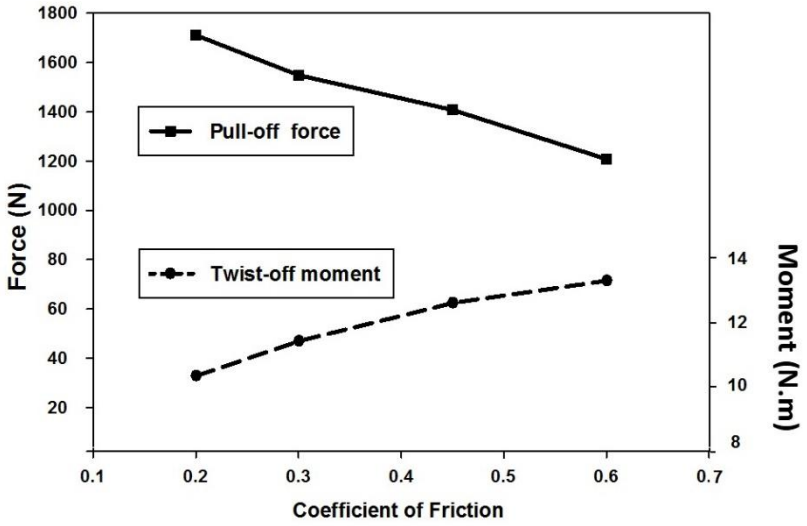

Figure 2.4– Pull-off force and twist-off moment determined for CoCr head/CoCr neck junction assembled with 3000 N with three friction coefficients of 0.20, 0.30 and 0.45.

2.3.2 Stress analysis under assembly load

No plastic deformation was found in the assembling process in all the head-neck combinations and all the deformations were in the elastic region of both the materials even under the highest assembly force. Figure 2.5a shows the contacting area between the CoCr head and titanium neck after an assembly force of 2840 N. As the Pressure stress contours show, the contact area contains localised stresses with a maximum magnitude of 407 MPa in this case. Over the contact area of the neck, the contact length was found to be in the range of 0.75 to 1.58 mm in different head-neck combinations as a result of varying assembly forces (Figure 2.5b). It was observed that the contact length increased as a function of assembly force. Moreover, the contact length was greater for the CoCr head/Ti neck combination, and the difference between CoCr/Ti and CoCr/CoCr increased with increasing assembly forces. This means that the titanium neck had the longest contacting region when matched with the CoCr head under the highest assembly load.

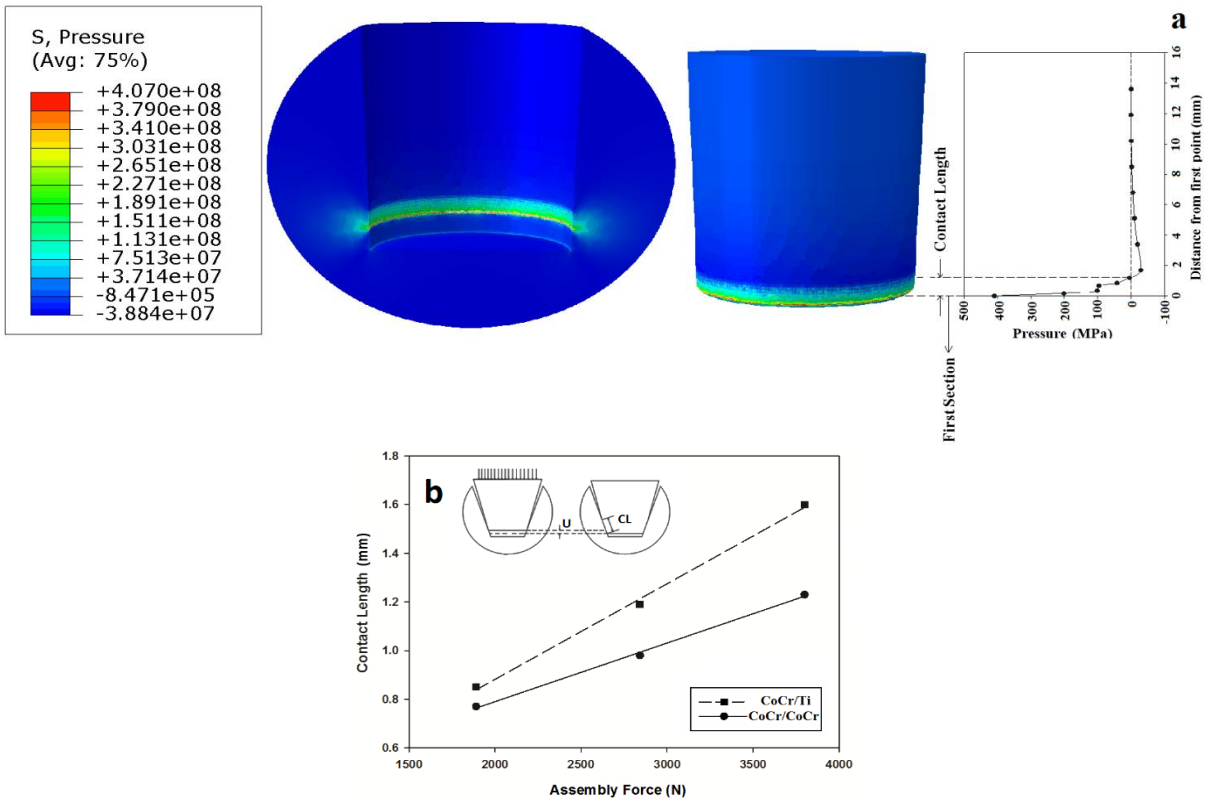

Figure 2.5– (a) Pressure contours in the CoCr head/Ti neck junction under 2840 N assembly force (stresses in Pa) along with pressure profile in the contacting area which determines contact length (CL) in the junction, (b) contact length (CL) in different head-neck combinations under different assembly forces.

The assembling process of the head and neck was understood to be considered as a press-fit process for which the dominant stress component in the contacting region was the pressure stress. This stress component was found to indicate that how firmly the head and neck are connected together. Figure 2.6 shows that how this pressure stress changes over the neck length as a result of its contact with the head. It is obvious that the pressure stress has its maximum magnitude at the first section (where the interaction between the head and neck initiates) because of a high stress concentration. The maximum pressure stress in all the head-neck combinations ranged from 375 MPa to 715 MPa. This maximum magnitude increased with increasing the assembly load. Generally, CoCr/CoCr combinations, which had a bigger mismatch angle compared to CoCr/Ti, had greater maximum pressure stresses under the same assembly load. This stress decreased significantly in magnitude over the contact length while it was still positive. After passing the contacting area, the pressure stress became negative for a few millimetres which then approached zero at points further away from the contacting

section. The presence of the negative pressure stress was understood to be because of the Poisson's effect and the bending load caused by the conical geometry of the neck and loading system. With increasing distance from the first section, this bending load decreased and the pressure stress tended to become zero. The point at which the pressure stress became zero for the first time represented the boundary between the contacting area and non-contacting area within the head-neck junction.

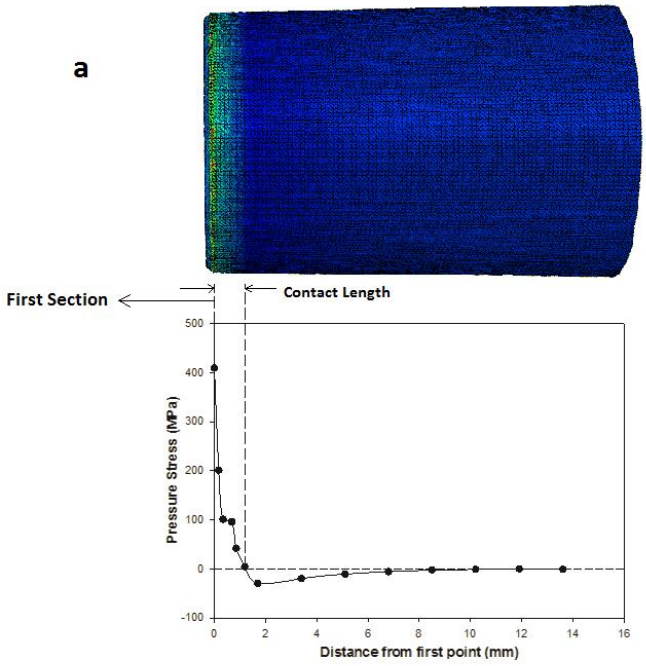

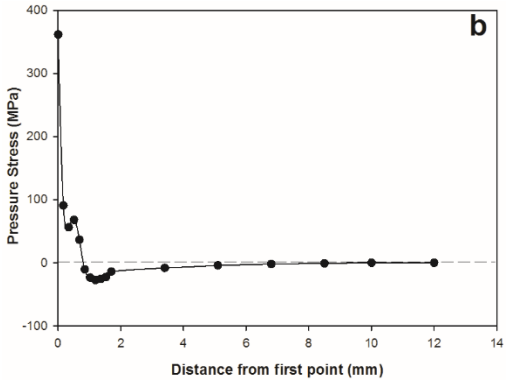

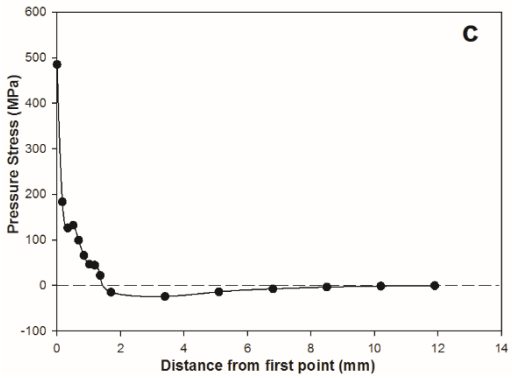

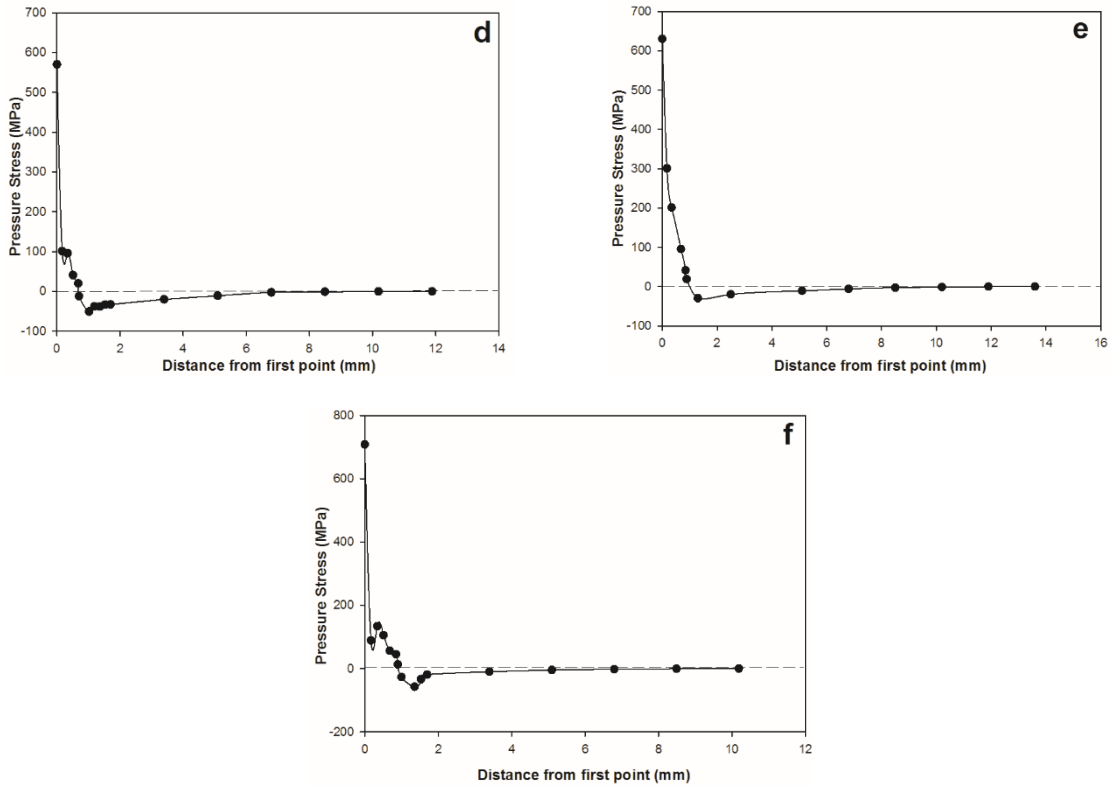

Figure 2.6– Pressure stress versus distance from the first section of the neck: (a) Ti neck/CoCr head under 2840 N push-on load, (b) Ti neck/CoCr head under 1890 N push-on load, (c) Ti neck/CoCr head under 3800 N push-on load, (d) CoCr neck/CoCr head under 1890 N push-on load (e) CoCr neck/CoCr head under 2840 N push-on load, (f) CoCr neck/CoCr head under 3800 N push-on load.

2.4 Discussion

The axial and torsional strengths of the head-neck junction are important in controlling fretting and corrosion. For the geometries and material combinations explored in this study and experimentally (Rehmer, Bishop et al. 2012), there was little difference in the axial pull-off strength, but the torsional strength was higher for the CoCr-Ti combination. Generally, the contact pressure stress and contact length were found as two important parameters that are responsible for this behaviour.

The contact length at the CoCr/Ti junction was longer in comparison with the CoCr/CoCr junction under the same assembly loads (Figure 2.5 b). This was understood to be because of the difference in the mismatch angle of the junctions and the modulus of elasticity of titanium and CoCr. As the mismatch angle of the CoCr/CoCr junction was larger, the contact length was

expected to be shorter than CoCr/Ti. Additionally, modulus of elasticity of Co–28Cr–6Mo alloy (240 GPa) is much greater than that of Ti–6Al–4V (112 GPa). This elastic characteristic causes the titanium neck to have more flexibility and create more interaction with the head compared to the CoCr neck during the assembling process. In addition, the pressure stress in the CoCr neck was greater than the Ti neck, particularly at the initial section of contact. This could be because of the difference in the mismatch angles. As the mismatch angle in CoCr/CoCr is bigger, the stress concentration particularly at the first contacting points is higher than CoCr/Ti.

The pull-off force was similar for the two material combinations (Figure 2.3), but the twist-off moment was significantly different. When a twist-off moment was applied to disassemble the junction, it decreased the friction force between the head and neck. Simultaneously, the vertical component of the pressure stress between the head and neck could overcome the friction force and pushed the head off of the neck (Figure 2.7). Under the twist-off moment, because of the conical geometry and complex three dimensional state of stress in the contact area, there was a lateral deformation of the femoral neck. Figure 2.8 shows the radial deformation contours with a scale factor of 200 in the Ti neck after an assembly load of 3700 N and when twist-off reached its maximum value of 19.8 Nm. Because of this lateral deformation, the pressure stress between the head and neck increased. Figure 2.8 shows the product of the average pressure in contact area (P_{ave}) and the contact length ($L_{contact}$) in two stages: after assembly load and when twist-of moment is maximum. It can be understood from Figure 2.9 that the $P_{ave}.L_{contact}$ parameter increases when the twist-off moment reaches its maximum value. But, the percentage of this growth is more significant in the CoCr/Ti combination compared to CoCr/CoCr.

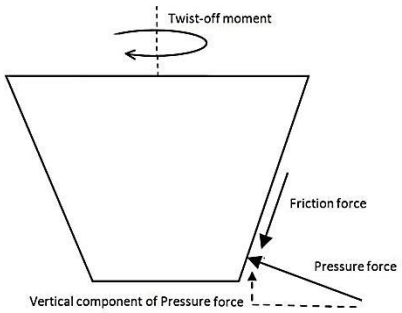

Figure 2.7– Free body diagram of the neck under pull-off and twist-off loads.

As the $P_{ave}.L_{contact}$ parameter has a direct relation with friction force, when $P_{ave}.L_{contact}$ increases, a larger twist-off moment is required to overcome the friction force between the head and neck. Thus, the maximum twist-off moment was higher in the CoCr/Ti junction. A comparing between "$P_{ave}.L_{contact}$ in maximum point" (Figure 2.9) and "maximum twist-off moment" (Figure 2.3) for two combinations, reveals that they have similar trends. For instance, under an assembly load of 2840 N, the $P_{ave}.L_{contact}$ in CoCr/Ti was 38% bigger than that of in CoCr/ CoCr and maximum magnitude of twist-off moment in CoCr/Ti was 42% higher compared with the CoCr/ CoCr junction. On the other hand, when the junction is disassembled by an uniaxial load, there is no such a lateral deformation, and hence the amount of $P_{ave}.L_{contact}$ is steady. As can be seen in Figure 2.9, at the first point of the time axis (end of the assembling process) there is no significant difference in the $P_{ave}.L_{contact}$ parameter between the two combinations under different assembly forces. Accordingly, there is no significant difference in the uniaxial strength between the two combinations.

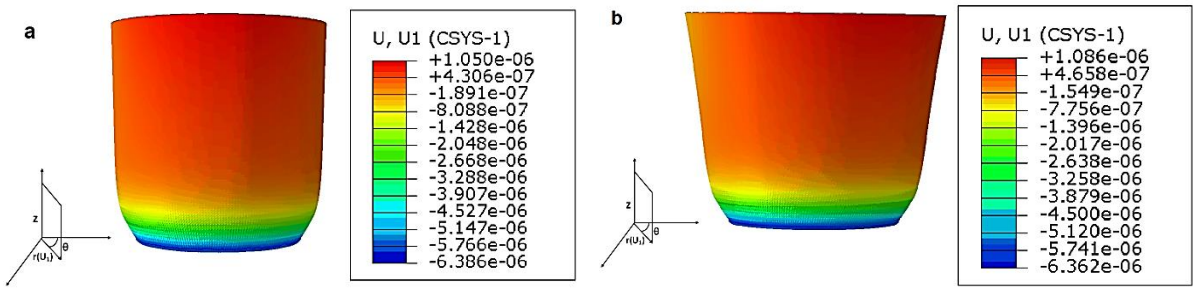

Figure 2.8– Radial deformation contours in the Ti neck with a scale factor of 200: (a) after assembly load of 3700 N, (b) when twist-off moment reaches its maximum value (19.8 Nm) (radial displacements are in m).

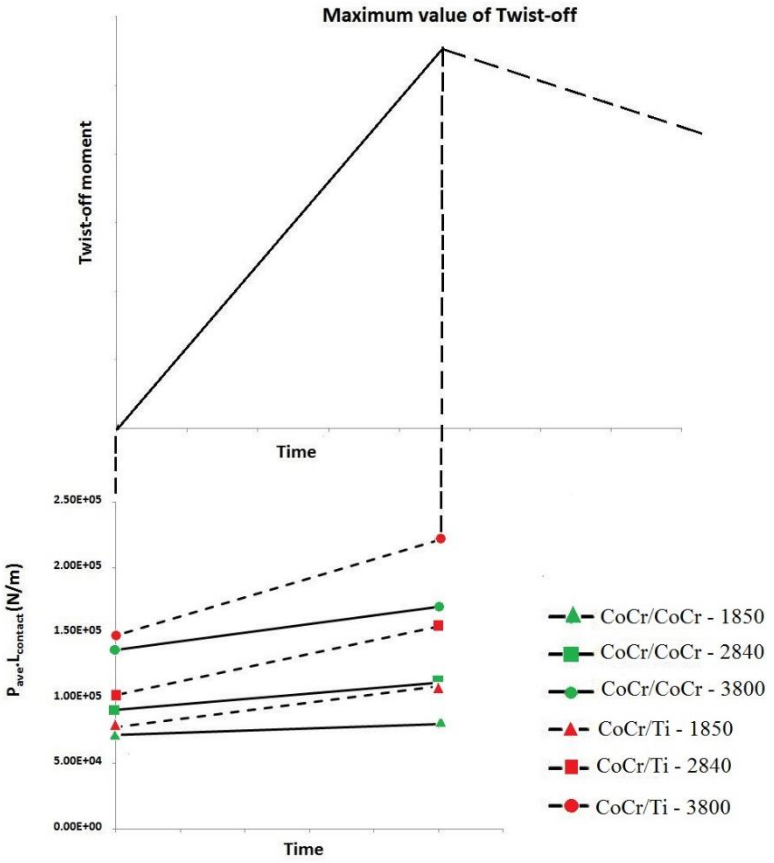

Figure 2.9– Variation of the $P_{ave}.L_{contact}$ after assembly and maximum value of the twist-off for the two material combinations subjected to varying assembly forces.

To understand the main reason for this behaviour, further simulations were performed through which two mismatch angles were applied to both material combinations (Figure 2.10). It can be seen from Figure 2.10 that the mismatch angle plays the most significant role in determining the twist-off moments and not the material combination. Decreasing the mismatch angle from 0.024° to 0.015° in CoCr/CoCr increased the torsional strength very significantly (109% under 3800 N) which was even higher than the torsional strength achieved by CoCr/Ti with the same mismatch angle.

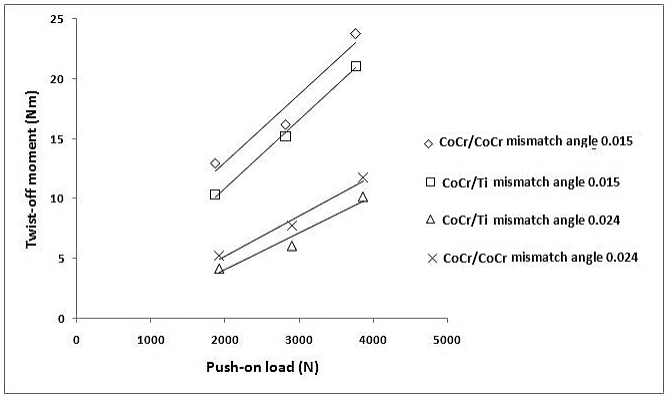

Figure 2.10– Twist-off moment versus assembly force for two mismatch angles and two material combinations.

Figure 2.11 shows torque is plotted against the twist angle for CoCr/CoCr combination assembled with push-on load of 2840 N. The torque-twist curve of the other cases also had the same trend. From the behaviour of torque-twist plot, it can be understood that until slip is initiated (coincident with maximum torque), elastic torsion is the dominant component of twist angle and the contribution of nonlinear micro motions at the contact surface were very small. After slip initiation between the contact surfaces, the torque which is required for relative twist motion started to decrease. The maximum value of twist-off moment for each case was demonstrated in Figure 2.3.

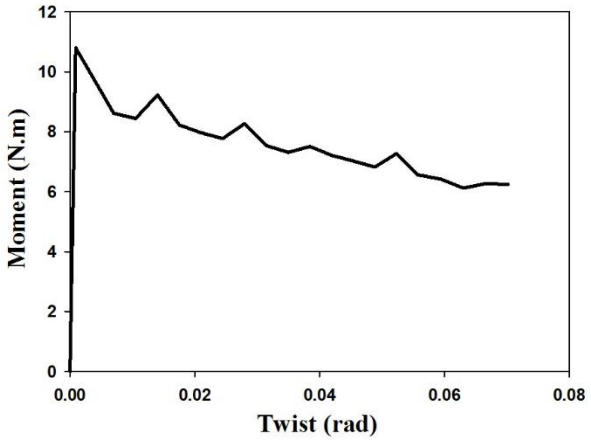

Figure 2.11– Moment versus twist angle for CoCr/CoCr combination assembled by push-on force of 2840 N.

2.5 Summary

A three dimensional finite element model of an isolated femoral head–neck junction was developed to explore the assembly and disassembly procedures, particularly the axial and torsional strengths for different material combinations and geometries. Under the same assembly load, the contacting length between the CoCr head and titanium neck was greater than that of in CoCr/CoCr. The contact length in the titanium neck was more sensitive to the assembly force when compared to the CoCr neck. For instance, with increasing the assembly force from 1890 to 3700 N, the contact length increased by 88% for CoCr/Ti and 59% for CoCr/CoCr junctions. The torsional strength of the junction is related to the lateral deformation of the neck material due to the applied moment. The angular mismatch existing between the head and neck components was found to play the main role in the torsional strength of the junction. The smaller mismatch angle the higher torsional strength. It is suggested to consider reducing the mismatch angle, particularly in CoCr/CoCr junctions, and ensure a sufficiently high assembly force is applied by impaction for this combination.

Chapter 3 The head-neck junction subjected to mechanical loads of daily activities

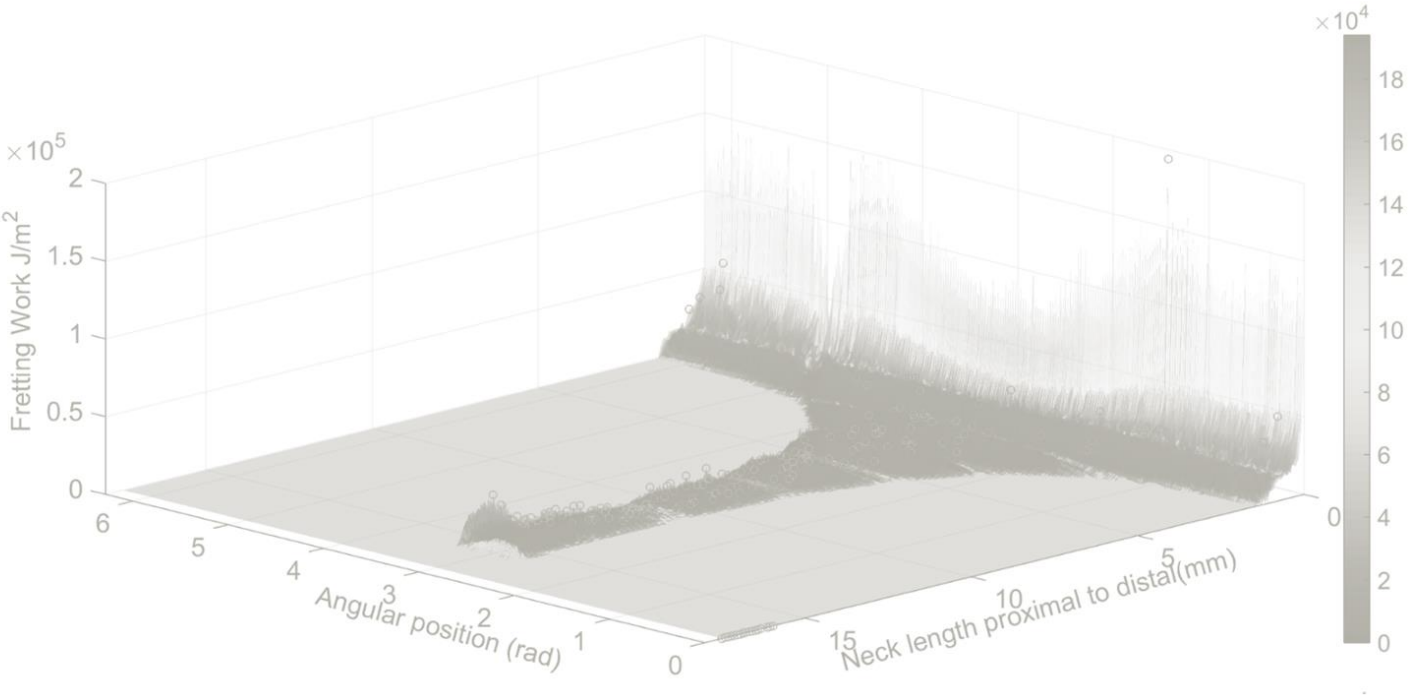

This chapter is based on the following publication:

Fallahnezhad, K.; Farhoudi, H.; Oskouei, R.H.; Taylor, M. A finite element study on the mechanical response of the head-neck interface of hip implants under realistic forces and moments of daily activities: Part 2, *Journal of the Mechanical Behavior of Biomedical Materials* **2017**, *77*, 164-170.

3.1 Overview

To date, many retrieval studies as well as *in-vitro* tests have been conducted to understand the occurrence and intensity of the fretting wear damage to the head and neck materials (Viceconti, Ruggeri et al. 1996, Viceconti, Baleani et al. 1997, Duisabeau, Combrade et al. 2004, Maruyama, Kawasaki et al. 2005). Geometric and mechanical parameters such as taper angle mismatch, head size, assembly force, head centre offset, body weight, material combination and surface finish were found as the main factors that play a role in fretting wear (Goldberg, Gilbert et al. 2002, Grupp, Weik et al. 2010, Langton, Sidaginamale et al. 2012, Del Balso, Teeter et al. 2015, Pourzal, Hall et al. 2016, Hothi, Eskelinen et al. 2017). The head-neck taper junction provides a complex three dimensional (3D) mechanical environment in which there are 6 degree of freedom loads (forces and moments), frictional contact and a tapered geometry with a mismatch angle. At present, *in-vitro* tests are performed under idealised conditions which may or may not reflect the *in-vivo* mechanical environment. Pin-on-disc tests have been performed across different ranges of normal contact stress and micro-motion ((Swaminathan and Gilbert 2012), (Maruyama, Kawasaki et al. 2005)). This raises the important question of what range of micro-motions and normal stresses should be used in these simplified *in-vitro* tests to represent the mechanical environment at the interface of the head and neck components under realistic loads of daily activities.

Although direct measurements of the mechanical environment are difficult, finite element (FE) analysis can be used to gain an understanding of the contact pressure and micro-motion throughout an activity (Chu, Elias et al. 2000, Donaldson, Coburn et al. 2014, Zhang, Harrison et al. 2014, Dyrkacz, Brandt et al. 2015). To achieve a reliable FE model, a precise loading pattern is of paramount importance. Some previous experimental studies have presented hip gait loading patterns induced by routine activities (Bergmann, Deuretzbacher et al. 2001, Bergmann, Graichen et al. 2004). Farhoudi et al. (Farhoudi, Oskouei et al. 2015) developed an analytical method to determine bending and torsional moments acting on the head-neck junction as a result of frictional sliding between the head and cup. Although there have been several studies on the geometric parameters and also loading parameters such as assembly force (Rehmer, Bishop et al. 2012, English, Ashkanfar et al. 2016), strength of the head-neck junction against torsional moments (Jauch, Coles et al. 2014) and mechanical behaviour of the junction

subjected to walking cyclic loading (Donaldson, Coburn et al. 2014), the influence of the loading regimes caused by different physical daily activities on the mechanical environment of the head-neck junction has not been investigated yet. Furthermore, the effect of the bending and torsional moments produced by the frictional sliding of the head and cup on the mechanical response of the head-neck junction is still unknown.

This chapter aims to evaluate the mechanical behaviour of the head-neck taper junction, in particular a CoCr/CoCr junction with a 12/14 taper design and a proximal mismatch angle of 0.024° that is subjected to mechanical loads of common daily activities. A range of contact stresses and relative micro-motions will also be determined which may be accordingly used in relevant *in-vitro* tests to represent a wide range of routine activities for this type of taper junction.

3.2 Materials and methods

The three-dimensional FE model of the head-neck junction that was developed in the previous chapter, and was verified by a set of experimental results (reported in (Rehmer, Bishop et al. 2012)), was further developed to investigate the mechanical behaviour of the head-neck junction subjected to the loads associated with six different activities of daily living: knee bending, sit to stand, stand to sit, stair up, stair down and one leg standing. It is noted that the results for walking are presented and discussed in (Farhoudi, Fallahnezhad et al. 2017), however, some comparisons and discussions are reported in this chapter.

As described in the previous chapter, in this study, a 12/14 taper with a proximal mismatch angle (in which the head angle is larger than neck angle) of 0.024° (Rehmer, Bishop et al. 2012) was modelled for a CoCr head/CoCr neck material combination. The simulation was accomplished in two stages. At the first stage, a 4 kN uniaxial push-on load was applied to assemble the head and neck components; and at the second stage, the loading of each activity was applied. As shown in Figure 3.1, the forces and moments in this model were applied to the neck while the external surface of the head sphere was fixed in all directions. For each activity, a combination of the forces (Bergmann, Deuretzbacher et al. 2001) and moments produced by the head and cup frictional sliding (Farhoudi, Oskouei et al. 2015) were applied to the head-neck junction (Figure 3.2). Micro-motion and contact pressure are found as the most important

mechanical parameters which can control fretting wear and thereby fretting corrosion (McColl, Ding et al. 2004, Swaminathan and Gilbert 2012). Accordingly, fretting work, as the resultant of friction coefficient, contact pressure and micro-motion, can help to understand how different loading regimes might result in damage to the head-neck materials. Therefore, a python code was developed to extract the contact pressure and micro-motion data of the contacting nodes at a critical loading instance during the gait cycle (the instance at which the resultant load and contact stress were maximum). Moreover, a MATLAB code was developed to compute relative displacements of the nodes in the contact area.

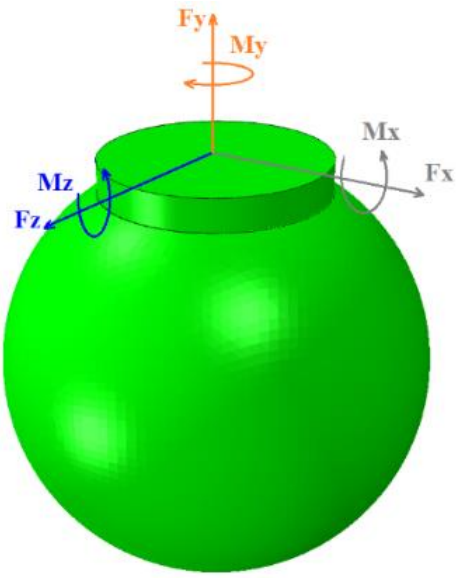

Figure 3.1– The head-neck taper junction model under three dimensional force and moment components.

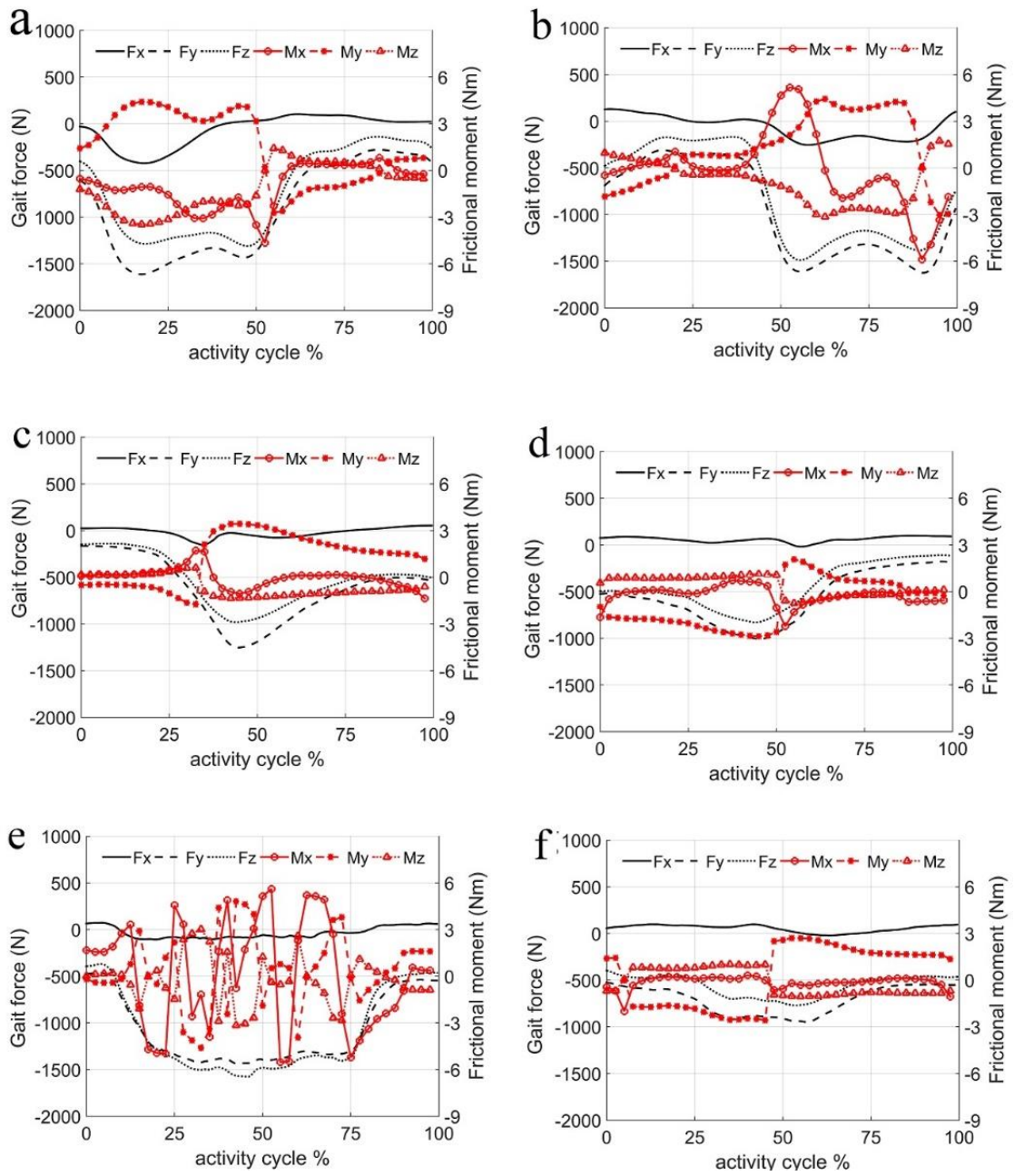

Figure 3.2– Force and moment profiles [26, 27] for: (a) Stair up, (b) Stair down, (c) Sit to stand, (d) Stand to sit, (e) One leg standing, and (f) Knee bending activity cycles.

3.3 Results

Figure 3.3 shows the distribution of contact stresses (contact pressure) in the superolateral region of the neck under the maximum resultant load of the six studied activities. The

superolateral region of the neck was found as the most critical region in terms of stress magnitudes and the size of contacting area. The contours clearly show the contacting area of the neck with the head where the contact stresses are positive. For a better demonstration of the contact area in the contours, the maximum magnitude of the contact stress was limited to 700 MPa for all the activities. This means that a very thin band from the proximal edge of the neck, at which there is a very high stress concentration, was excluded from the contours. However, the maximum magnitude of the contact stress is still included in the legend of the contours.

Figure 3.4 illustrates fretting work per unit of area (J/m^2) versus the length and perimeter of the neck for all the activities. It can be seen that the proximal side of the neck, which is firmly fixed to the head (because of the assembly force), has the maximum fretting work in all the activities. Figure 3.4 also shows that in stair up, stair down and one leg standing, the distal side has higher levels of fretting work compared with the middle side of the neck (between the proximal and distal sides). This is due to the bending effect caused by the loading pattern in these three activities. As shown in Figures 3.2(a,b,e), the maximum magnitude of F_y and F_z, that are dominant forces, is approximately 1,500 N for stair up, stair down and one leg standing, while for the other activities, these are about 1,000 N. Therefore, for stair up, stair down and one leg standing, F_y and F_z are big enough to cause bending over the neck length which influences more the distal side and makes a contact between the head and neck in this side as well.

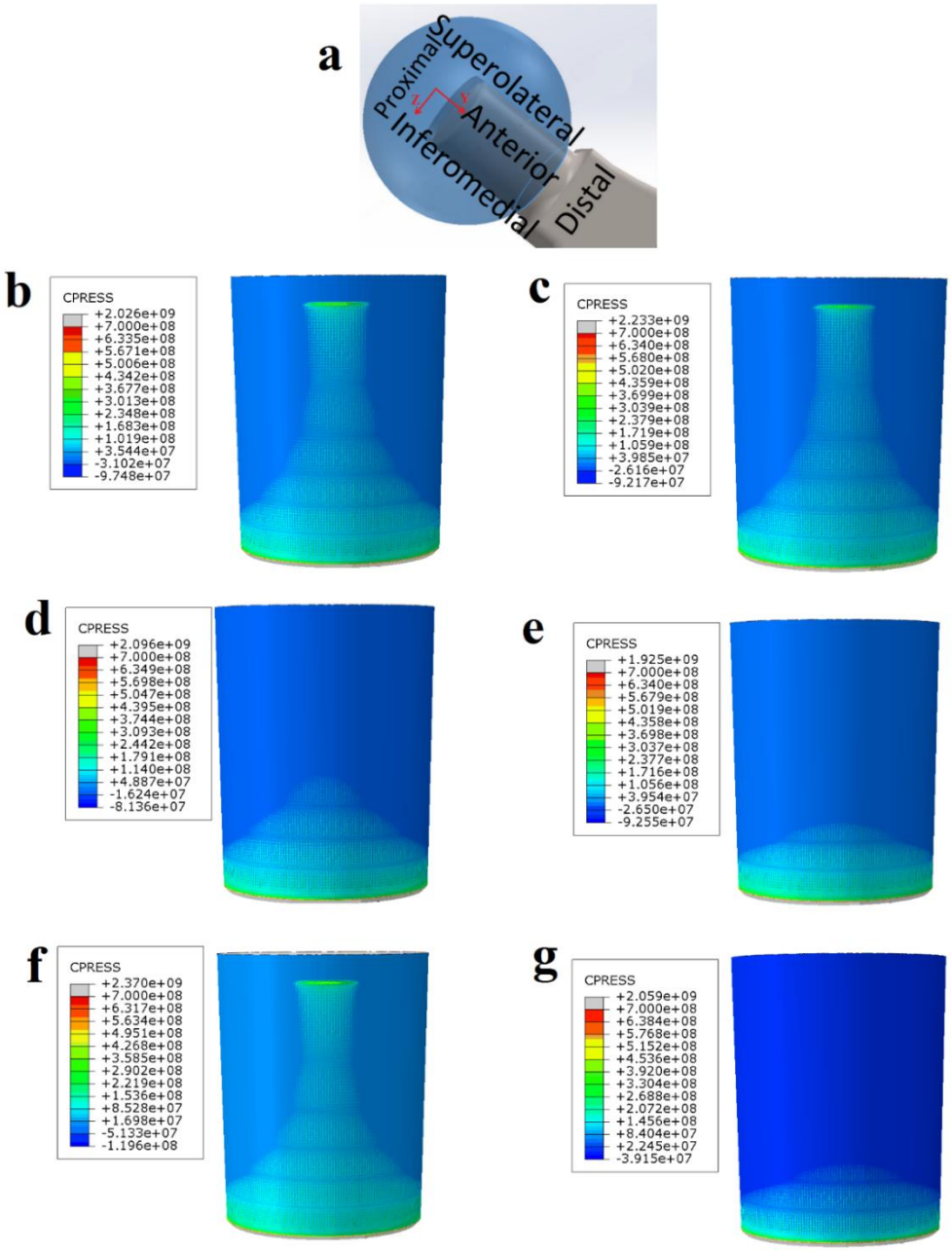

Figure 3.3– Contact stress distribution in the superolateral region of the neck at the critical loading instance (when the resultant load and contact stress were maximum): (a) the head-neck junction with its regions, (b) stair up, (c) stair down, (d) sit to stand, (e) stand to sit, (f) one leg standing, and (g) knee bending. Stresses in Pa. (Maximum

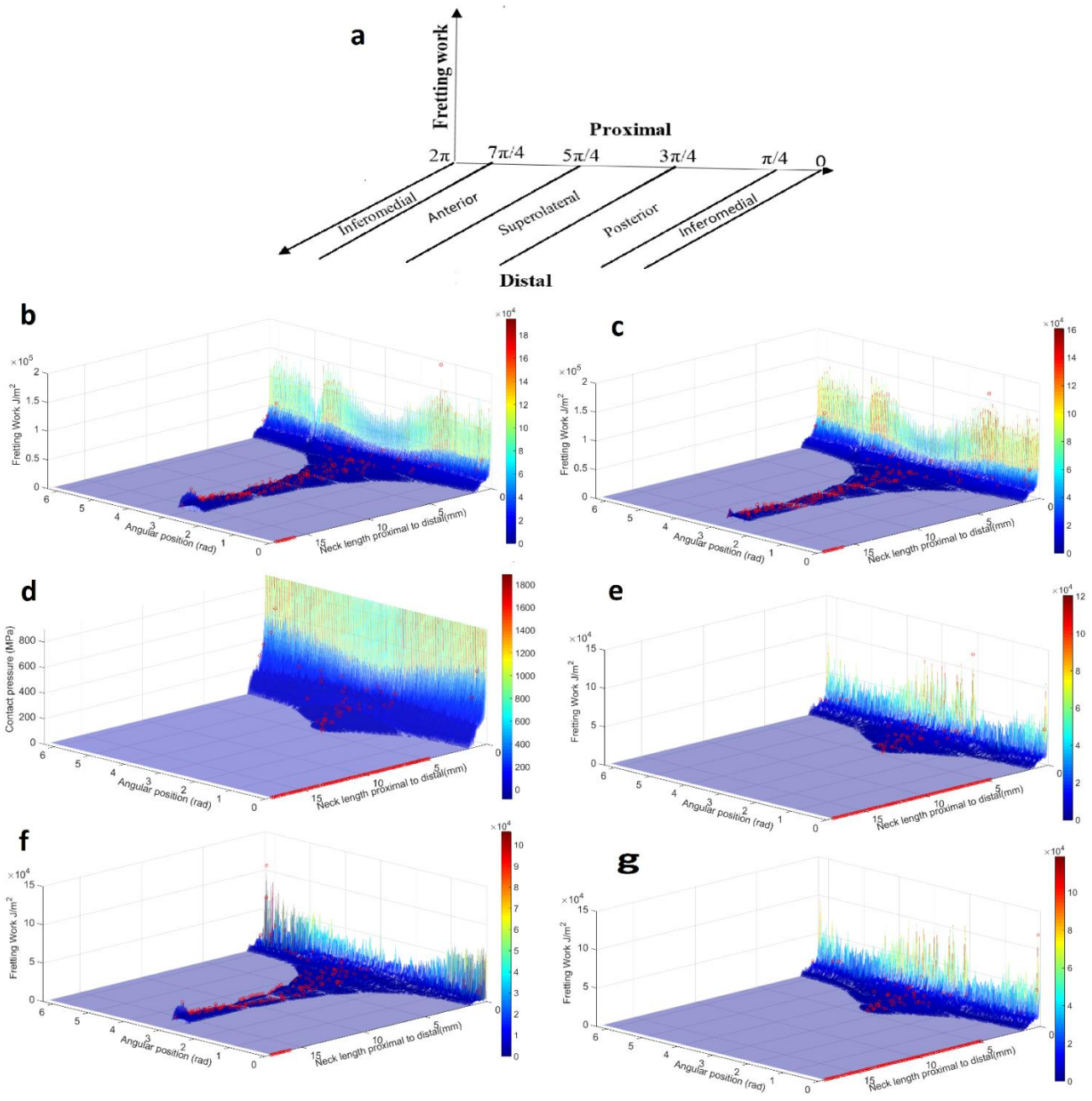

Figure 3.4– Fretting work per unit of area (J/m^2) versus the length and perimeter of the neck at the critical loading instance (when the resultant load and contact stress were maximum): (a) regions and angles over the neck surface, (b) Stair up, (c) Stair down, (d) Sit to stand, (e) Stand to sit, (f) one leg standing, and (g) Knee bending.

In Figure 3.4, the superolateral region was found as the most critical region of the neck in terms of fretting work. The maximum values of fretting work in each division of the neck length over the neck circumference were identified and shown in the profile of each activity with small red circles. The track of the fretting work maximum values over the length of the neck for all the

activities is shown in Figure 3.5. The same method was used to produce similar graphs for normal contact stresses, shear stresses and relative micro-motions.

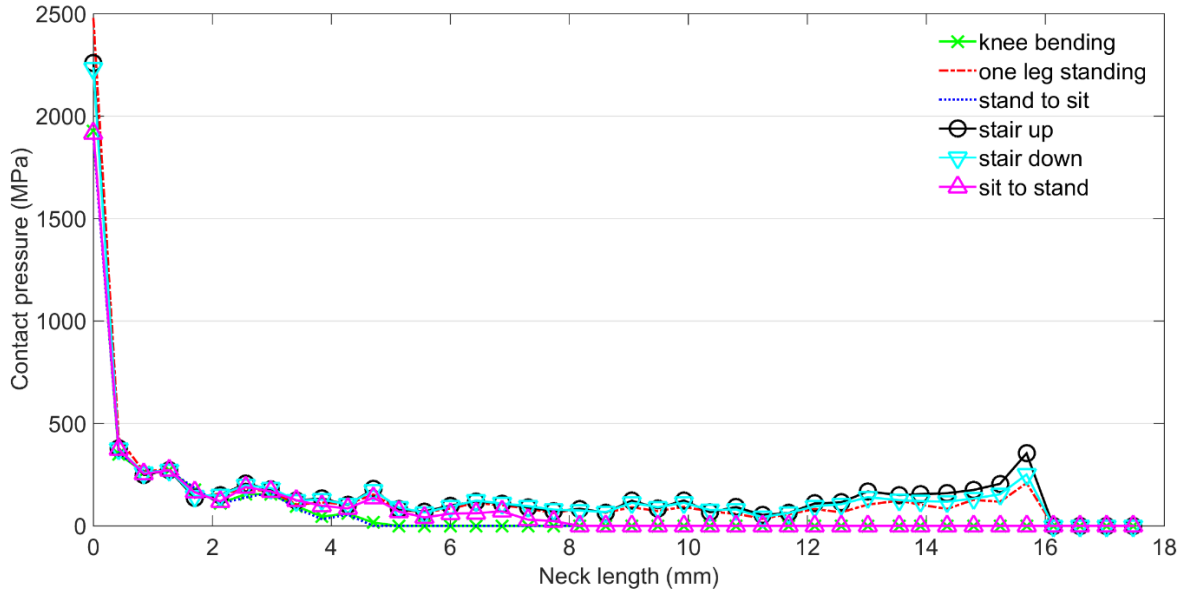

Figure 3.5– Maximum values of fretting work per unit of area (J/m^2) across the neck circumference versus the neck length.

As can be seen in Figure 3.5, the maximum fretting work per unit of area for all the activities occurred at the proximal side. Stair up had the highest fretting work per unit of area 4,720 (J/m^2). This was followed by stair down, sit to stand, one leg standing, knee bending and stand to sit activities with 4320, 4020, 3140, 2520 and 2320 (J/m^2), respectively. While for stand to sit, knee bending and sit to stand, the fretting work per unit of area becomes zero after approximately 5-8 mm from the proximal side, for the other three activities, the fretting work is non-zero over the entire length of the neck and increases in magnitude at the distal side.

As Figure 3.6 shows, the highest contact pressure (2,500 MPa) is induced by one leg standing; and knee bending causes the lowest contact pressure (1,940 MPa) both at the highly stressed edge of the proximal side. However, all contact stresses drop significantly to less than 500 MPa immediately after this edge (only 0.4 mm away) for the remainder of the neck length towards the distal side. A similar pattern is observed for shear stresses (a reduction from 563 MPa to less than 100 MPa right after the edge), as shown in Figure 3.7.

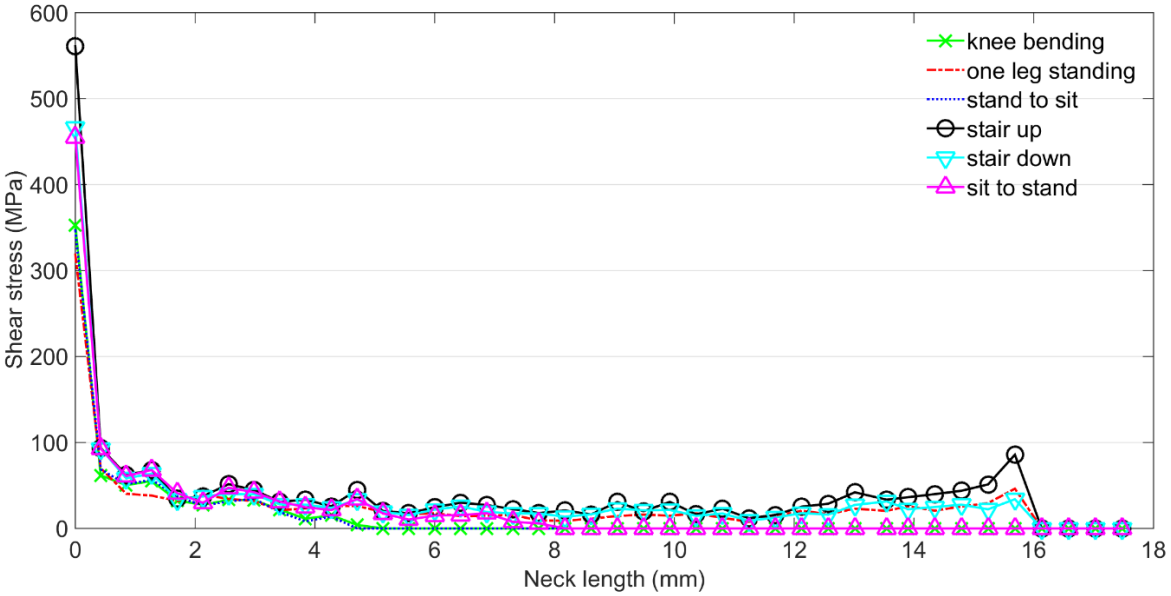

Figure 3.6– Maximum magnitudes of contact stress (pressure) across the neck circumference versus the neck length.

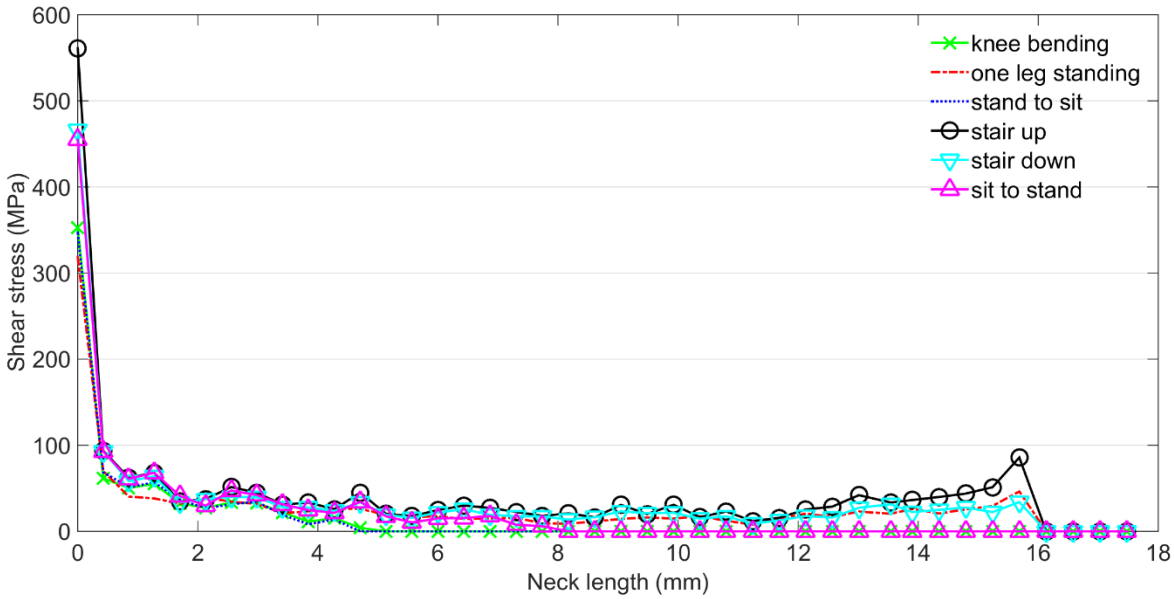

Figure 3.7– Maximum magnitudes of shear stress across the neck circumference versus the neck length.

As demonstrated in Figure 3.4, the superolateral region was the most critical region for all the activities. Stair up, stair down and one leg standing were the three activities in which the contacting area was greater compared to the other activities. From Figure 3.6, the contact length over the neck surface for the activities can be found as: 4.4 mm (stand to sit), 4.6 mm (knee

bending), 8.2 mm (sit to stand), 16 mm (one leg standing, stair up and stair down). The last three activities made a complete longitudinal contact between the head and neck in the superolateral region. Figure 3.8 shows the contact stress contours of the head for stair up and sit to stand as two activities that can represent the activities with a complete and incomplete contact between the head and neck, respectively, at the critical loading instance. The legend of the contours was limited to 400 MPa to better demonstrate the contact area. Unlike the sit to stand activity, there is a complete longitudinal contact in the superolateral region of the head for stair up.

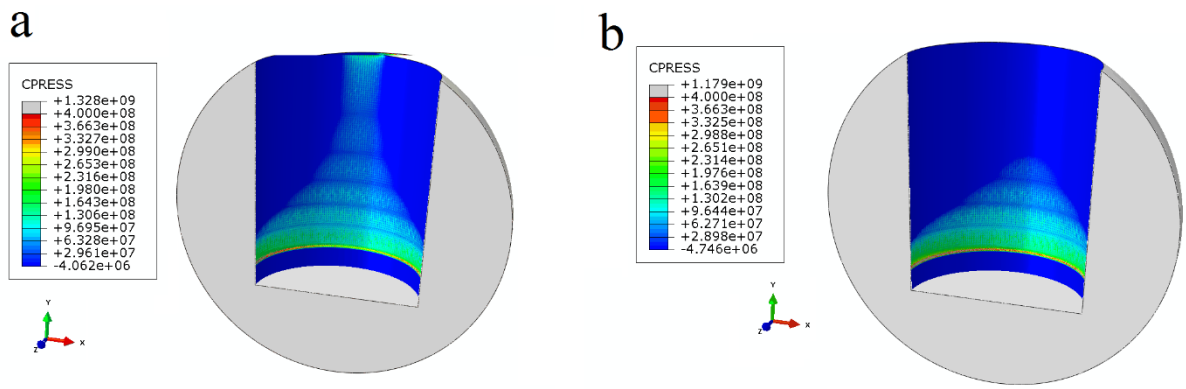

Figure 3.8– Contact stress (Pa) contours of the head for: (a) Stair up, (b) Sit to stand. (Maximum stress is always at the proximal edge of the head, however, to better demonstration, maximum magnitude of the contact stress was limited to 400 MPa for both activities).

As mentioned previously, fretting work per unit of area could be a good indicator for comparing the effect of various activities on the fretting wear of the junction, as its formulation includes both the relative micro-motion and contact stress components. The area under the curve of fretting work per unit of area (Figure 3.5) was computed for each activity. This gives fretting work per unit of length (FWPUL). The bar chart of Figure 3.9 shows FWPUL calculated for all the activities including walking. Stair up was found as the most critical activity with the highest FWPUL (1.62×10^4 J/m), while knee bending and stand to sit with 1.96×10^3 J/m had the lowest FWPUL. Such a 720% difference between these activities indicates the effect of type of physical activity on the fretting wear of the head-neck junction. The FWPUL for walking was also computed as 1×10^4 J/m.

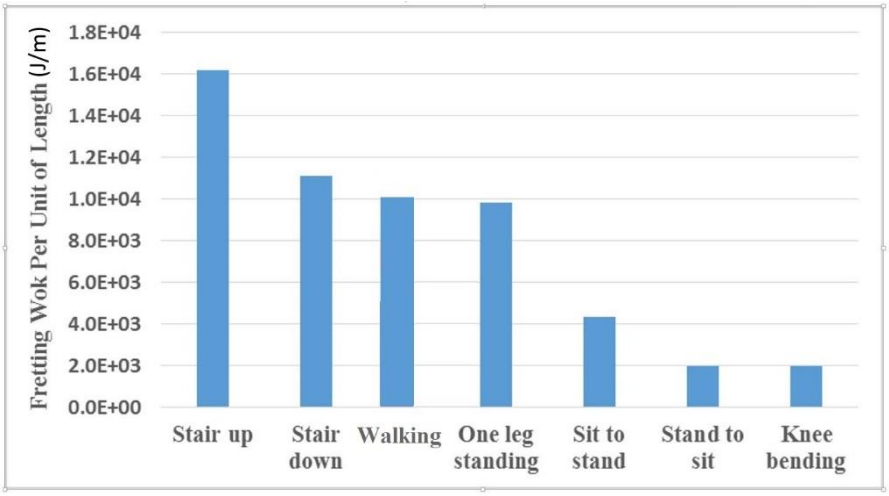

Figure 3.9– Fretting work per unit of length determined for each activity.

It can be seen from Figure 3.10 that the relative micro-motions for the studied activities are not more than 32 μm which is related to stair up. It is also obvious from this figure that the relative micro-motion for stair up, stair down and one leg standing is remarkably higher than the other activities particularly in the distal side of the neck.

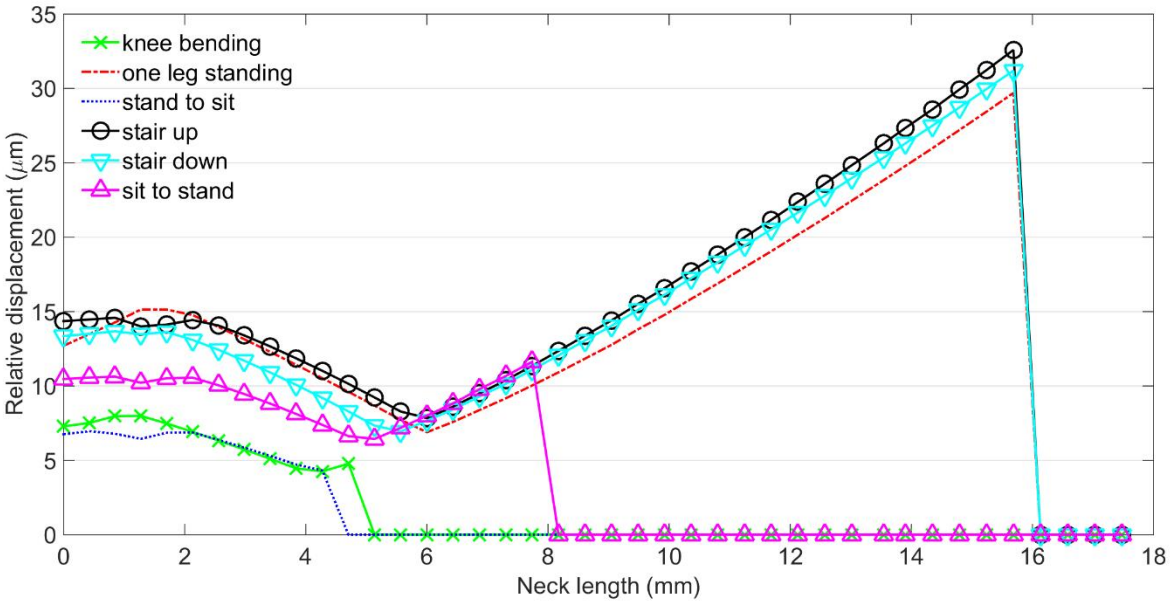

Figure 3.10– Maximum values of relative displacement across the neck circumference versus the neck length.

Figure 3.11 shows the maximum contact stresses versus their corresponding relative displacements and the maximum relative displacements versus their corresponding contact stresses at several divisions through the neck length. From this figure, it can be understood that most of the critical points of the neck have a contact stress in the range of 0-350 MPa and a relative displacement in the range of 0-32 μm. It is noted that for each activity, there is a data point having a high contact stress which was due to the stress concentration at the edge of the proximal side of the neck. Therefore, these points were excluded from the reasonable ranges as shown with the red lines.

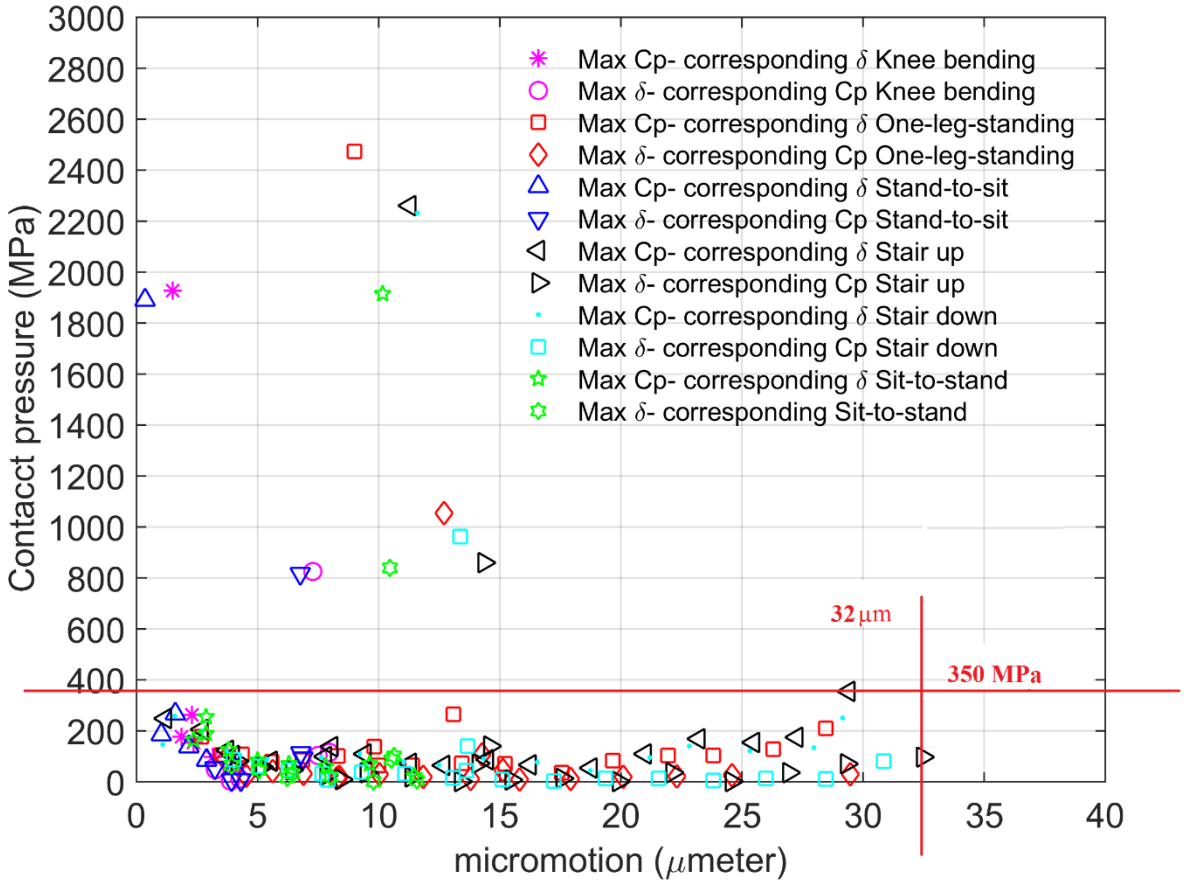

Figure 3.11– Maximum contact stresses and maximum relative displacement through the neck length for different activities.

3.4 Discussion

As pointed out in the previous section, superolateral sector was the most critical sector of the junction, in aspects of having the higher magnitude of contact stress and fretting work. This

can be fully justified by focusing on the loading structures of different activities. Figure 3.2 shows that F_y (toward junction axis) and F_z (toward superolateral sector) are the most dominant load components that are being applied to the junction. The significant magnitude of F_z has caused superolateral sector to become the most critical sector of the junction.

It was found from Figure 3. 10 that after stair up and stair down, walking was the most critical activity. Generally, it can be said from Figure 3.10 that activities in which patients raise one leg for a while during a cycle of the activity, such as stair up, stair down, one leg standing and walking, have greater FWPUL values in comparison with the activities having both legs in contact with the ground. This could be explained by the load components of each activity (Figure 3.2). For stair up, stair down and one leg standing, their F_y and F_z components reach approximately 1,500 N during the gait cycle. This amount of force not only increases the normal and shear stresses between the contacting surfaces, but also can lead to a complete contact between the head and neck, due to the bending caused by the F_z component.

In Figure 3.11, the contact stress and micro-motion ranges obtained for the six activities were close to the contact stress and micro-motion ranges obtained for the walking activity in the first part of this paper (275 MPa for contact stress and 31 μm for micro-motion). This may suggest that to develop *in-vitro* tests close to the real mechanical environment of the head-neck junction, the contact pressures and relative micro-motions should be within the range of 350 MPa and 32 μm, respectively, so that most common daily activities of a patient are covered in the tests. Comparing these findings with previous *in-vitro* tests, Swaminathan et al. (Swaminathan and Gilbert 2012) applied greater magnitudes (contact stresses of 0-1,100 MPa and micro-motion of 50 μm) which are found to be conservative. In another pin-on-disc study (Maruyama, Kawasaki et al. 2005), the micro-motion was 25 μm which is well in the range of micro-motions suggested by the present work. Moreover, the contact stresses were 1 MPa, 3 MPa and 5 MPa which seem very low for the 350 MPa range in this work. In a pin-on-disc experiment conducted by Geringer et al. (Geringer, Forest et al. 2005), they applied micro-motion of 40 μm, while the contact surface was under normal stress of 12-25 MPa. In this experiment, although micro-motion is very close to the proposed range, applied normal stresses are too low to cover the proposed range of stress, in this study. This study can help to understand fretting wear related parameters and accordingly the severity of the damage and its

location that may be caused by mechanical fretting wear. Referring to wear relations such as Archard equation (Eq. 1),

$$\frac{V}{S} = k\frac{F}{H} \qquad (3.\ 1)$$

where V is the lost volume, S is the amplitude of sliding, k is the wear coefficient, F is the normal force and H is the hardness of material (Archard 1953), it is apparent that the volume loss is directly proportional to the normal load (normal stress) and amplitude of the relative micro-motion. Hence, these two parameters that are investigated in this study can be good indicators of the damage caused by fretting wear.

It should be noted that in this work a particular design and a CoCr/CoCr material combination was used. Moreover, assembly force of 4 kN and a medium walking loading regime was applied to the junction. To have a more comprehensive range of results, further research is required to investigate the influence of variation of the mentioned parameters on mechanical behavior of the junction. In addition, the behavior of the head neck junction under cyclic loading and the influence of rhythmic loading on the junction need to be investigated.

3.5 Summary

The 3D FE model, developed in the Chapter 2 was used in this chapter to investigate mechanical responses of head-neck interface under forces and moments of real daily activities. The activities included stair up, stair down, sit to stand, stand to sit, one leg standing and knee bending. To present the real mechanical environment of the junction, in addition to the force components, the frictional moments produced by the frictional sliding of the head and cup were applied to a CoCr/CoCr junction having a 12/14 taper with a proximal mismatch angle of 0.024°. This study revealed that stair up with the highest fretting work per unit of length (1.62×104 J/m) was the most critical activity, while knee bending and stand to sit with 1.96×103 J/m were the least critical activities. For all the activities, the superolateral region of the neck was identified as the most critical region in terms of having larger values of fretting work per unit of area. This study showed also that the relative micro-motions and contact stresses occurring at the head-neck interface for all the studied activities are mostly in the range of 0-38 μm and 0-350 MPa, respectively. These ranges may be accordingly employed for

conducting relevant in-vitro tests to more realistically represent the mechanical environment of taper junctions with the same materials and geometry studied in this work.

Chapter 4 Development of fretting wear model for the head-neck junction

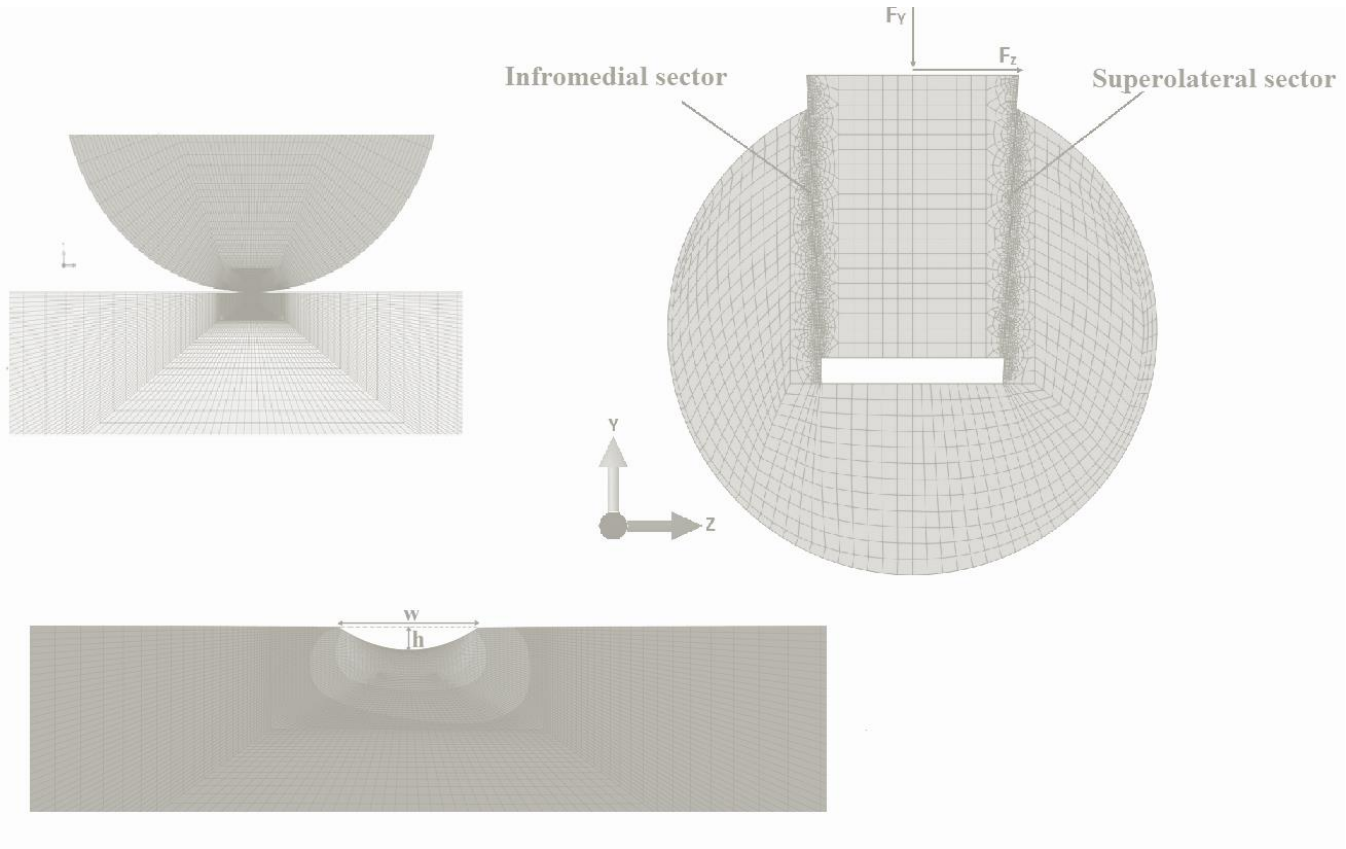

This chapter is based on the following publications:

Fallahnezhad, K.; Oskouei, R.H.; Badnava, H.; Taylor, M. An adaptive finite element simulation of fretting wear damage at the head-neck taper junction of total hip replacement: The role of taper angle mismatch. *Journal of the Mechanical Behavior of Biomedical Materials* **2017**, *75*, 58-67.

Fallahnezhad, K.; Oskouei, R.H.; Badnava, H.; Taylor, M. The influence of assembly force on the material loss at the head-neck junction of hip implants in physiological body fluid subjected to cyclic fretting wear. Manuscript being submitted to *Materials*.

4.1 Overview

As was mentioned in Chapter one, the metallic debris caused by fretting corrosion can have adverse effects on local tissues (Doorn, Campbell et al. 1998, Walter, Marel et al. 2008, Oskouei, Fallahnezhad et al. 2016). Hence, the amount of material loss in the head-neck junction over the life of implant inside the body together with the mechanism of fretting wear in this junction are important problems for investigation. This has been the subject of several in-vitro studies (Viceconti, Baleani et al. 1997, Duisabeau, Combrade et al. 2004, Maruyama, Kawasaki et al. 2005, Grupp, Weik et al. 2010). Using a pin-on-disc set-up, Maruyama et al. (Maruyama, Kawasaki et al. 2005) investigated the fretting wear behaviour of CoCr on CoCr in both air and a phosphate buffered saline (PBS) solution. They applied a 25 µm reciprocating displacement under contact normal stresses of 1 MPa, 3 MPa and 5 MPa. There was less wear damage in PBS compared to that of in air. Moreover, the coefficient of friction was larger in PBS (approximately double). Duisabeau et al. (Duisabeau, Combrade et al. 2004) performed fretting wear experiments on Ti-6Al-4V and 316L stainless steel in air and Ringer's solution. They concluded that the solution has a significant effect on the fretting regime such that introducing a corrosive lubricant leads to the modification of the fretting regime.

Due to the long exposure of implants to cyclic loading of daily activities, material loss related factors, complexity of the junction geometry and mechanical loads, it is very hard and expensive to study the fretting wear mechanism by means of in-vitro tests. Hence, finite element (FE) simulations have been recently developed as a more convenient and practical method for studying fretting wear and material loss in modular junctions of hip implants (Donaldson, Coburn et al. 2014, Zhang, Harrison et al. 2014).

Elkins et al. (Elkins, Callaghan et al. 2014) investigated the stability and trunnion wear in large diameter metal-on-metal hip implants. Based on a previously validated finite element model, they reported that with increasing the head diameter, the stability of the head-neck junction can improve; however, it will increase the wear. They performed all the simulations under only one cycle of sit-to-stand loading. They also used a perfect contact (zero mismatch angle) between the head and neck components, as no mismatch angle was reported in their work. It is however noted that there is always a subtle mismatch between the head and neck taper angles which can provide an interference fit to lock the junction (Bisseling, Tan et al. 2013, Hernigou, Queinnec

et al. 2013, Hussenbocus, Kosuge et al. 2015). English et al. (English, Ashkanfar et al. 2015) developed a FE model to estimate the amount of material loss and contact pressure at a head-neck junction subjected to two million cycles of a walking gait loading. They used a CoCr head and titanium neck combination with a perfect contact between the head and neck. In another work (English, Ashkanfar et al. 2016), they investigated the effect of assembly force on the wear behaviour. It was reported that with increasing the impaction force to at least 4 kN, a significant reduction in the amount of wear debris can be achieved. Zhang et al. (Zhang, Harrison et al. 2013) developed a 2D axisymmetric model of the head-neck junction to predict wear in high cyclic gait loading. They applied a uniaxial cyclic load to simulate the gait loading. The material combinations were a CoCr head with a direct metal laser sintering (DMLS) Ti-6Al-4V neck and a CoCr head with a forged Ti-6Al-4V neck. DMLS Ti-6Al-4V was found to be more resistant against the fretting wear.

The material combinations used in the previous models included CoCr for the head and titanium for the neck. Also, all the simulations that have been developed to date are based on the material properties (such as wear coefficient and friction coefficient) obtained in a dry condition. More importantly, mismatch angle at the junction has been neglected in previous finite element studies, in spite of its important effect on the mechanics of the interface and thus potentially on the fretting wear.

This chapter aims to develop an adaptive FE model to simulate fretting wear at the head-neck junction of hip implants. To this aim, a FORTRAN code was developed to apply Archard equation to the head-neck junction interface, through the UMESHMOTION ABAQUS subroutine. The model was used to explore the influence of the junction environment (dry and phosphate buffered solution (PBS) conditions) to compare the fretting wear behaviour of the head-neck junction in both conditions.

4.2 Materials and methods

The material combination used in this study was a CoCr head with a CoCr neck. A two dimensional model was developed to simulate the fretting wear process at the most critical section of the head-neck junction. The key steps in the development of this model are given in Figure 4.1.

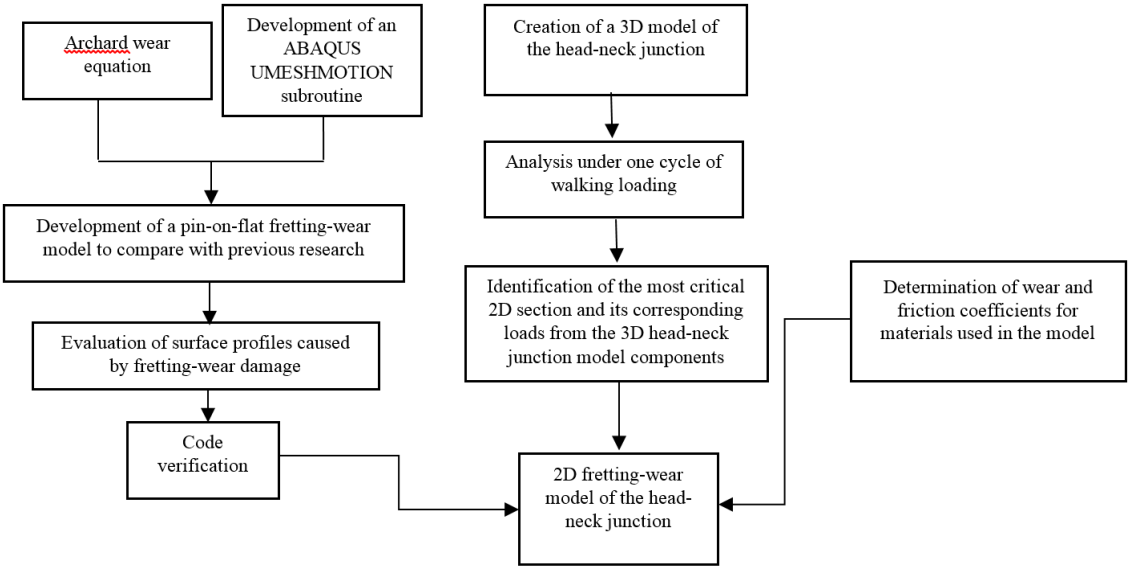

Figure 4.1– The algorithm of the key steps implemented in the development of this model.

4.3 Verification of the fretting wear code

To model the fretting wear, a FORTRAN code was developed that can control the position of the surface nodes through the ABAQUS UMESHMOTION subroutine within an adaptive meshing constraint. The Archard wear equation was the main formulation that was used in this simulation (Eq. 1).

$$\frac{V}{S} = k\frac{F}{H} \tag{4.1}$$

where V is the lost volume, S is the amplitude of sliding, k is the wear coefficient, F is the normal load and H is the material hardness. The Archard wear law was originally proposed by Archard (Archard 1953), and was validated for a wide variety of materials under sliding wear by Archard & Hirst (Archard and Hirst 1956). This model has the ability to become localized, and therefore can be used by finite element method. Moreover, the Archard equation has been used to simulate fretting wear through numerical methods such as finite element by previous researchers and has been verified by experimental tests (Johansson 1994, Ding, Leen et al. 2004, McColl, Ding et al. 2004).

The algorithm of this code was previously used by McColl et al. (McColl, Ding et al. 2004) and Ding et al. (Ding, Leen et al. 2004) to model fretting wear in a pin-on-flat system. They

presented surface profiles after different cycles of fretting wear tests. To verify the UMESHMOTION code, which was used to simulate fretting wear in the head-neck junction of this work, a pin-on-flat model was first developed which was very similar to the Ding's models in terms of material, geometry, element size, meshing structure, normal load and sliding frequency and amplitude. The surface profiles of the flat were produced and compared with the ones that were presented by Ding et al. (Ding, Leen et al. 2004) (Figure 4.2). Good agreement was found between the profiles that verified the UMESHMOTION code and its accuracy used in this study. The surface of the disc after the fretting wear process was evaluated (Figure 4.3) and compared with the results reported by Ding et al. (Ding, Leen et al. 2004). Table 1 provides a comparison between the results of this study and those presented by Ding et al. (Ding, Leen et al. 2004) in terms of the width and height of the wear profile for the disc which shows a very good level of agreement verifying the UMESHMOTION code and its accuracy used in this study.

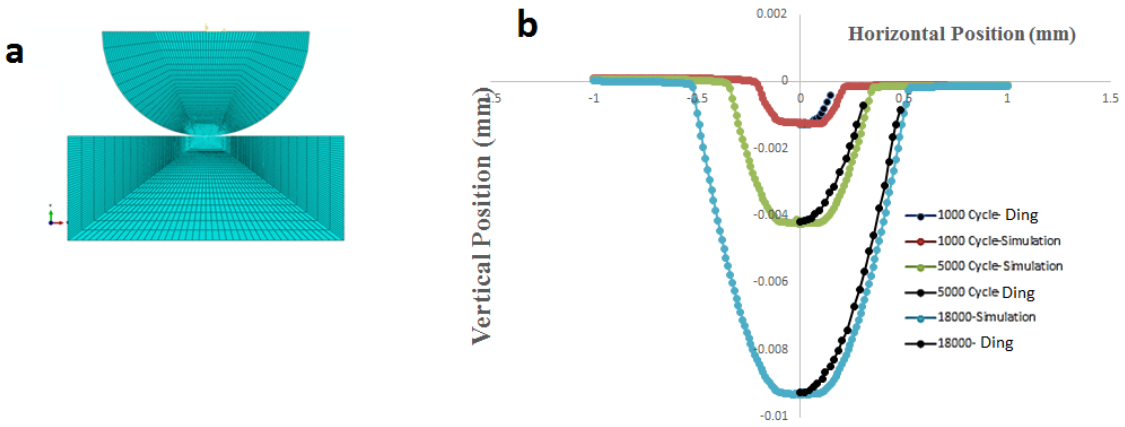

Figure 4.2– Verification of the fretting wear code developed in this work: (a) meshing structure of the model in this study, and (b) a comparison between surface profiles of the flat component presented by Ding (Ding, Leen et al. 2004) and those produced in this study.

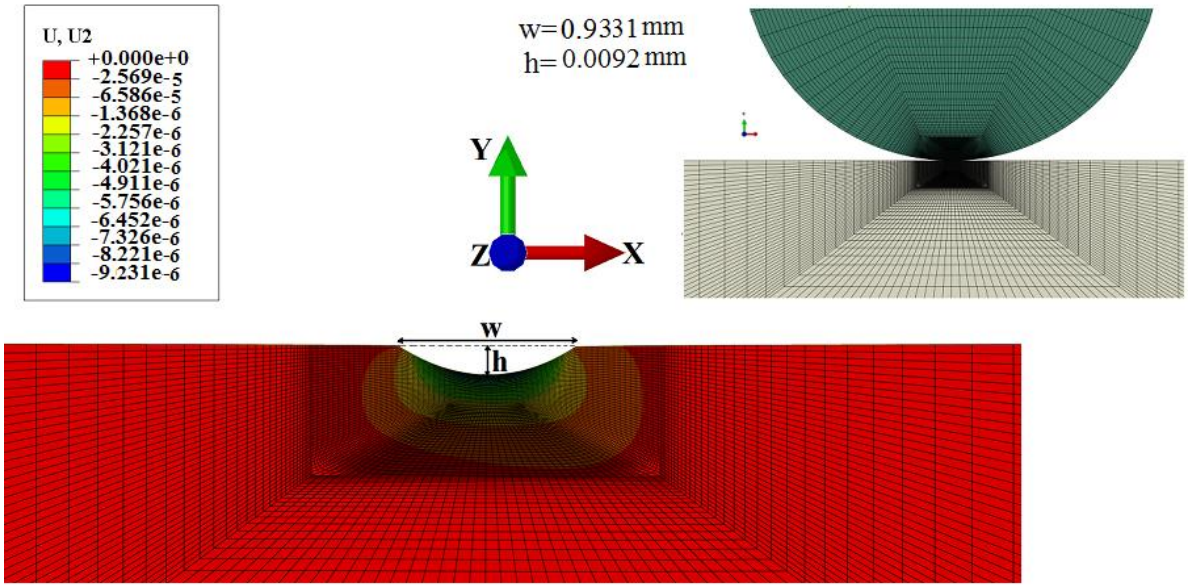

Figure 4.3– The distribution of displacement in Y axis (in meters) representing material removal from the surface of the disc under a normal force of 1,200 N and a sliding amplitude of 10 µm after 18,000 cycles of fretting wear.

Table 4.1 The width and height of the wear profile for the disc after various fretting wear test cycles; a comparison between the computational results of this work and those presented by Ding et al. (Ding, Leen et al. 2004).

	Wear profile parameters on the surface of the disc	After 1,000 cycles	After 5,000 cycles	After 18,000 cycles
Results of this work	Width, w (mm)	0.3512	0.7123	0.9331
	Height, h (mm)	0.0013	0.0042	0.0092
Results reported by Ding et al. (Ding, Leen et al. 2004)	Width, w (mm)	0.3834	0.7644	0.9754
	Height, h (mm)	0.0013	0.0042	0.0092

4.4 FE model

A two-dimensional plane strain model was developed to investigate the fretting wear mechanism in the head-neck junction. Although the two-dimensional model cannot provide the

volume of the lost material, it can simulate fretting wear process at the most critical section of the junction. This is a good indicator of the junction behaviour under cyclic gait loading. To do this, the most critical section of the head-neck junction subjected to level gait loading, had to be determined. Thus, a 3D model of the same CoCr-CoCr head-neck junction that had been previously developed [9] was used to analyse the junction under walking load profiles reported in (Farhoudi, Oskouei et al. 2015, Farhoudi, Oskouei et al. 2016). The junction had a proximal contact with a mismatch angle of 0.024° (Chapter 2). The materials, geometry and the mismatch angle of the junction were in accordance with the taper junction (12/14 taper design and 32 mm head) that had been measured and reported by Rehmer et al. (Rehmer, Bishop et al. 2012). Figure 4.4a shows the von Mises stress contours in the junction and more specifically in the neck under the maximum force and moment over the gait cycle. With implementation of a Python code, the results of contact pressures and displacements were extracted for all the contacting nodes of the head and neck surfaces at the maximum force and moment instance.

A MATLAB code was then implemented to determine micro-motions (relative displacements) and fretting work at the contacting nodes of the interface. The results indicated that the mid-plane of the superolateral region of the neck was the most critical section in terms of contact stresses and micro-motions. The corresponding load components of this critical section were also identified for applying to the 2D fretting wear model. The 2D meshed model and the load components are shown in Figure 4.5 a. The right and left sides in this figure represent the superolateral and inferomedial sectors of the junction, respectively. For the contact area, linear 2D elements (4-node bilinear) were used for both the head and neck models. The main body of the head and neck models were also structurally meshed with the same elements except the layers close to the contacting layer which were freely meshed using linear 2D elements, as shown in Figure 4.5a. Different geometric parameters of the junction are schematically shown in Figure 4.5b. In this figure, contact length is illustrated and depth of wear is shown with exaggeration for a better visibility and presentation. A convergence study was developed to find the most appropriate size of the elements, particularly at the contact area in which the Archard equation is being applied. A convergence study was developed to find the most appropriate size of the elements, particularly at the contact area in which the Archard equation is being applied.

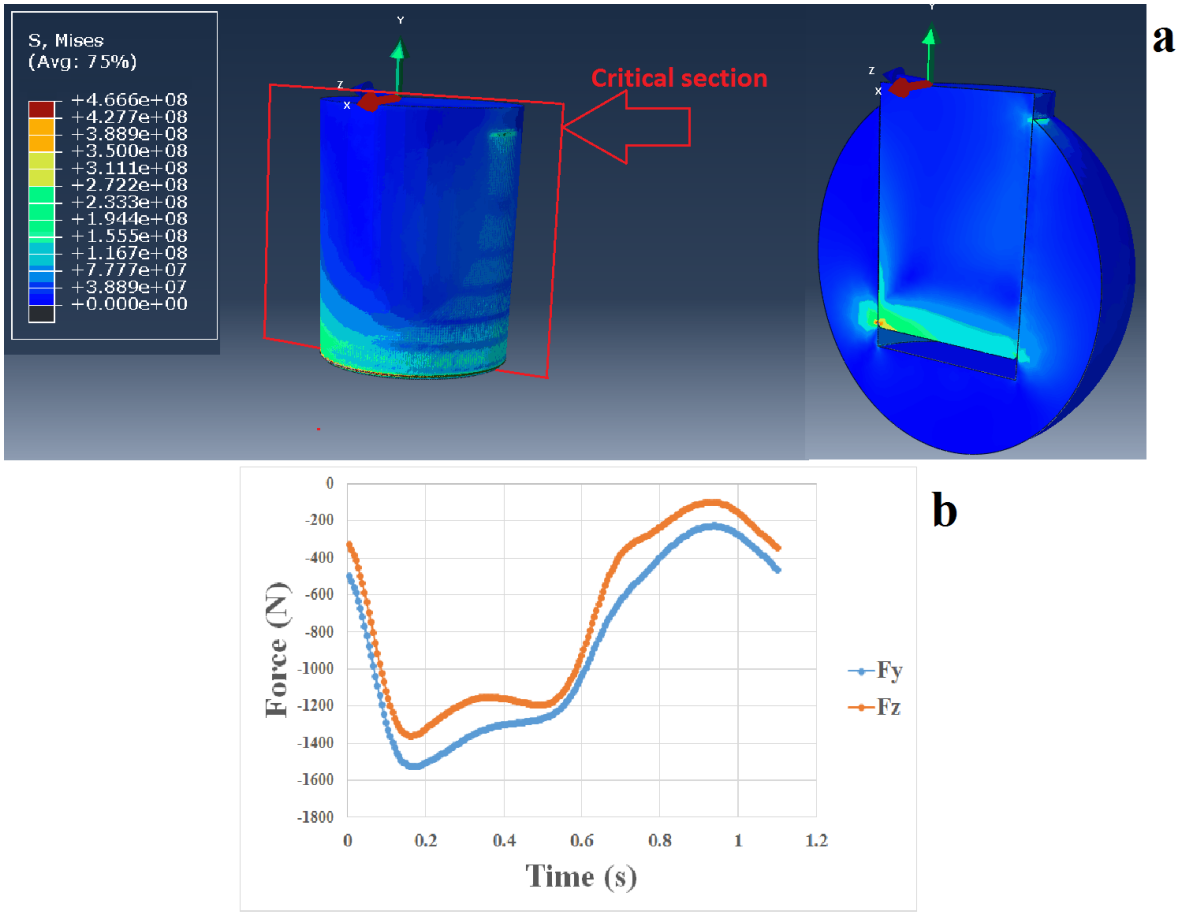

Figure 4.4– The most critical section of the head-neck junction subjected to walking loading: (a) von Mises stress distribution, stresses in Pa, and (b) corresponding load components of the critical section in the superolateral region.

The Archard equation (Eq. 1) can be re-written as Eq. 2 by dividing both sides of the equation by the area:

$$h = K.S.p.\Delta N \qquad (4.2)$$

where h is the depth of wear, K is the wear coefficient divided by hardness (k/H), p is the normal stress and ΔN is the load cycle update interval which will be discussed more in the following sections. This equation has the ability to be localized and can be used in a FE model. To apply the Archard equation to the head-neck model, first, the value of K for the contacting materials should be determined. The material combination in this study was a CoCr head with a CoCr neck for which a K factor for CoCr on CoCr was required. For this purpose, a set of experimental results conducted by Maruyama et al. (Maruyama, Kawasaki et al. 2005) were

used to identify the wear coefficient for the CoCr-CoCr combination. They conducted pin-on-flat tests for different normal stresses and sliding cycles in both a dry condition and a phosphate buffered saline (PBS) to simulate the corrosive medium of the human body. For each testing condition, they applied 50,000, 200,000 and 600,000 cycles and presented the amount of material loss and surface profiles. Having the geometric properties of the test samples, and the density of CoCr alloy, and using the Archard equation, the coefficient of wear was computed for each case in this study. For each condition (dry and PBS), 9 wear coefficient-to-hardness ratios (*K*) were obtained. The *K* values for each condition were very close (with a difference of less than 10%). Accordingly, for each condition, the average of the *K* factors was used for the CoCr-CoCr combination in that condition. This indicated that the Archard equation was able to estimate the amount of material loss with a constant value of *K* for each condition. *K* values for dry and PBS conditions were obtained as:

Dry condition: $K = 1.68\text{E-}14\ \text{Pa}^{-1}$

PBS: $K = 0.17\text{E-}14\ \text{Pa}^{-1}$

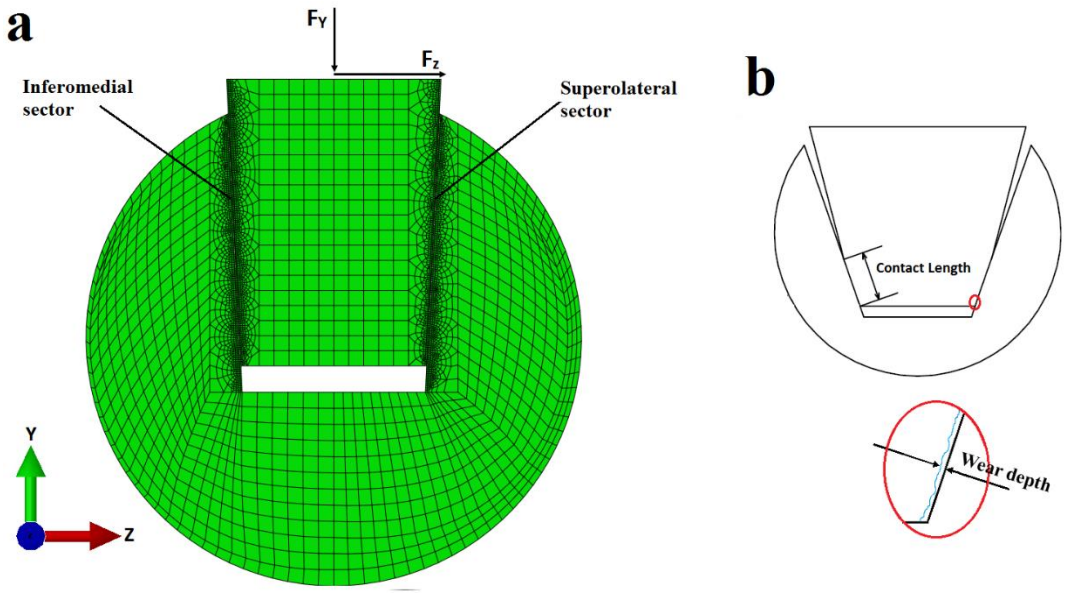

Figure 4.5– (a) Two dimensional meshed model of the most critical section of the junction and the applied load components, and (b) contact length at the interface and wear depth onto the neck surface.

The friction coefficient for both conditions was based on the results reported in Maruyama et al. (Maruyama, Kawasaki et al. 2005). They presented graphs of the friction coefficient versus

number of cycles for both the dry and PBS conditions for different magnitudes of contact stress. Their graphs revealed that, regardless of the contact stress magnitude, the friction coefficient in the dry condition reaches approximately a constant coefficient of 0.30 after 100 sliding cycles. In the PBS condition, the friction coefficient stabilizes at 0.60 after 5,000 cycles. These constant friction coefficients were then used for the dry and PBS conditions in the simulations of the present work.

To simulate fretting wear in a two dimensional head and neck model, an algorithm that had been previously verified against experimental results of Ding [16] (Section 2.1.) was used. This model was used to simulate the fretting wear process for four million cycles. In order to reduce the computation cost, an adaptive wear simulation (Ding, Leen et al. 2004) was used which assumes that the wear rate remains constant during a pre-determined number of cycles (ΔN). After several attempts to find the most optimized ΔN, it was found that the effect of ΔN is not the same at different stages of the simulation. Due to the head-neck junction geometry (proximal and distal contact types with positive and negative angular mismatches, respectively (Kocagöz, Underwood et al. 2013)), at the beginning of the simulation, there are large contact stresses at the small contacting area which cause the effect of ΔN to become more significant. During the process of fretting wear, the contact area gradually increases and as a result the contact stresses reduce. Hence, in this model, the ΔN factor was varied during the fretting process. The optimized ΔN factors that were used in the simulations are shown in Figure 4.6.

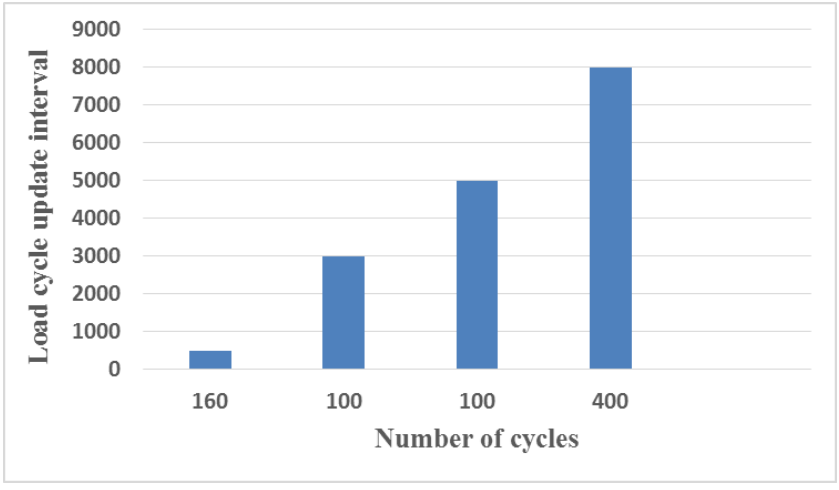

Figure 4.6– Load cycle update interval, ΔN, versus number of cycles in which ΔN is applied.

4.5 Optimization of load cycle update interval (ΔN) and element size

Figure 4.7 illustrates the verification of the ΔN factors used for different stages of the simulations. In this figure, the difference between the employed load cycle update interval and smaller factors is presented at different stages of the simulation for a model with a proximal mismatch angle of 0.024° (Case 1 in Table 1). No significant differences were observed which could verify the accuracy of the ΔN factor used at each stage.

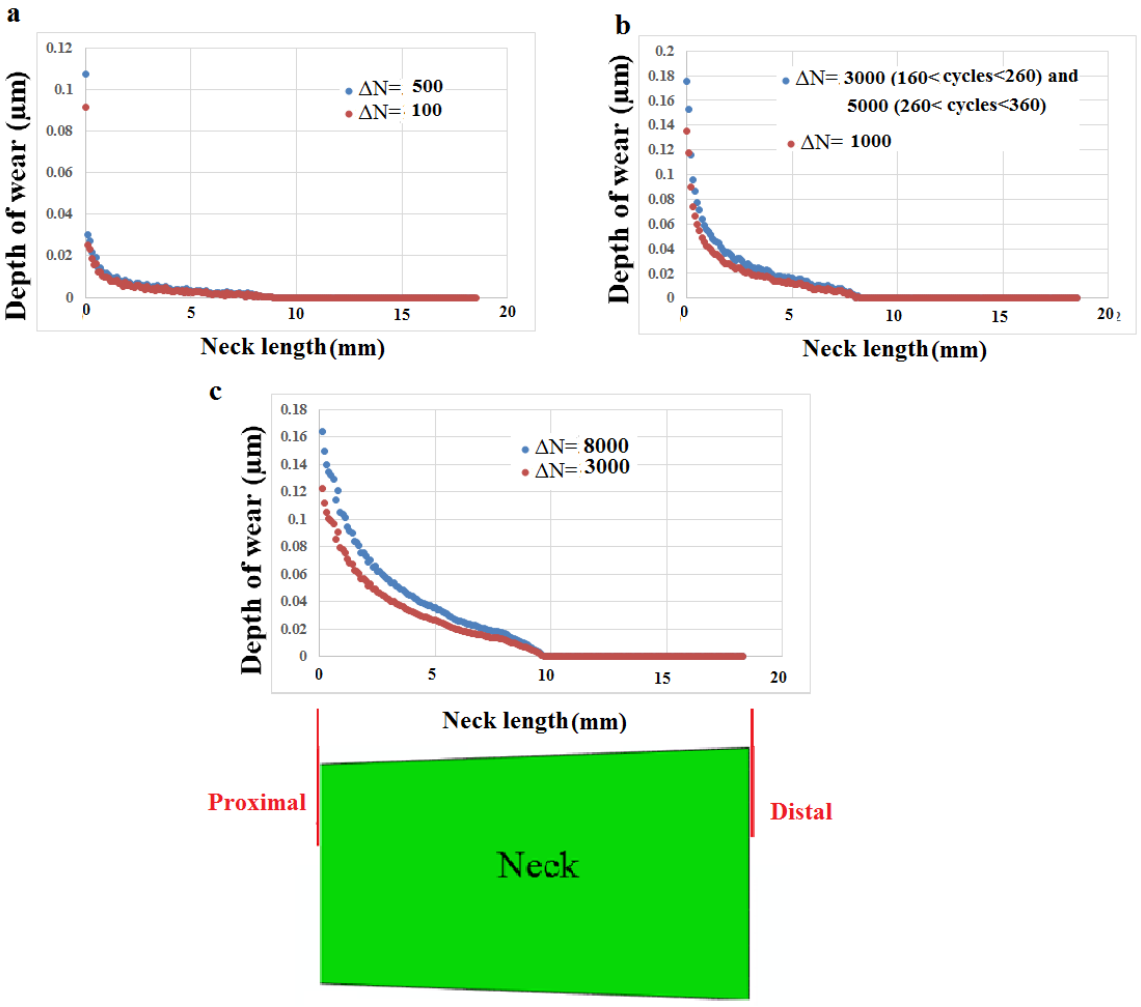

Figure 4.7– A comparison between the used ΔN factor and a smaller factor for case 1: (a) first 160 cycles, (b) between 160 and 360 cycles, and (c) between 360 and 760 cycles.

The size of the elements, especially at the contact area, was refined several times in order to obtain a converged solution. 0.10 mm was obtained as the most suitable element size (the length of the element edge in the critical contact region) to provide mesh-independent results. Figure 4.8 shows the element size effect on the wear depth over the length of the neck when the size is reduced from 0.10 mm to 0.05 mm. A maximum of 10% was found as the difference in the wear depth after 4,080,000 cycles.

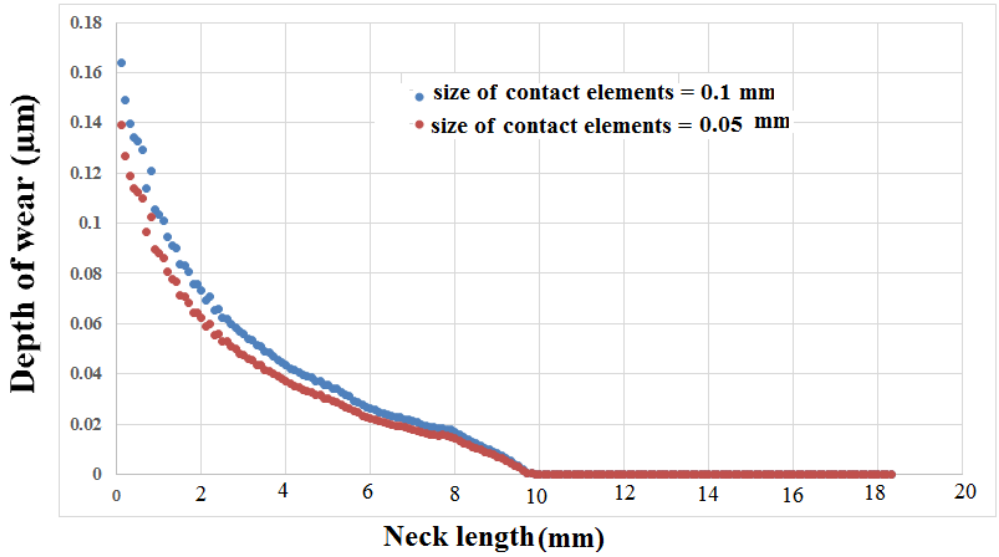

Figure 4.8– A comparison between the wear depth of the neck with two element sizes (the simulations were for Case 1 and after completing 4,080,000 cycles of fretting wear).

4.6 Dry and PBS conditions

Figure 4.9 shows the variation in the lost area of the inferomedial side (left side) of the neck (as specified in Figure 4.5) versus the number of cycles for a perfect contact (zero mismatch angle) for both the dry and PBS conditions. This area loss was computed by calculating the area under the curve of wear depth versus the neck length. As can be seen in Figure 4.8, there are significant differences between the lost areas of the two conditions at different cycles. While the lost area for the dry condition after 4,080,000 cycles was 0.028 mm2, this value for the PBS condition was only 0.011 mm2. This 150% difference between these two conditions reveals that the assumption of dry condition for fretting wear studies is a major simplification. The main differences between these two conditions are in their friction coefficient and wear

coefficient, as specified in Section 2.2. Although friction coefficient can play an important role over the process of fretting wear (by influencing the sliding and shear stress parameters), according to the Archard wear equation, wear coefficient and hardness, together with the normal stress applied to the contact surface contribute directly to the amount of material loss caused by wear (Eqs. 1 and 2). Given the wear coefficient-to-hardness ratio of the material in the PBS condition was significantly lower than that of in the dry condition, the lost area of the PBS is lower in comparison with the dry condition. In order to develop more realistic simulations and avoid the major simplification of the dry condition, the fretting wear simulations of the head-neck junction with varying mismatch angles were further analysed only for the PBS condition in this study.

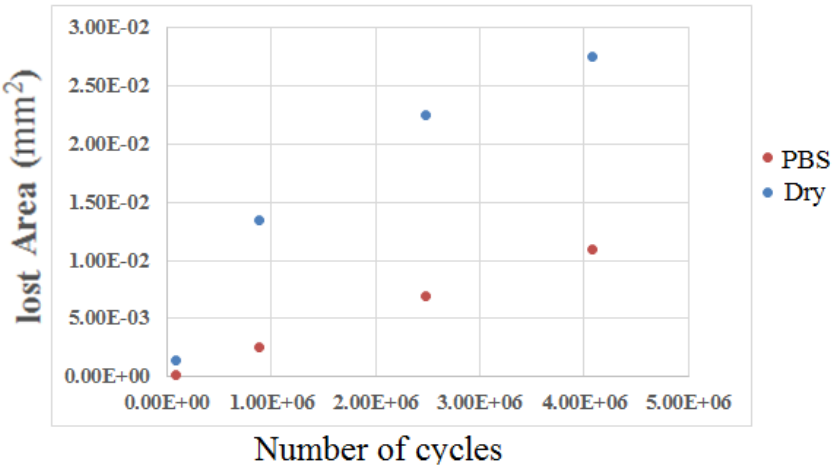

Figure 4.9– Area loss versus number of cycles for both dry and PBS conditions.

4.7 Summary

An adaptive finite element simulation was developed to predict fretting wear in a head-neck taper junction of hip joint implant through a two dimensional (2D) model and based on the Archard wear equation. This model represents the most critical section of the head-neck junction which was identified from a 3D model of the whole junction subjected to one cycle of level gait loading. In addition, the model was used to explore the influence of the junction environment (dry and phosphate buffered solution (PBS) conditions) with comparing the fretting wear behaviour of the head-neck junction in both conditions. The fretting wear model

developed in this work can be used to investigate the influence of assembly force, material combinations and other design parameters (e.g. head size) on the material loss. Moreover, in this model, loading of the other daily activities can be applied to the taper junction. This model will be used in the next two chapters to investigate the influence of the angular mismatch and assembly force on the fretting wear process and the volume of lost material in the head-neck junction.

Chapter 5 The influence of taper angle mismatch on material loss

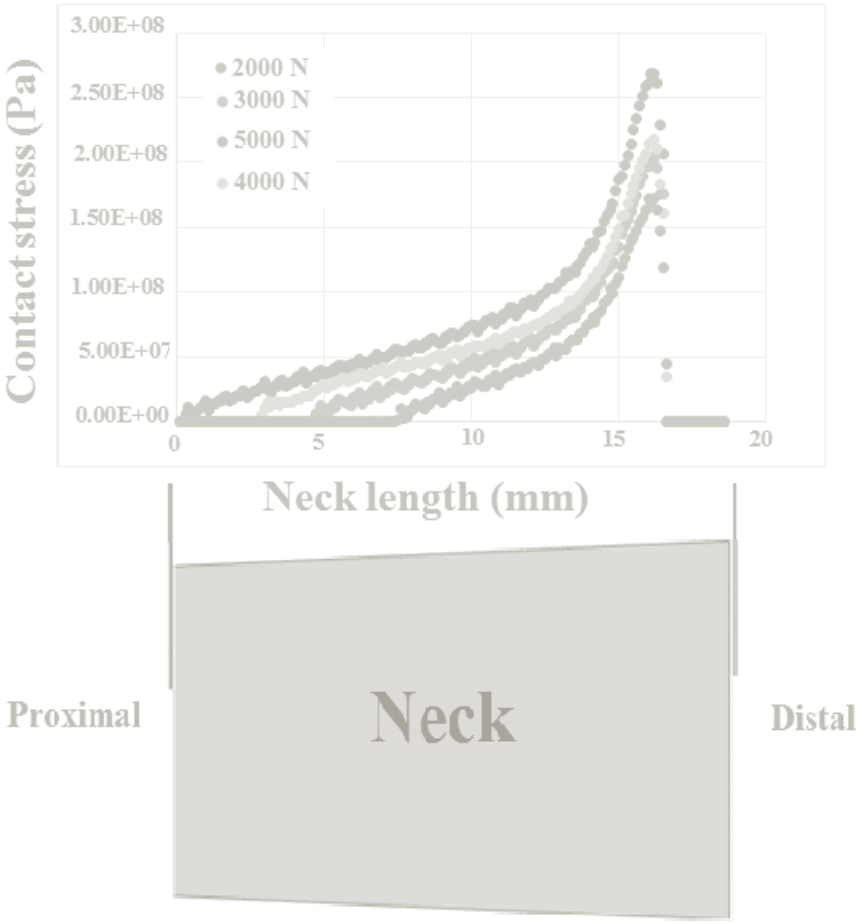

This chapter is based on the following publication:

Fallahnezhad, K.; Oskouei, R.H.; Badnava, H.; Taylor, M. An adaptive finite element simulation of fretting wear damage at the head-neck taper junction of total hip replacement: The role of taper angle mismatch. *Journal of the Mechanical Behavior of Biomedical Materials* **2017**, *75*, 58-67.

5.1 Overview

As was pointed out in the first chapter, the angular mismatch plays an important role in the mechanical behaviour of the head-neck junction. Based on the studies developed by previous researchers and the outcomes of the second chapter of this work, mismatch angle can significantly affect the contact length, contact pressure, relative micro-motion and shear stress at the interface of the head-neck junction. However, the influence of the mismatch angle on the fretting wear process and material loss of the head-neck junction is still unknown. In this chapter the fretting wear model, developed in the previous chapter, was used to investigate such an influence.

5.2 The influence of mismatch angle on material loss

The fretting wear model developed in the previous chapter was used to investigate the effect of mismatch angle on the fretting wear mechanism and the lost material at the critical section of the junction. Five different cases were investigated as given in Table 1. As mentioned previously, the angular mismatch of 0.024° was used according to the experimental measurements of the same CoCr-CoCr taper junction presented by Rehmer et al. (Rehmer, Bishop et al. 2012). Moreover, Donaldson et al. (!!! INVALID CITATION !!! (Donaldson, Coburn et al. 2014)) studied a range of angular mismatches between 0° to 0.2° in both proximal and distal contacts. Another mismatch angle of 0.124° was chosen in this work to represent approximately twice their standard deviation. Hence, a junction with an angular mismatch of 0.124° was also modelled for both the proximal and distal contact situations. The head and neck, in all cases, were assembled with an assembly force of 4 kN and then subjected to F_Y and F_Z force components, as illustrated in Figure 5.3b. A PYTHON code together with a MATLAB code were developed to compute the lost material in the form of worn area from the contacting surfaces at various number of cycles of walking activity (up to 4,080,000 cycles) as well as depth of wear over the length of the neck for each case.

Table 5.1 – Type of contact in the head-neck junction, and mismatch angle for five different cases studied in this work.

Case	Type of contact	Mismatch angle between the head and neck
1	Proximal	0.024°
2	Proximal	0.124°
3	Perfect	0°
4	Distal	0.024°
5	Distal	0.124°

5.3 Contact pressure

Figure 5.1 shows the variation in contact stress (pressure) over the neck length of 5 cases at different number of cycles. Generally, it can be seen that the contact pressure decreases with increasing the number of cycles. The maximum magnitude of the contact pressure for cases 1, 2, 4 and 5 decreases from 288 , 604, 159 and 493 MPa at 80,000 cycles to 116, 186, 95 and 130 MPa at 4,080,000 cycles, respectively. For the perfect contact (case 3 with a zero mismatch angle), the contact pressure does not vary significantly over the neck length. The average magnitude of contact pressure for case 3 at 80,000 cycles is approximately 50 MPa which remains almost unchanged after 4,080,000 cycles. The contact pressure graphs can also help to identify the contacting area between the head and neck. It is apparent that where contact pressure is zero, there is no contact between the head and neck. Based on this, Figure 5.2 was produced to show the contact length (summation of both inferomedial and superolateral sides of the interface) versus the number of cycles in all the cases with a mismatch angle. The contact length was found to increase with increasing the number of cycles, in general. The interesting point is that in the proximal cases, case 1 which has the smaller mismatch angle was more sensitive to the number of cycles compared with case 2. In contrast, for the distal cases, case 5 which has the bigger mismatch angle was more sensitive to the number of cycles.

5.4 Micro-motion

Figure 5.3 shows the relative micro-motion between the head and neck after 80,000 and 4,080,000 cycles at areas with non-zero contact pressures. For all the cases, the micro-motion increases from the proximal side to the distal side. Case 2 had the largest micro-motions in comparison with the other cases with a range of 0.54 - 1.65 μm. It can be understood from Figure 5.3 that the dependence of cases 2, 3 and 4 on the number of cycles was insignificant, while cases 1 and 5 were more dependent on the number of cycles. The maximum difference between case 1 (at 80,000) and case 1 (at 4,080,000) was 0.18 μm and this was 0.1 μm for case 5 (at 80,000) and case 5 (at 4,080,000).

Number of cycles	Left side	Right side
80,000	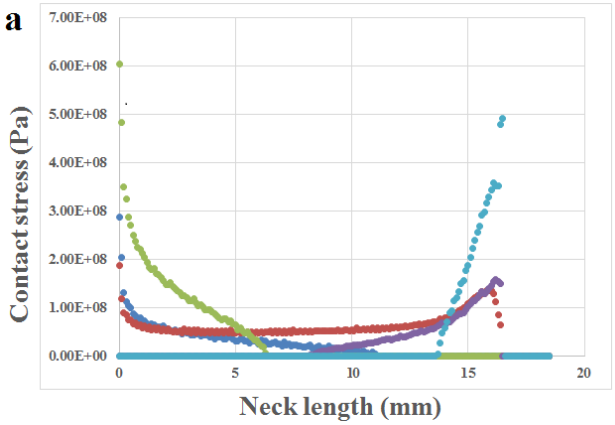	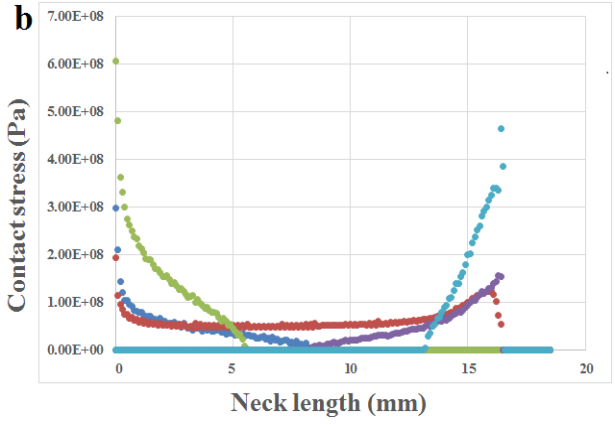
880,000	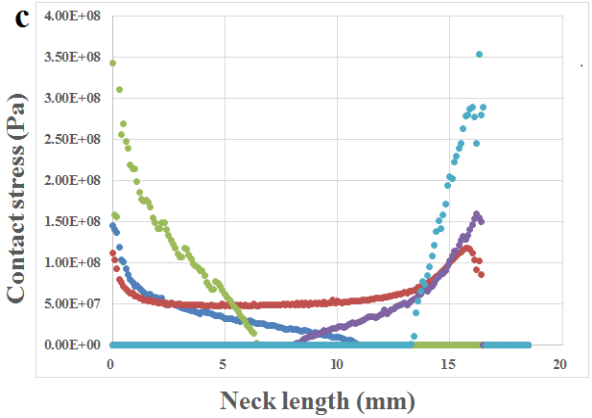	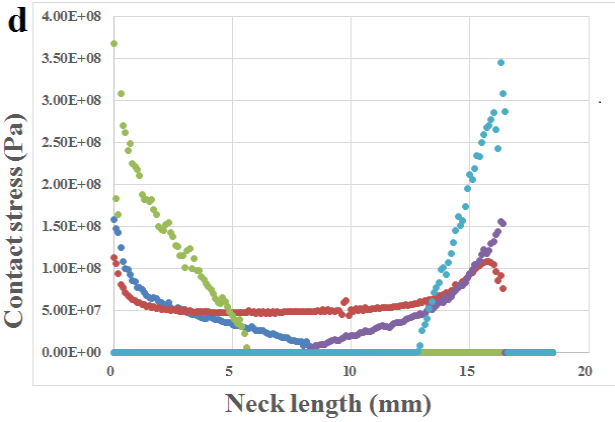

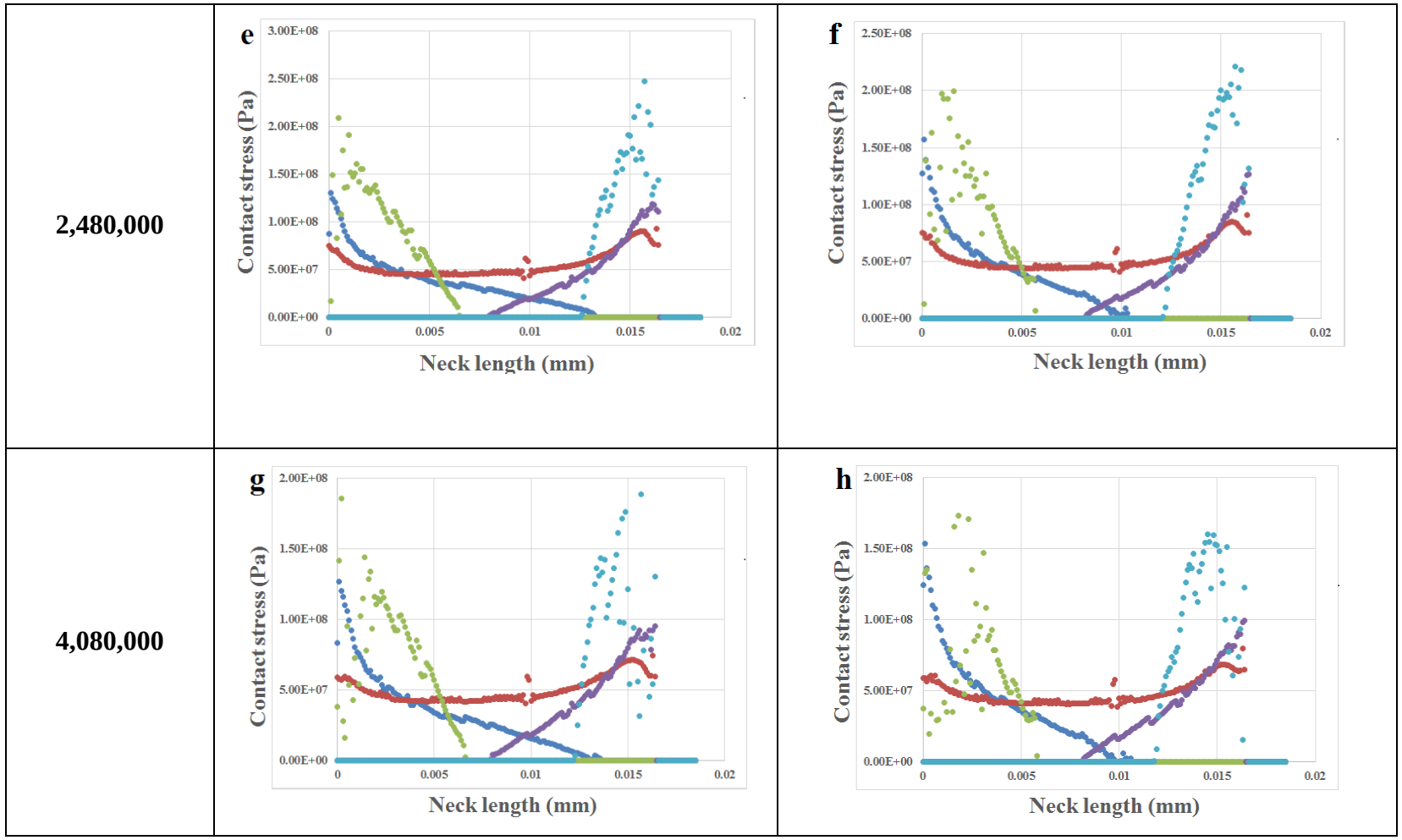

Figure 5.1– Contact stress in neck versus the neck length (inferomedial and superolateral sectors) for 5 cases after different number of cycles (a-f).

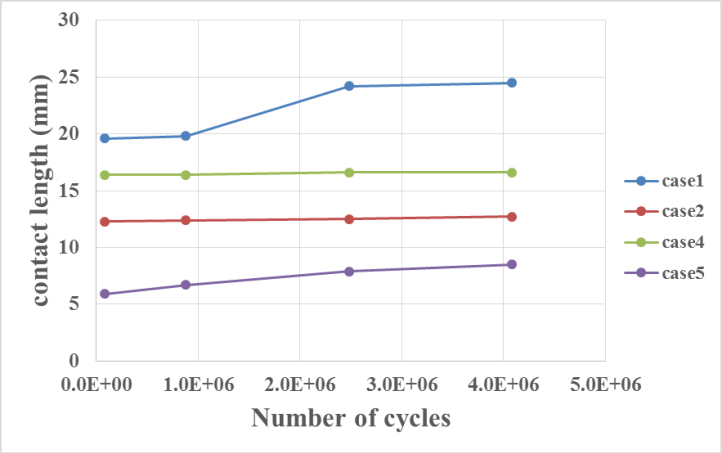

Figure 5.2– Contact length (summation of both inferomedial and superolateral sectors of the interface) versus number of cycles.

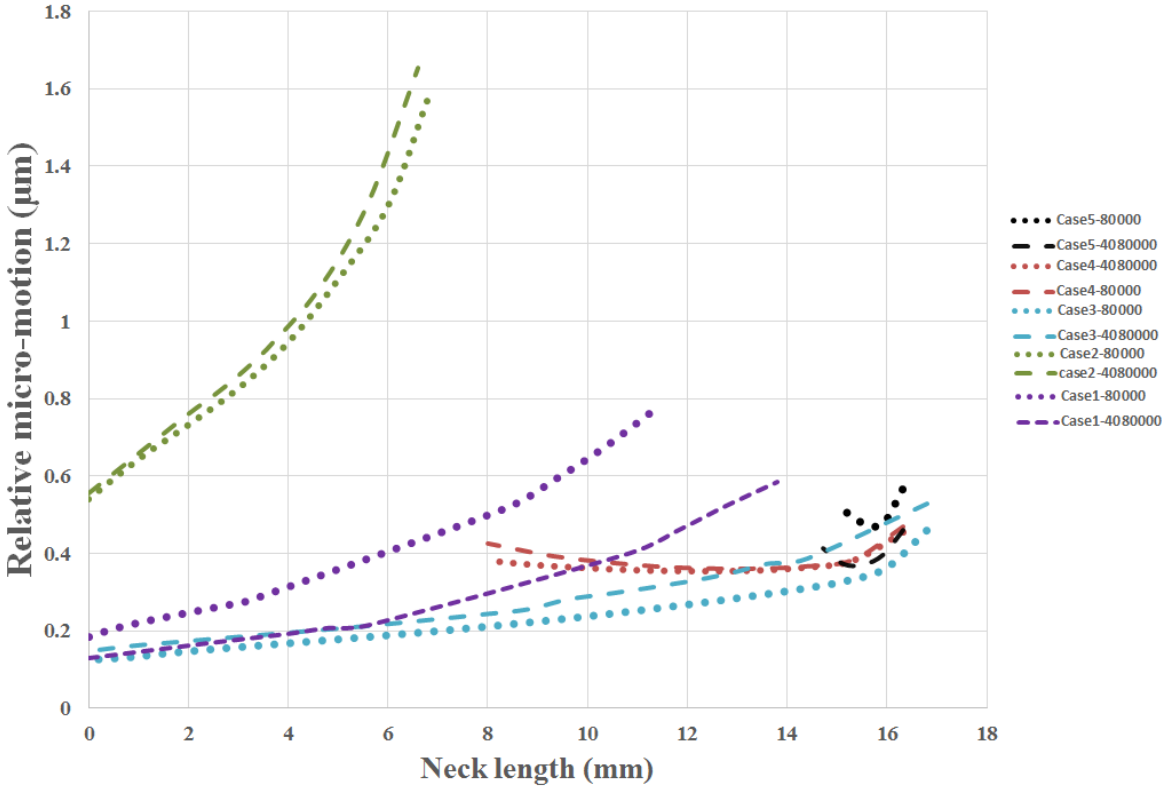

Figure 5.3– Relative micro-motion between the head and neck over the neck length for 5 different cases after 80,000 and 4,080,000 cycles.

5.5 Area loss

The lost areas in the neck and head versus the number of loading cycles are shown in Figure 5.4. It is evident that the trend of the lost area over cycles is almost linear for all the studied cases. The values of the lost area for different cases and at different cycles are almost equal in both the head and neck. Furthermore, Figure 5.4 indicates that with increasing the mismatch angle, the lost area increases in both distal and proximal contacts. For instance, when the proximal mismatch angle increases from 0.024° to 0.124° (cases 1 and 2) the lost area increases from 5.40E-03 mm^2 to 1.86E-02 mm^2 in the neck. This increase is from 4.30E-03 mm^2 to 1.17E-02 mm^2 when the distal mismatch angle increases from 0.024° to 0.124° (cases 4 and 5). These results reveal that the mismatch angle has a significant effect on the amount of material loss. According to Figure 5.4, it can be also understood that the cases with proximal mismatch angles have larger levels of lost area in comparison with the cases with distal mismatch angles. After 4,080,000 cycles, the lost area in the neck and head for case 2 was 1.86E-02 and 1.92E-02 mm^2, respectively. While these are 1.17E-02 and 1.14E-02 mm^2 for case 5. Such a difference can also be seen between cases 1 and 4. The results showed a total area loss ranking (from lowest to highest) of cases 4, 1, 3, 5 and 2 suggesting that the proximal contact with 0.124° had the highest total area loss and the distal contact with 0.024° offered the lowest total area loss.

Figure 5.5 and 14 shows the effect of mismatch angle on the rate and location of fretting wear (at different number of cycles) in the neck. Very similar depth of wear results and patterns are also observed for the head at the same number of cycles (Figure 5.6). These graphs not only help to compare the wear depth at different cases, but also show the location of the wear at the interface. It can be seen that the wear depths in case 2 (maximum 5.39 μm) and case 5 (maximum 3.36 μm) that have the bigger mismatch angle (0.124°) are significantly higher than that of in case 1 (maximum 1.15 μm) and case 4 (maximum 1.77 μm) with the smaller mismatch angle (0.024°).

5.6 Stress distribution

The von Mises stress distribution in the neck component for cases 2, 3 and 5 after 80,000, 880,000, 2,480,000 and 4,080,000 cycles is shown in Figure 5.7. This figure shows that the equivalent stresses generally decrease with increasing the number of loading cycles. It is apparent that cases 2 and 5 are more critical in comparison with case 3 in aspect of the stress magnitude. In case 2, the maximum equivalent stress decreased from 600 MPa (at 80,000 cycles) to 312 MPa (at 4,080,000 cycles). This reduction was 539 to 390 MPa for case 5 and 200 to 71 MPa for case 3. The most critical area for case 2 was the edge of the proximal side which also had the maximum contact stress (Figure 5.7). For case 5, the most critical area was the distal edge in which there are maximum contact stresses between the head and neck (Figure 5.7). For case 3, the critical area was a combination of two previous cases. Although there is a perfect contact between the head and neck, the edge of the proximal and distal sides were the most critical regions.

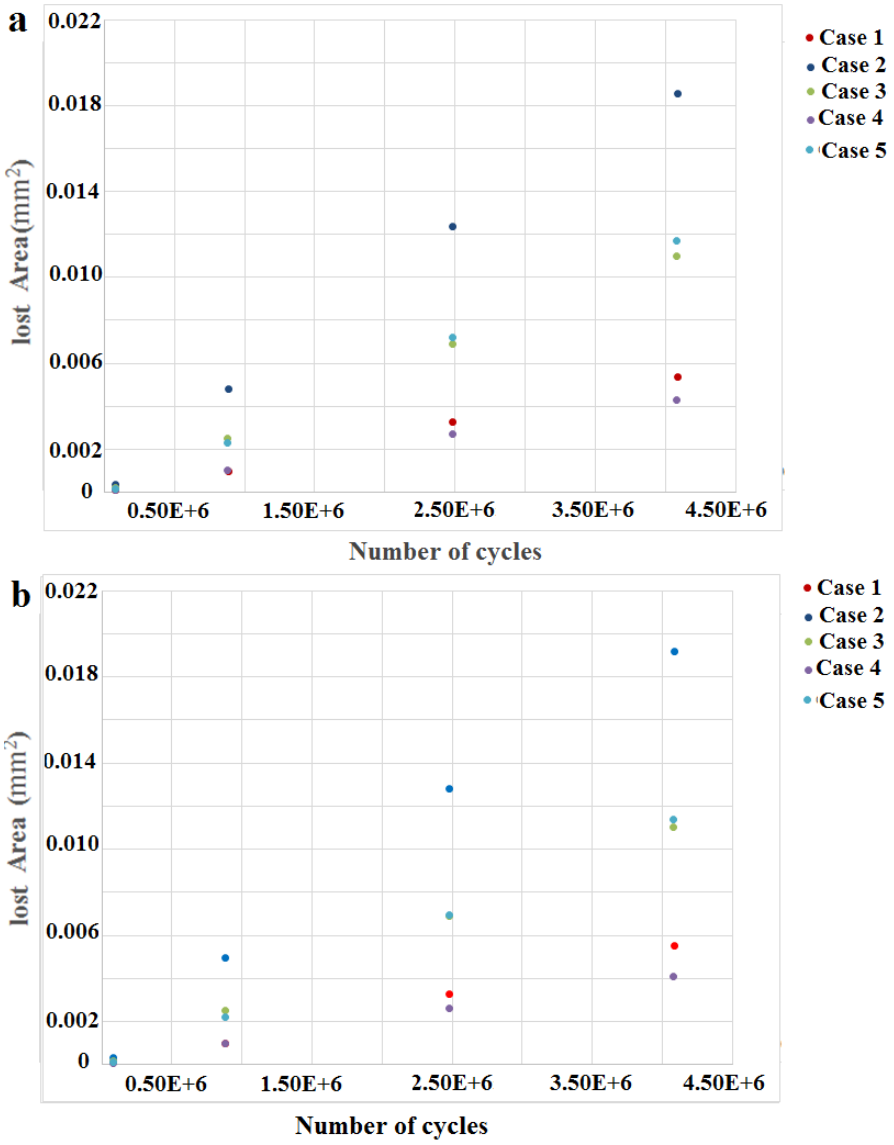

Figure 5.4– Lost area versus number of cycles for different cases: (a) neck, and (b) head.

Number of cycles	Inferomedial sector	Superolateral sector
80,000	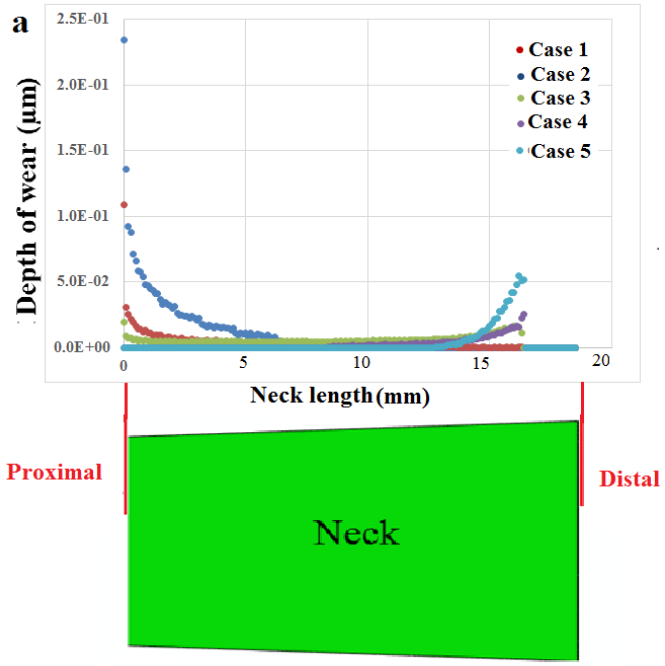	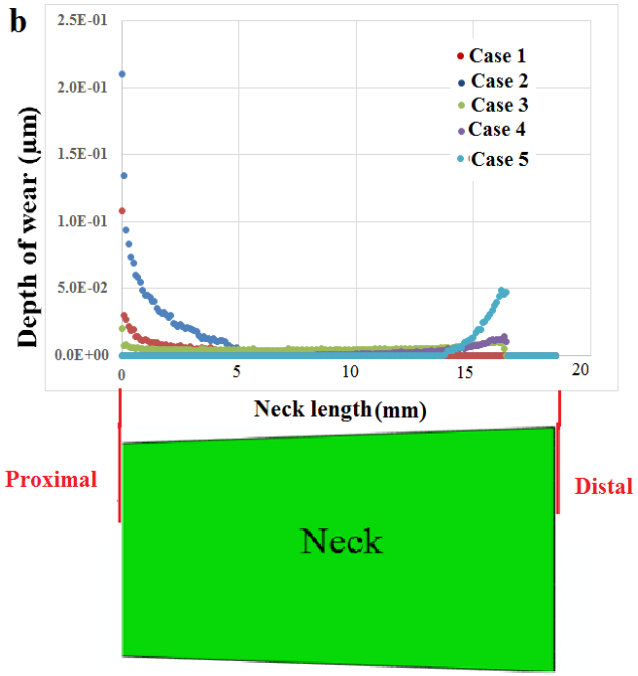

880,000	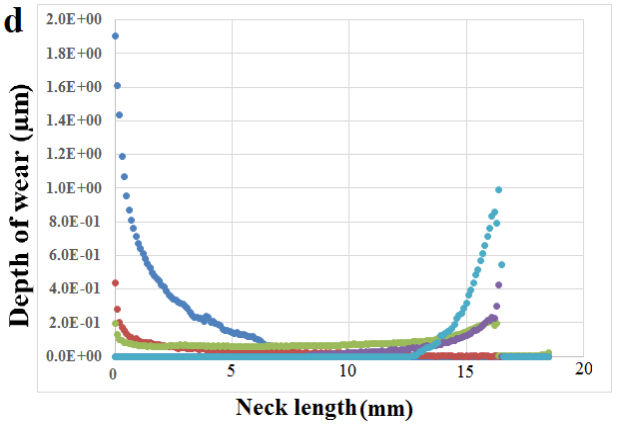	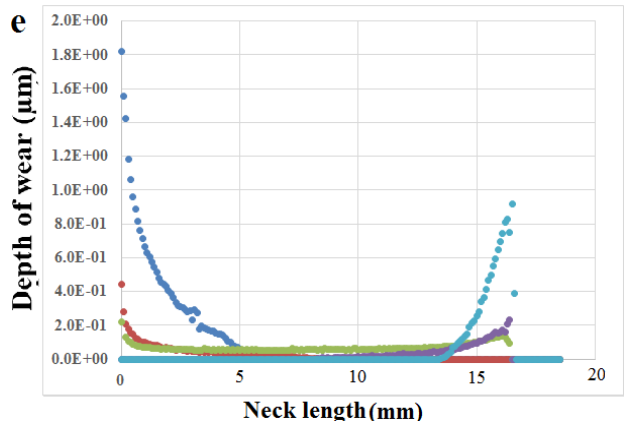
2,480,000	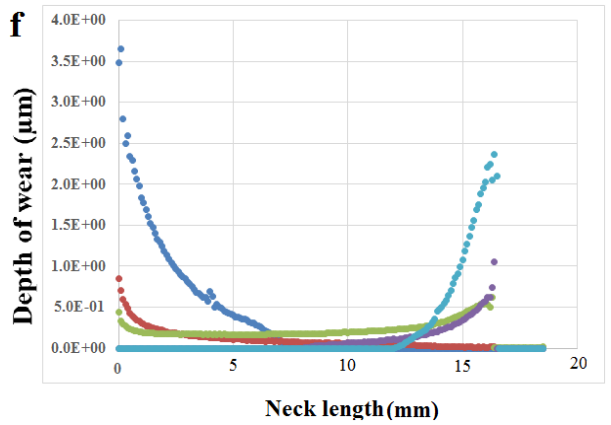	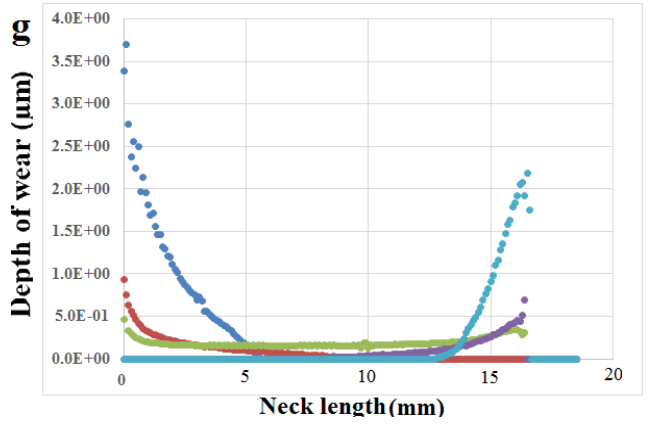

4,080,000	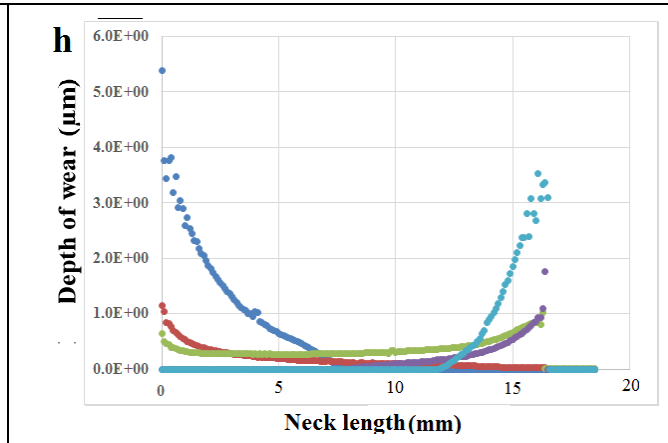	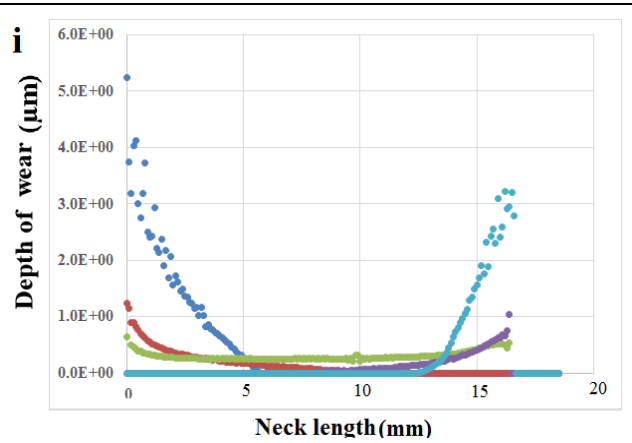

Figure 5.5– Fretting wear in neck showing depth of wear versus the neck length at different number of cycles for both the inferomedial and superolateral sectors of the neck (a-f).

Number of cycles	Left side	Right side
80,000	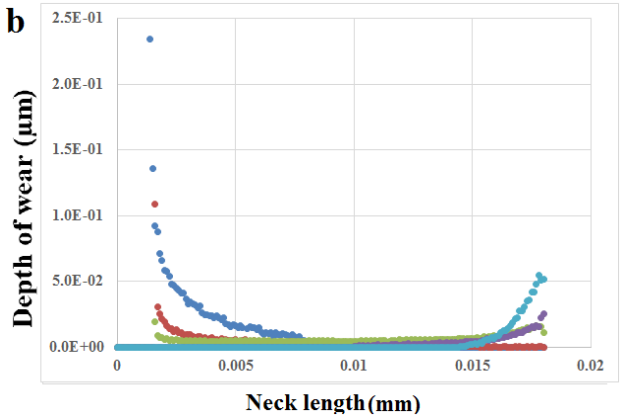	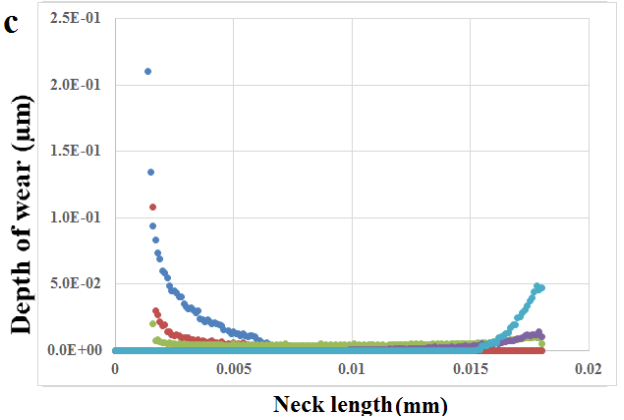
880,000	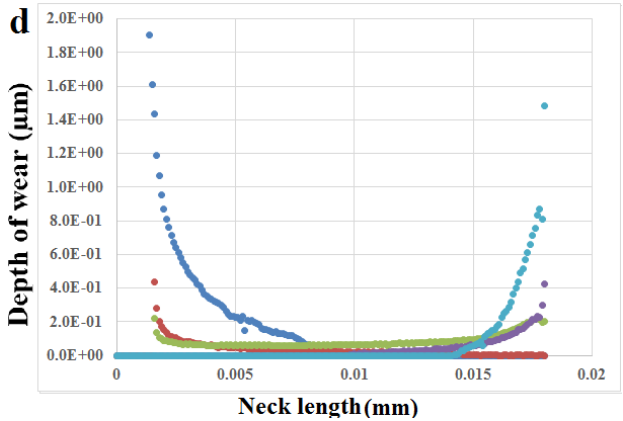	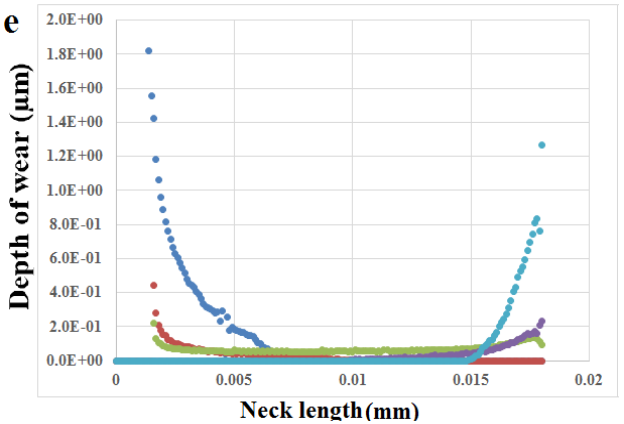

2,480,000	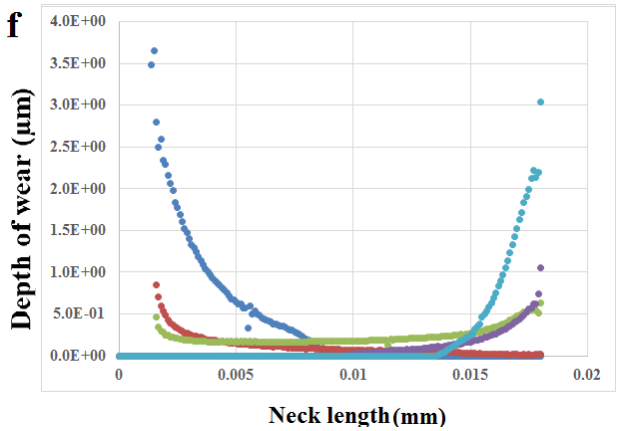	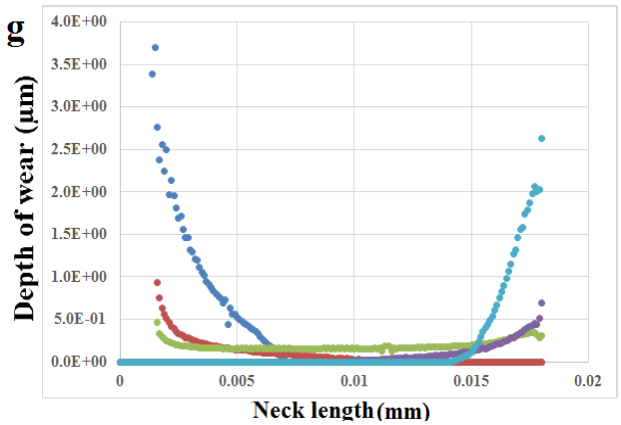
4,080,000	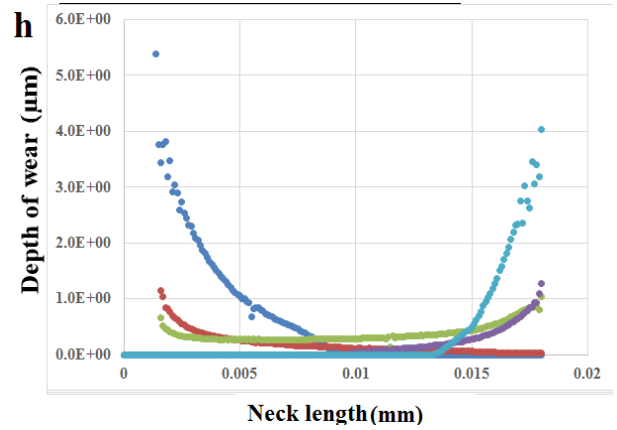	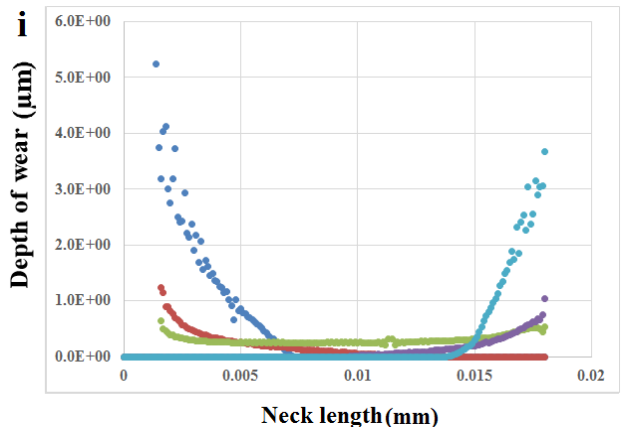

Figure 5.6– Fretting-wear in head (a) Area lost versus number of cycles for different cases, (b), (c), (d), (e), (f), (g), (h) and (i) Depth of wear versus neck length for different number of cycles.

Number of cycles	Case2	Case3	Case5
80,000	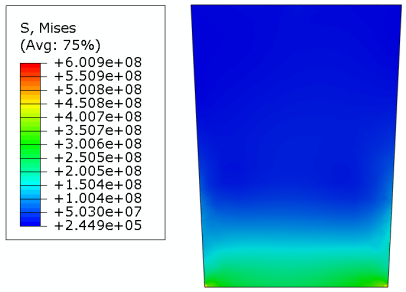	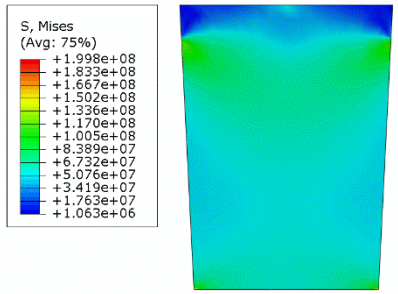	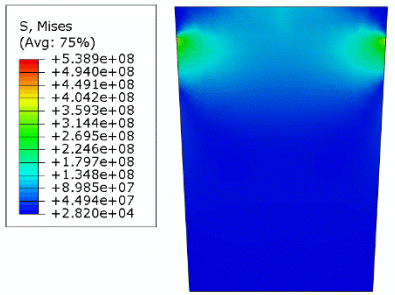
880,000	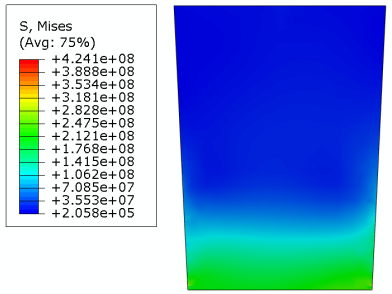	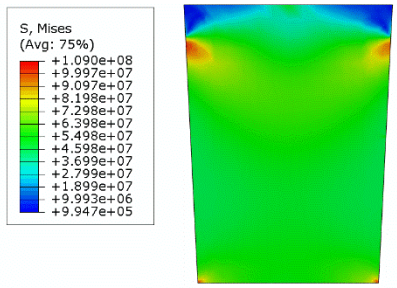	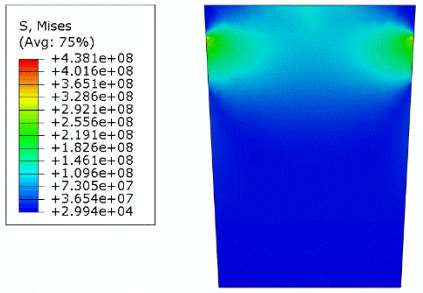
2,480,000	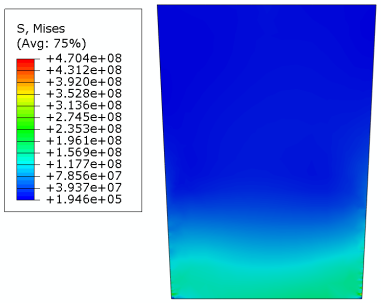	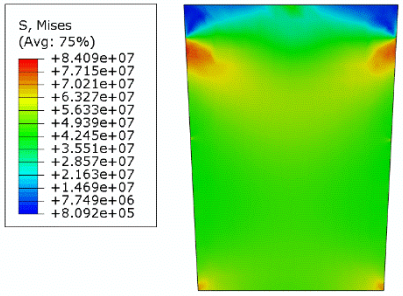	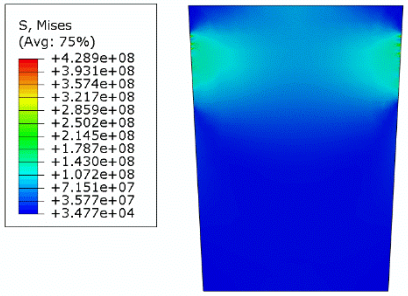

4,080,000	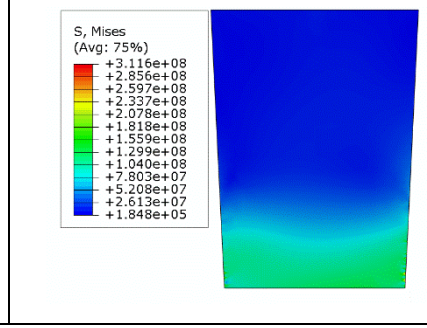	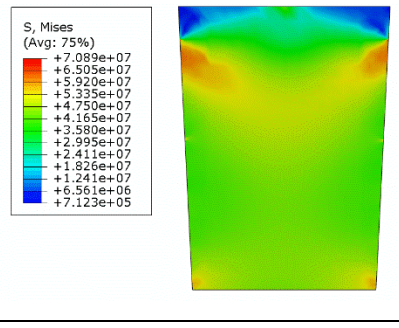	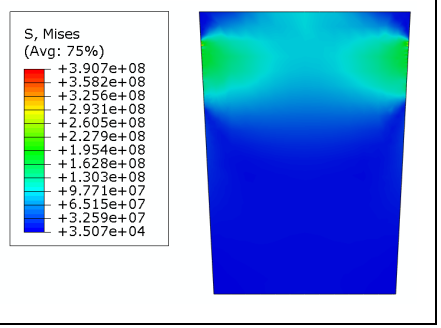

Figure 5.7– The von Mises stress distribution in the neck for cases 2, 3 and 5 at different number of cycles (stresses are in Pa).

5.7 Discussion

Head-neck taper junctions of hip implants are known to experience fretting wear and corrosion under physiological loading in the body (Goldberg, Gilbert et al. 2002, Higgs, Hanzlik et al. 2013). Due to the effect of fretting wear, particulate debris (in the range of micro- to nano-meters) have been detected in the surrounding tissues (Bitounis, Pourchez et al. 2016). At revision surgery, particularly in cases with large amounts of metallic wear, signs of fluid collection, soft tissue damage and pseudotumours can be clearly seen around the implant (Chana, Esposito et al. 2012, Fricka, Ho et al. 2012). Chana et al. (Chana, Esposito et al. 2012), based on a retrieval analysis, reported that the angular mismatch in a taper junction facilitated the release of metal debris and consequently pseudotumour formation requiring revision. Given the significance of angular mismatch, in this study, an adaptive FE model was implemented to simulate the process of fretting wear and material loss in a CoCr-CoCr head-neck junction with various taper angle mismatches and in a phosphate buffered solution (PBS) condition.

The wear results revealed that the angular mismatch between the head and neck components plays an important role in the location and depth of wear damage as well as the degree of material loss. In addition, the type of taper contact (proximal and distal) was found to play a role in the wear process and material loss be effective. It is noted that the assembly force required to connect the head and neck was kept constant as 4 kN for all the models. Also, the junction was subjected to two dominant load components of the level gait cycle, the axial and lateral loads. The lowest lost areas for both the head and neck were generated by case 4 (distal with 0.024°) and then case 1 (proximal with 0.024°). However, the highest worn areas were generated by case 2 (proximal with 0.124°) and then case 5 (distal with 0.124°). These findings showed that in both the studied mismatch angles, distal contact offered lower lost areas in comparison with the proximal contact. Importantly, the smaller mismatch angle (0.024°) resulted in lower lost areas (in both distal and proximal contacts) when compared to the bigger angle (0.124°). Case 3 (perfect contact with zero mismatch angle) was found to have an intermediary position between the distal and proximal contact cases with the two studied mismatch angles. According to the Archard equation, two parameters that can affect the wear damage are contact stress and amplitude of sliding (relative micro-motion between the head and neck in this study). Figure 5.9 shows that cases 2 and 5 with the mismatch angle of 0.124°

have the highest contact stresses during the process of fretting wear. Then, cases 1 and 4 with the mismatch angle of 0.024° have higher contact stresses compared to case 3 with zero mismatch angle. Case 2 has also the largest micro-motions which consequently results in the largest material loss.

The other important parameter that should be taken into account, while investigating the fretting wear damage, is the contact length. Case 3, with a perfect contact between the head and neck, has the longest contact length between all cases. Hence, in spite of having significantly lower contact stresses compared with case 5, the lost area for these two cases during the fretting wear process is almost the same. The results related to cases 1 and 4 illustrate the effect of contact length on the fretting wear damage. Case 1 and 4 have higher contact stresses compared with case 3. Case 4 has even larger micro-motions in comparison with case 3, over 4,080,000 loading cycles. However, a perfect contact length has caused case 3 to have a greater lost area compared to cases 1 and 4. Generally, it can be concluded that fretting wear damage does not have a linear relationship with the taper mismatch angle. There seems to be an optimum mismatch angle for both the proximal and distal contact types in which the fretting wear damage would be minimum. This appears to be biased towards a distal contact type; however, further research is required including a new series of simulations with systematically selected geometries offering a wide range of taper angle mismatches and a set of well-designed *in-vitro* experiments for validation.

Contact pressure, relative micro-motion and contact length were found as the main parameters that contribute to the amount of material loss. These parameters can be changed and controlled by varying the mismatch angle at the taper junction. The results of this work (Figures 5.12 and 13) revealed that taper designs with distal contact are more resistant to the fretting wear damage in comparison with proximal contact designs provided they both have the same angular mismatch. Although the average magnitude of contact stresses for the proximal and distal contacts with the same mismatch angle are very close (Figure 5.8), proximal cases have greater micro-motions and longer contact lengths which cause them to be more vulnerable against

fretting wear. The fretting wear model developed in this work can be used to investigate the influence of assembly force, material combinations and other design parameters (e.g. head size) on the material loss. Moreover, in this model, loading of the other daily activities can be applied to the taper junction. Such future investigations together with the results provided in this work can help manufacturers move towards implant designs that are more resistant to fretting wear. Furthermore, future studies can provide surgeons with more information about a range of assembly forces and selection of material combinations that may generate less fretting wear and material loss in the body.

5.8 Summary

The 2D model developed in the Chapter 4 was used to investigate the effect of angular mismatch between the head and neck components on the material loss and fretting wear process over 4 million gait cycles of walking. Generally, junctions with distal angular mismatches showed a better resistance to fretting wear. The largest area loss in the neck after 4 million cycles of loading was 1.86E-02 mm^2 which was found in the junction with a proximal mismatch angle of 0.124º. While, the minimum lost area (4.30E-03 mm^2) was found in the junction with a distal angular mismatch of 0.024º. Contact stress, amplitude of sliding and contact length were found as the key parameters that can influence the amount of material loss and the process of fretting wear damage. These parameters vary over the fretting wear cycles and are highly dependent on the type and magnitude of the taper angle mismatch. This study also showed that lost area does not have a linear relationship with the mismatch angle of taper junction.

Chapter 6 The influence of assembly force on the material loss at the head-neck junction

This chapter is based on the following publication:

Fallahnezhad, K.; Oskouei, R.H.; Badnava, H.; Taylor, M. The influence of assembly force on the material loss at the head-neck junction of hip implants in physiological body fluid subjected to cyclic fretting wear. Manuscript being submitted to *Materials*.

6.1 Overview

The mechanical behaviour of the taper connection is dependent on a number of parameters. The material combination used at the taper, as mentioned in the Chapter 2, and the taper mis-match angle (Kocagöz, Underwood et al. 2013, Donaldson, Coburn et al. 2014, Gührs, Körner et al. 2017) can be controlled by the design and the manufacturing process. As the components are assembled intraoperatively, the assembly force is important not only to avoid loosening and diassociation (Georgiou, Siapkara et al. 2006, Rehmer, Bishop et al. 2012) after implantation but also to establish a favourable mechanical environment to minimise fretting. There is variation between manufacturers recommendations on how to impact the femoral head (Ramoutar, Crosnier et al. 2017), from a single light tap to several sharp hammer blows. The impaction forces generated by surgeons can varying significantly, from approx. 300N to in excess of 7500N (Nassutt, Mollenhauer et al. 2006).

To date, the majority of studies (Pennock, Schmidt et al. 2002, Rehmer, Bishop et al. 2012, Scholl, Longaray et al. 2015, Bitter, Khan et al. 2017) investigating the influence of the assembly force have focussed on the dis-association force as the metric to assess the performance of the taper. Assembly forces from 2kN to 15kN have been investigated and a linear relationship with the dis-association force has been reported (Pennock, Schmidt et al. 2002, Rehmer, Bishop et al. 2012). The dis-association force is always lower, varying between 42% (Scholl, Longaray et al. 2015) and 91% (Bitter, Khan et al. 2017) of the assembly force. Rehmer et al (Rehmer, Bishop et al. 2012) reported a similar linear relationship between the assembly force and the twist off torque. Increasing the impaction force has also been shown to increase the contact area (Gührs, Körner et al. 2017) and reduce the micromotion (Dyrkacz, Brandt et al. 2015, Bitter, Khan et al. 2017) between the head and the trunnion. These studies generally suggest that a high assembly force can achieve a high degree of initial stability and fixation in the head-neck junction to more reliably withstand mechanical loads of daily activities without disconnection.

However, the previous studies have not addressed the important question of whether the assembly force has an influence on the material removal by fretting wear over an extended period of time. Bitter et al. (Bitter, Khan et al. 2017) developed a combined experimental and finite element study to analyze the influence of assembly load on the fretting wear mechanism in total hip replacement. They reported a drop in the fretting wear as assembly forces increase. In their experimental results, although they reported the pattern of the wear, they did not calculate the volume of the material loss. They also developed a one cycle FE model for three daily activities. According to the modified version of Archard equation, they used contact pressure and relative micrimotion to produce a wear score parameter. However, their model was not able to track the fretting wear process, over the several cycles of sliding. They concluded that wear is more affected by relative micromotion compared with contact pressure. Using a FE analysis, English et al. (English, Ashkanfar et al. 2015) modelled a CoCr head and a titanium neck with a zero angular mismatch to estimate the material loss and contact pressure at the junction subjected to two million cycles of walking gait loading. This work was extended to explore the influence of assembly force, and they reported that higher assembly forces resulted in lower fretting wear (English, Ashkanfar et al. 2016); however, they still used the critical simplification of zero mismatch angle for the junction in the dry condition. The materials modelled in the previous studies were CoCr and titanium for the head and neck, respectively. Also, the existing taper angle mismatch between the head and neck components has been ignored in the previous fretting wear studies; whereas, the angular mismatch has been found to significantly influence the mechanics of the junction; and therefore, it could have a significant effect on fretting wear as a mechanically driven process. More importantly, the previous FE simulations have assumed a dry condition for the contacting materials of the junction; however, the existence of the body fluid at the interface of the junction may control the frictional and wear characteristics which may then influence the fretting wear behaviour.

In this chapter, the main research objective was to evaluate the effect of assembly force on the material loss and fretting wear process, using the adaptive FE model developed in the third chapter. This work aims to simulate the fretting wear process and predict the material removal

in a CoCr/CoCr head-neck junction through an adaptive finite element modelling approach. To achieve more realistic outcomes, the taper junction was modelled to have a distal contact with a real angular mismatch between the head and neck with the presence of a simulated physiological body fluid.

6.2 Contact pressure and contact length

As shown in Figure 6.1, with increasing the assembly force from 2,000 N to 5,000 N contact pressure increased in magnitude over the length of the neck, and the contacting region between the head and neck (contact length) also increased towards the proximal side of the neck. This confirms that a higher assembly force can further push the neck into the head inducing greater normal contact forces; thereby, larger contact pressures and more engagement between the head and neck surfaces (longer contact). As more loading cycles were applied (increase in the number of cycles), the peak contact pressure decreased in magnitude. The maximum magnitude of contact pressure for cases with assembly forces of 2,000 N, 3,000 N, 4,000 N, and 5,000 N decreased from 206, 257, 265 and 337 MPa at 25,000 cycles to 169, 243, 258 and 294 MPa at 1,025,000 cycles, respectively in the superolateral sector of the neck. These graphs can also help to investigate the contact length between the head and neck. Non-zero contact stresses at any region of the surface indicate that there is contact between the head and neck in that region. After 25,000 cycles, the percentage of the neck which is in contact with the head for cases with assembly forces of 2,000 N, 3,000 N, 4,000 N, and 5,000 N were 48%, 64%, 75%, and 79%, respectively. These total contact lengths remained almost constant after 1,000,000 cycles of fretting wear.

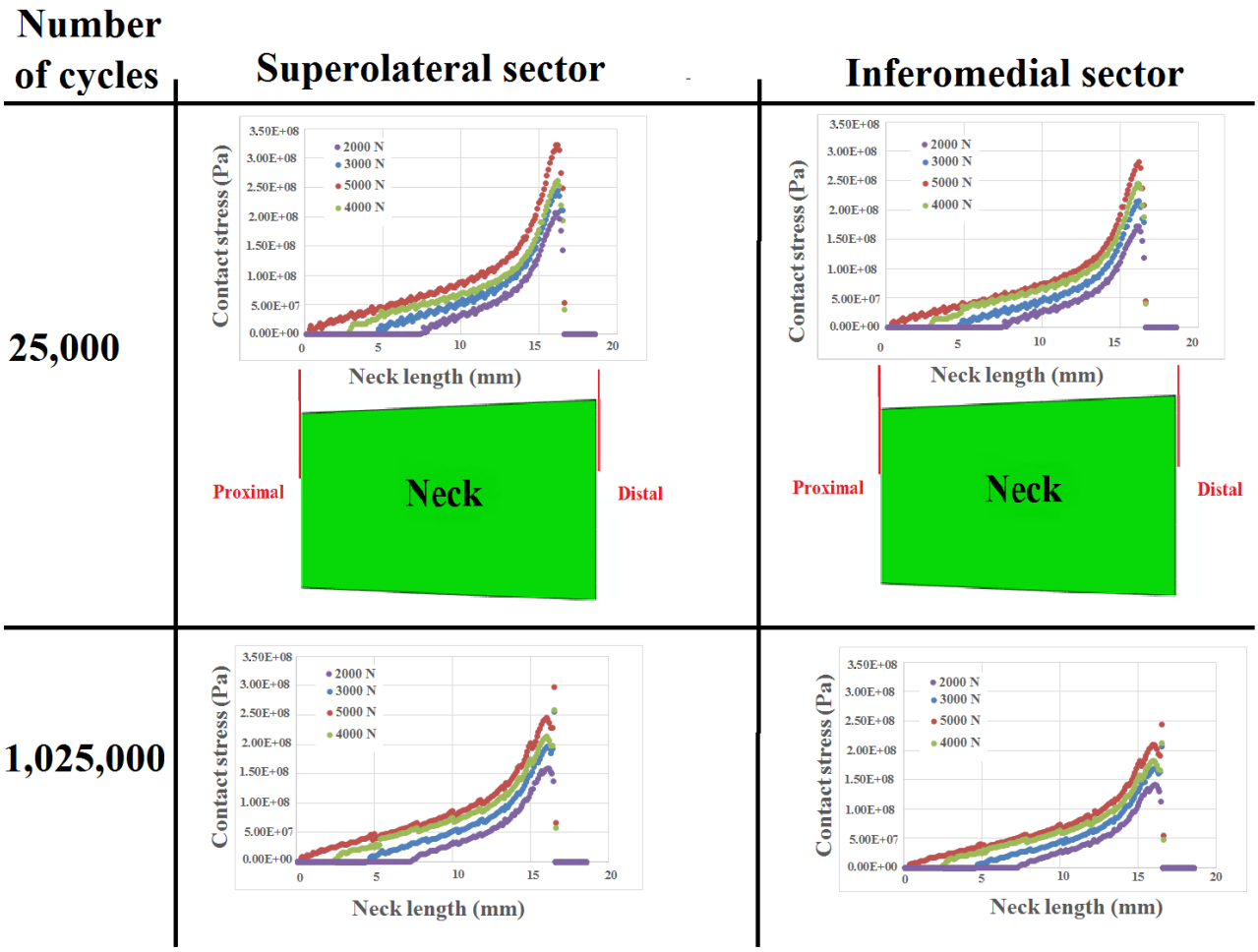

Figure 6.1– Variation of normal contact stress over the neck length in both superolateral and inferomedial sectors under different assembly forces and after 25,000 and 1,025,000 loading cycles.

6.3 Micro-motions

For all the assembly forces, the micro-motion at the contacting interface tends to increase from the proximal side to the distal side (Figure 6.2) and that the magnitude of the micromotion reduces with increasing the assembly force. The junction assembled with 2,000 N had the

largest micro-motions compared to the other cases with a range of 0.41-0.51 µm. There appears to be minimal change in the micro-motion after 1,000,000 load cycles (Figure 6.2).

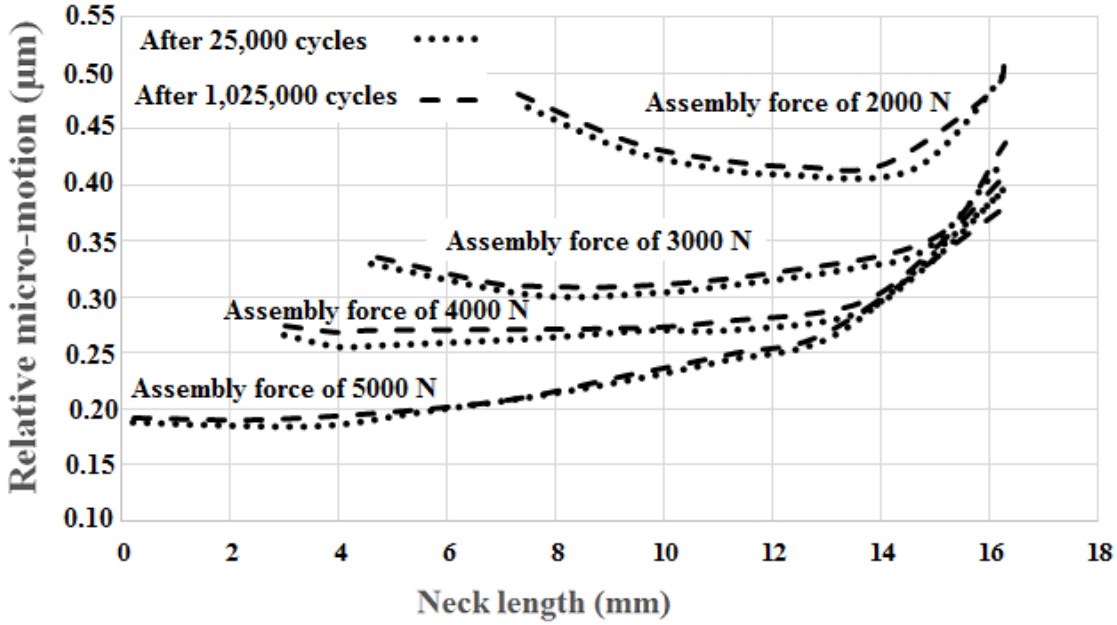

Figure 6.2– Relative micro-motion at the contacting interface over the neck length (superolateral sector) for different assembly forces after 25,000 and 1,025,000 cycles.

6.4 Material loss

Material removal over the neck length was calculated as the total area under the curve of wear depth versus the neck length in both the superolateral and inferomedial sectors. This represents the lost area from the original edges (superolateral and inferomedial sectors) of the 2D model. It can be seen in Figure 6.3 that the trend of the lost area over the number of loading cycles is linear for all of the assembly forces studied. The values of area loss for different assembly forces and at different cycles were almost equal in both the head and neck; and thus, this figure only presents the area losses of the neck. Increasing the assembly force results in an increase in the lost area at the taper junction. For instance, when the assembly force was increased from

2,000 N to 5,000 N, the area loss increased from 5.28E-03 mm^2 to 16.3E-03 mm^2 in the neck after 1,025,000 cycles.

Figure 6.4 shows the effect of assembly force on the rate and location of the fretting wear damage in the form of wear depth (after 25,000, 125000, 625000, and 1,025,000 number of cycles) in the neck. It is noted that very similar depth of wear results were found in the head at the same number of cycles. These graphs can help to compare the wear depth at different assembly forces, and locate the wear damage at the interface. It can be seen that the wear depths in the assembly force of 5,000 N (with a maximum 0.779 µm) was significantly higher than that of in the assembly force of 2,000 N (with a maximum 0.413 µm).

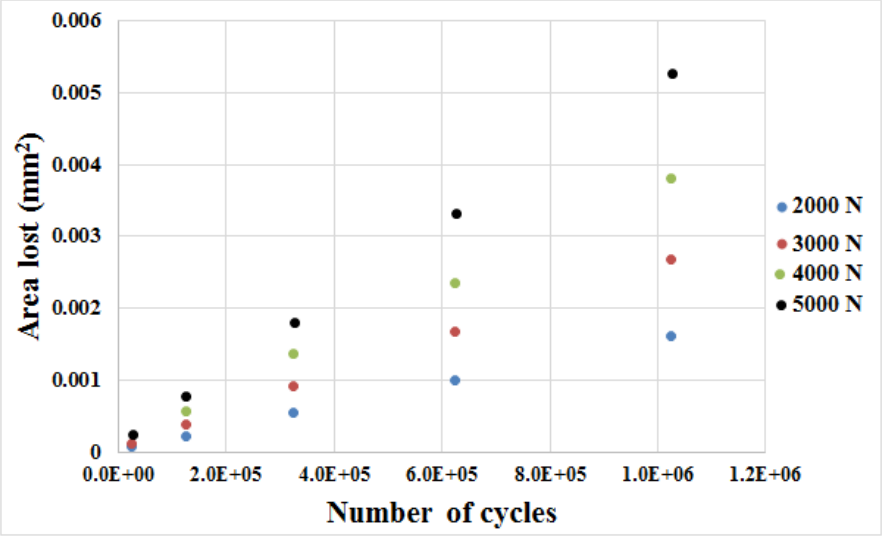

Figure 6.3– Lost area versus number of cycles for different assembly forces

Number of cycles	Inferomedial sector	Superolateral sector
25,000	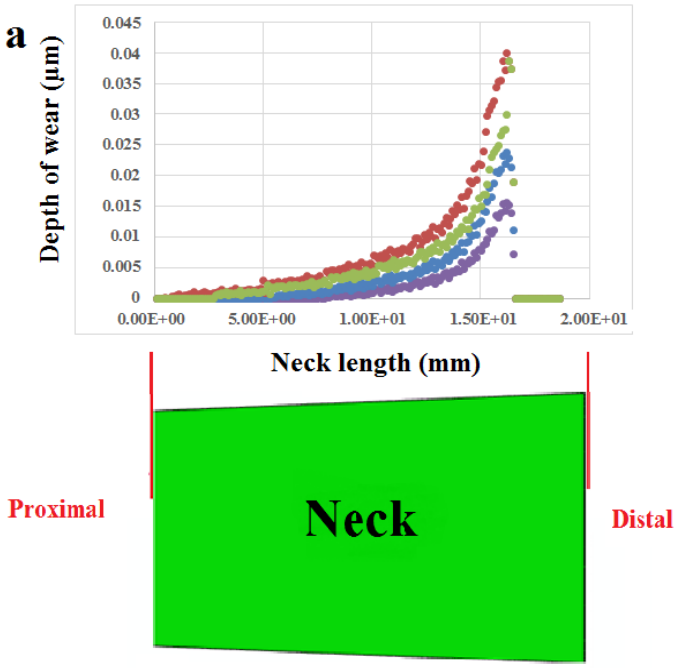	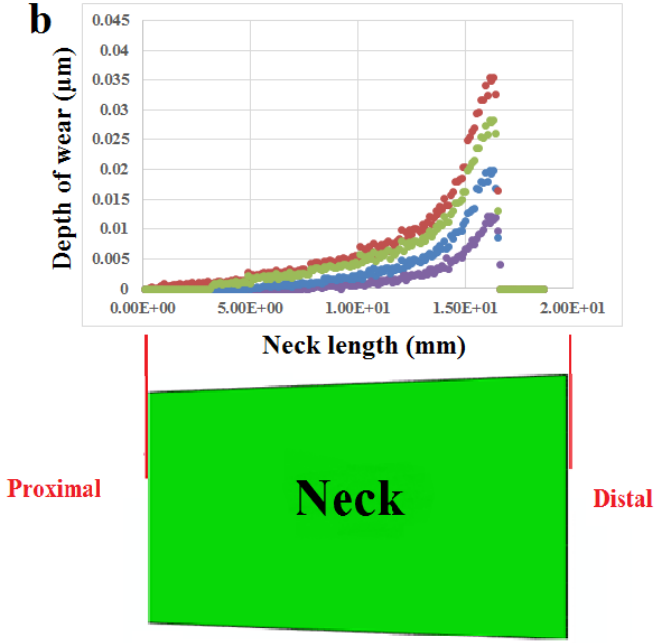

125,000	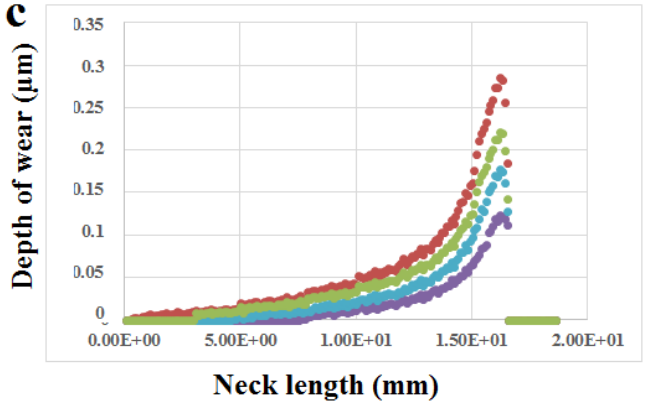	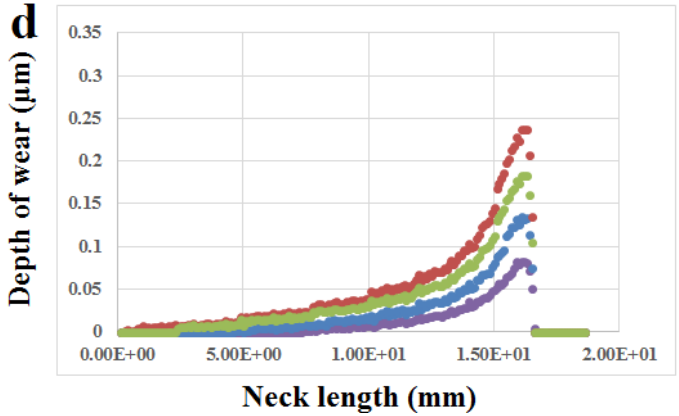
625,000	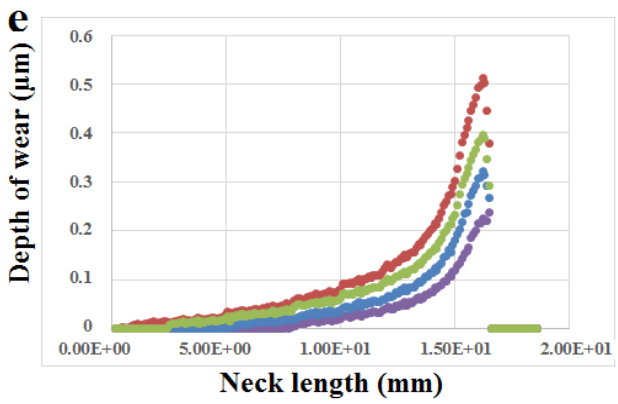	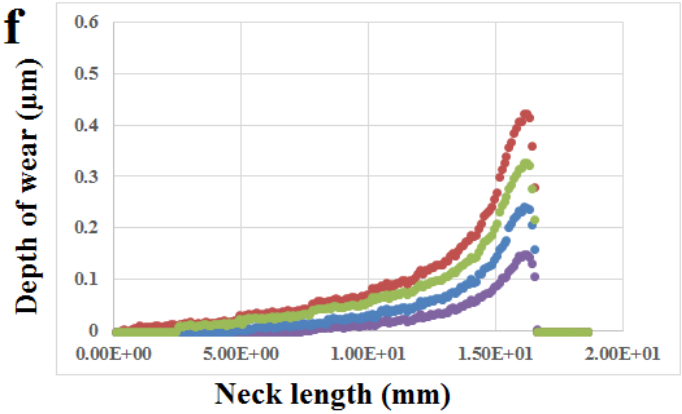

1,250,000	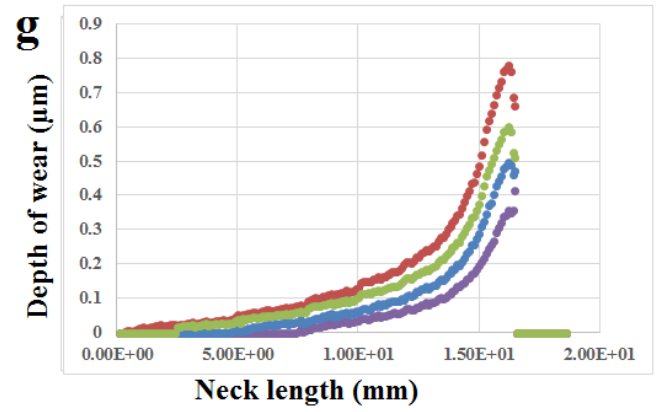	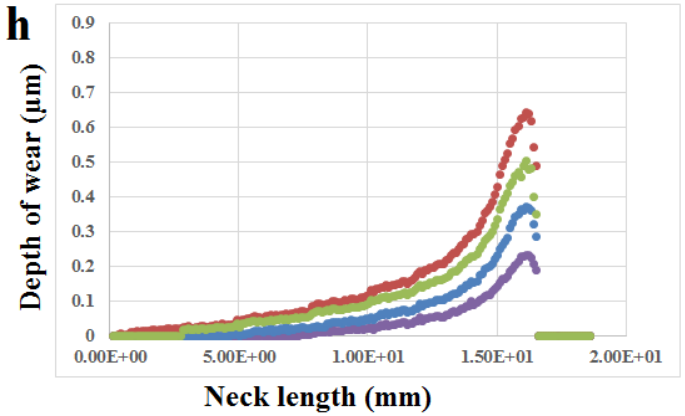

Figure 6.4– Depth of wear over the neck length after (a) and (b) 25,000 cycles, (a) and (b) 25,000 cycles, (c) and (d) 125,000 cycles, (e) and (f) 625,000 cycles, (g) and (h) 125,000 cycles.

6.5 Discussion

In this work, the fretting wear mechanism and material loss were investigated in a CoCr/CoCr head-neck junction with a real mismatch angle in a PBS solution and under a normal walking gait loading. The junction was assembled with various forces ranging from 2-5 kN to represent low-to-high impaction forces applied by surgeons in practice. The area loss from the edges of the most critical plane of the junction, as an indicator of material loss in the junction) showed a linearly increasing pattern over the fretting wear cycles. This could help to estimate the degree of material loss after several million cycles of fretting wear.

The results of this work revealed that contact pressure, contact length and relative micro-motion at the interface of the junction are the key parameters that can influence the material loss caused by fretting wear. Figure 6.5 showed that with increasing the assembly force, relative micro-motions between the head and neck components reduce considerably which offers more stability to the junction. According to the Archard equation, wear is proportional to both the contact pressure and relative micro-motion (amplitude of sliding). Even though the relative micro-motions decrease in the firmly assembled junctions, the significant increase in the contact pressure induced over greater contact regions leads to a net increase in fretting wear and consequently material removal. The results showed that a higher assembly force can induce a longer contact at the interface. This can extend the surface on which fretting wear occurs and can therefore increase the extent of material removal. As shown in Figure 6.6a, (for the studied taper design and material combination) increasing the assembly force results in more material loss. This is in contrast with the English's results (English, Ashkanfar et al. 2016). As was mentioned in the introduction, they concluded that higher assembly forces resulted in lower fretting wear. The immediate difference of this work with their study is the material combination. In this study the material combination was CoCr/CoCr, while they used a Ti/CoCr combination. However, further to the different material combinations, it seems that mismatch angle is the major difference between this work and English's model. The existence of mismatch angle have a great influence on the contact length between head and neck. In their work, the contact length is always constant (due to having no mismatch angle) and therefore increasing of the assembly force magnitude reduces the relative micromotion in head-neck interface and accordingly reduces the amount of the material loss. However, as in this work the

contact between head and neck is not perfect, increasing of the assembly load increases the contact length in head-neck junction which results in increasing of the material loss.

Assembly force, as an intraoperative surgical parameter, can play an important role in the fretting wear damage to the head and neck components. According to the previous studies (Rehmer, Bishop et al. 2012), high assembly forces can enhance the stability and strength of the junction. It was therefore suggested to apply impaction forces of at least 4 kN. However, based on the results of this work, increased assembly forces, particularly from 4 kN to 5 kN, can result in more significant material removal from the head and neck components caused by the effect of fretting wear. This may therefore suggest not to exceed surgeons typical impaction forces that are approximately 4 kN (Heiney, Battula et al. 2009) in the interest of enhanced stability. It should be noted that this study was developed for a particular design, a CoCr/CoCr material combination with a distal angular mismatch of 0.01°. Further research is required to investigate the influence of assembly force on the fretting wear behaviour, considering various angular mismatches, different material combinations and loading profiles of the other daily activities.

6.6 Summary

The adaptive finite element model developed in the Chapter 4 was used to simulate fretting wear in a CoCr/CoCr head-neck junction with an angular mismatch of 0.01°. The junction was assembled with 2, 3, 4 and 5 kN and then subjected to 1,025,000 cycles of normal walking gait loading. IT was revealed that material removal due to fretting wear increased with increasing the assembly force. High assembly forces induced greater contact pressures over larger contact regions at the interface which in turn resulted in more material loss and wear damage to the surface when compared to lower assembly forces. Although a high assembly force (greater than 4 kN) can further improve the initial strength and stability of the taper junction, it appears that it also increases the degree of fretting. Thus, a maximum force of 4 kN is suggested. Further

studies are needed to investigate the assembly force in the other taper designs, taper angle mismatches, and material combinations.

Chapter 7 Development of a fretting corrosion model for metallic interfaces using adaptive finite element analysis

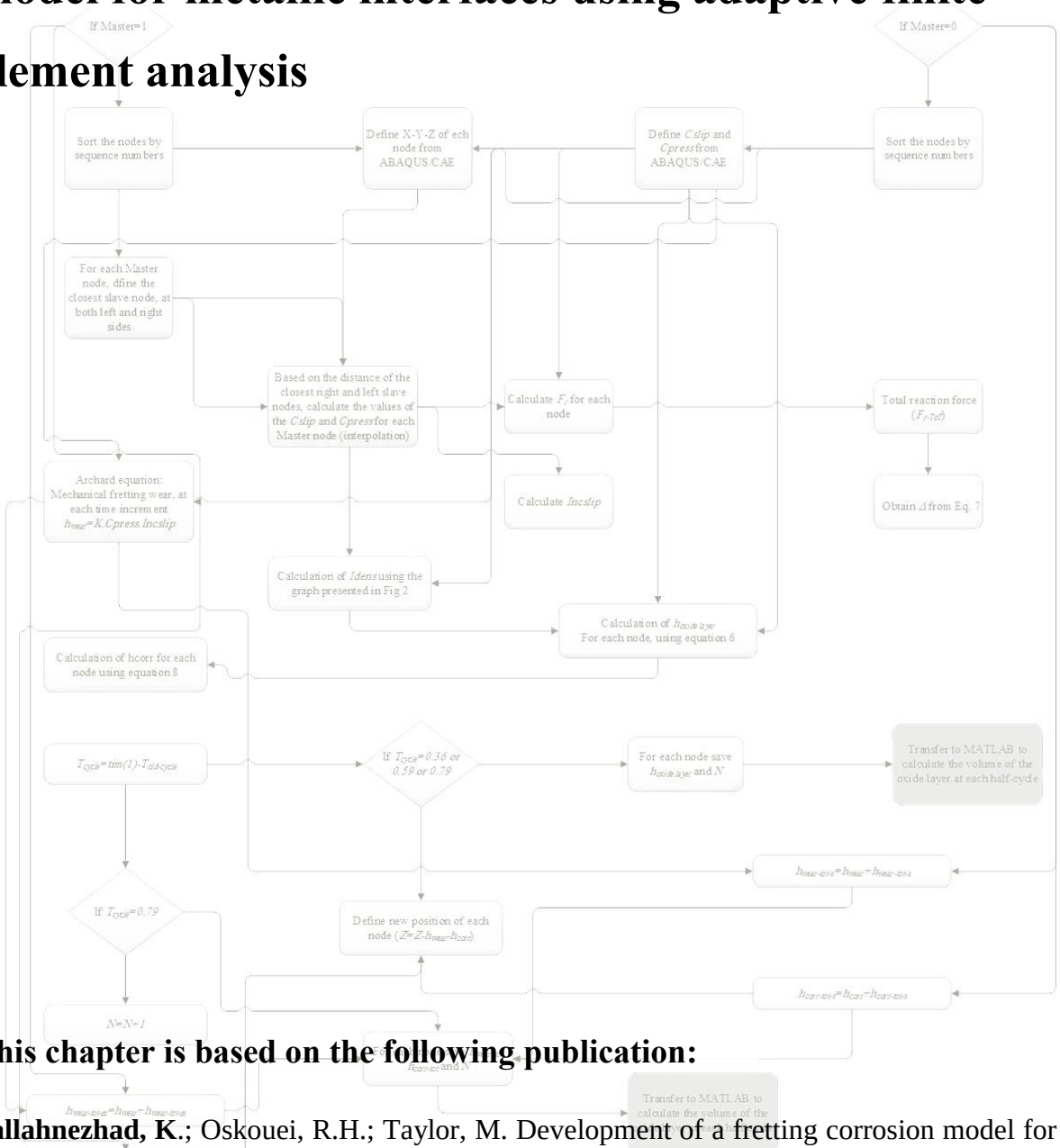

This chapter is based on the following publication:

Fallahnezhad, K.; Oskouei, R.H.; Taylor, M. Development of a fretting corrosion model for metallic interfaces using adaptive finite element analysis. *Finite Element in Analysis and Design*, in press (accepted on 14 May 2018).

7.1 Overview

As was mentioned in Chapter 1, fretting corrosion (a type of mechanically assisted corrosion) is known to occur in metallic contacting components that are cyclically subjected to fretting wear in a corrosive environment. Metallic implants such as modular taper junctions of total hip replacement are an example of this failure type where mechanical loads of daily activities can induce fretting wear at the metallic interface in the presence of the corrosive body fluid. Over the process of fretting corrosion, the passive oxide layer, that plays an important role in enhancing the corrosion resistance of metallic materials, can be mechanically disrupted. Such a disruption provides a condition for the metal (or metal alloy) to lose material through the associated chemical reactions in order to re-create a new oxide layer (repassivation) and also the process of metallic dissolution (Goldberg, Gilbert et al. 2002, Rodrigues, Urban et al. 2009, Mali 2016, Oskouei, Fallahnezhad et al. 2016).

To date, attempts have been made to propose a general model for mechanically assisted corrosion to predict the behaviour of metallic alloys taking into account the mechanical and electrochemical parameters. Goldberg et al. (Goldberg and Gilbert 1997) used a model of surface oxide fracture and a repassivation equation, that had been previously proposed by Ambrose (Ambrose 1983), to justify the electrochemical response of CoCrMo alloys to fracture and reformation of its oxide layer. To do this, they employed an electrochemical scratch test method in which they used a diamond pin to scratch a CoCrMo sample in a phosphate-buffered saline (PBS) medium. They developed an equation that can determine the oxide layer thickness of CoCrMo alloys.

Swaminathan et al. (Swaminathan and Gilbert 2012) proposed a theoretical model which incorporates both the mechanical and electrochemical parameters of fretting corrosion. They conducted experimental tests in which different combinations of Ti-6Al-4V and CoCrMo alloys were subjected to fretting wear loading in a PBS condition. In their model, they proposed

a relation between the mechanical and electrochemical properties such as normal load, amplitude of sliding, surface properties, potential and current.

Due to the complexity of the fretting corrosion process, the existence of various designs for implants (in terms of geometry and size), and the limitations of physical tests, it is difficult and expensive to study fretting corrosion in metallic implants by means of *in-vitro* tests. Similar difficulties and limitations apply to other situations where fretting corrosion occurs (e.g. clamped joints (Molent 2015), leaf springs (D'Silva and Jain 2014) and ball or roller bearings (Lai and Stadler 2016)). Hence, finite element (FE) method could be employed as a convenient and practical way to explore complex geometries subjected to complex load cases.

As was pointed out in the previous chapters, in the area of modular taper junctions of hip implants, several finite element simulations have been developed to evaluate the mechanical response of the contacting components (Donaldson, Coburn et al. 2014, Dyrkacz, Brandt et al. 2015). These studies showed that the geometric parameters such as taper angle mismatch, material combinations, and assembling load can directly affect the mechanical-related parameters such as relative micro-motions and contact stresses at the interface. These studies were limited to exploring the contact mechanics of the junction subjected to a single gait loading cycle. It is however noted that material loss due to the effect of fretting wear and corrosion occurs under cyclic gait loading. As was mentioned in Chapter 4, recently, finite element method has been used to predict the amount of material loss in the taper junction as a result of fretting wear over a few million cycles of loading (Zhang, Harrison et al. 2014, English, Ashkanfar et al. 2015, English, Ashkanfar et al. 2016). Moreover, we developed a finite element fretting wear model, in Chapter 4, for the contacting materials of a CoCr/CoCr head-neck taper junction in a PBS condition. We used the Archard wear equation to simulate the mechanical fretting wear process. All of these models have simulated only the mechanical fretting wear process and have neglected the effects of corrosion, in particular passivation/repassivation and consequent material loss due to corrosion.

A literature review confirms that, to date, no finite element model has been developed to simulate the fretting corrosion phenomenon in contacting surfaces of metallic materials under fretting wear loading and in a corrosive environment where passivation and repassivation repeatedly occur. In this chapter, therefore, a new finite element model was developed to simulate the process of fretting corrosion and predict material loss due to the both mechanical fretting wear and corrosion. The equation of the oxide film regeneration (proposed by Swaminathan (Swaminathan and Gilbert 2012)) together with the Archard wear equation were implemented in an FE code to simulate fretting corrosion for a CoCr/CoCr material combination. This model is able to predict the amount of material loss caused by corrosion; and also, to determine the volume of detached material caused by mechanical fretting wear. Moreover, this model was able to determine the amount of oxide layer removed from the material surface during the fretting corrosion process.

7.2 Materials and methods

The fretting corrosion process is a combination of two damaging components; mechanical wear and electrochemical corrosion. These two components are not independent processes; for instance, fretting wear can intensify corrosion (mechanically assisted corrosion). The details and procedure for developing an adaptivefinite element model for this complex phenomenon applied to a CoCrMo/CoCrMo material combination are presented in the following sections.

2.1. Main equations

To model the mechanical fretting wear, Archard wear formulation was used to determine the depth of material loss over the surface (Eq. 7. 1).

$$\frac{V}{S} = k\frac{F_N}{H} \quad (7.1)$$

where V is the lost volume, S is the amplitude of sliding, k is the wear coefficient, F_N is the normal load and H is the material hardness. This equation was the core of a wear algorithm developed by McColl et al. (McColl, Ding et al. 2004) and Ding et al. (McColl, Ding et al. 2004) to model fretting wear in a pin-on-disc system. This wear equation was also used in Chapter four to develop an algorithm for a two dimensional FE model of a head-neck taper junction in which the Archard equation was re-written in the form of Eq. 7. 2:

$$h_{wear} = K.Incslip.C_{Press} \quad (77.2)$$

where h_{wear} is the depth of wear, K is the wear coefficient-to-hardness ratio *(k/H)*, *Incslip* is the relative displacement of each node of the contact surface at each time increment and C_{Press} is the normal contact stress. The K ratio for the CoCr/CoCr material combination was presented as $1.68\text{x}10^{-14}$ Pa^{-1} in Chapter four.

Swaminathan et al. (Swaminathan and Gilbert 2012) developed an equation for the re-generation of passive oxide layers (Eq. 7. 3) from which the oxide layer thickness can be determined. To propose and verify this equation, they conducted experimental work in which a pin-on-disc system of different materials was subjected to cyclic fretting wear, in a (Phosphate Buffered Salain) PBS medium.

$$I_{film} = \left(\frac{\rho nF}{M_w}\right).2\frac{V_{nom}}{\Delta}\frac{d\delta}{dt} \quad \text{(a)} \quad (7.3)$$

$$I_{film} = 4\left(\frac{\rho nF}{M_w}\right).\frac{V_{nom}}{\Delta}\delta\nu \quad \text{(b)}$$

where I_{film} is the oxide film formation current, ρ is the density of the oxide, M_w is the molecular weight of the oxide, n is the effective valence of the oxide, F is Faraday's constant (96,500 C/mol), V_{nom} is the nominal volume of the oxide layer, Δ is the average inter-asperity distance

in the sliding direction (further details can be found in (Swaminathan and Gilbert 2012)), δ is the amplitude of sliding and v is the frequency of one cycle. Eq. 7. 3b can be used to define the current film of the fretting corrosion process for one complete cycle. The additional factor of 2 in this equation is because that both the top and bottom surfaces are present in contact. The assumptions for the development of this equation include: the repassivation rate is limited to the oxide abrasion rate, ionic dissolution currents are small in comparison with the oxide film currents and generation of metal particles without oxidation is ignored (Swaminathan and Gilbert 2012). For a CoCr/CoCr combination, the passive oxide layer is assumed to be Cr_2O_3 (Goldberg and Gilbert 1997). Hence, the oxide layer for this alloy has a density of ρ = 5,210 kg/m^3, oxide effective valence of n = 3, and molecular weight of M_w = 0.152 *kg/mol*.

To make this equation applicable for a finite element modelling, it needs to be localised so that it can be directly applied to the nodes of the material model. Therefore, the equation should be re-arranged in a way that could be solved within small increments of time and position of the nodes. To do this, both sides of Eq. 7. 3b are divided by area A to yield Eq. 7. 4 as follows:

$$\frac{Ifilm}{A} = \frac{1}{A}.\left(\left(\frac{\rho nF}{Mw}\right).2\frac{V_{nom}}{\Delta}\frac{d\delta}{dt}\right) \Rightarrow$$

$$I_{Density} = \left(\left(\frac{\rho nF}{Mw}\right).2\frac{h}{\Delta}\frac{d\delta}{dt}\right) \tag{7. 4}$$

where $I_{Density}$ is the average fretting corrosion current density and h is the oxide layer thickness. In this equation, all the constants can be substituted with K_{corr}:

$$I_{Density} = K_{corr}.\left(\frac{h}{\Delta}\frac{d\delta}{dt}\right) \quad (7.5)$$

$$\left(K_{corr} = \frac{2\rho nF}{Mw}\right)$$

$$I_{Density} = K_{corr}.\left(\frac{h}{\Delta}.\ \frac{Incslip}{t_{increment}}\right) \quad (77.6)$$

where *Incslip* is the relative micro-motion between the surface nodes at each time increment ($t_{increment}$). Equation 7. 6 can be then applied to each node of the contact surface to model the electrochemical corrosion.

7.2.1 Modelling procedure

To apply Equation 7. 6 to each surface node of the model, a FORTRAN code was developed that can locate the position of the surface nodes through the ABAQUS UMESHMOTION subroutine within an adaptive meshing constraint. A 3D FE model was developed to simulate the fretting corrosion process in a CoCr/CoCr pin-on-disc system that was the same as the experiments used by Swaminathan et al. (Swaminathan and Gilbert 2012). The diameter of the pin was 0.35 mm. The friction coefficient of the contact surface was defined as a function of normal contact stress (Figure 7.1)

As presented in (Swaminathan and Gilbert 2012), the average inter-asperity distance in the sliding direction, Δ, is a function of normal load, F_N, (Eq. 7. 7) for the CoCr/CoCr combination. Hence, at each time increment, the normal reaction force of the contact surface (which is the summation of all the reaction forces of the surface nodes) was computed. The resultant normal load was then used to determine the Δ factor using Equation 7. 7. The average fretting corrosion current density ($I_{Density}$) versus normal contact stress was reported at a sliding frequency of 1.25 Hz (Swaminathan and Gilbert 2012) (Figure 7.2). It should be noted that although Δ is defined as the average inter-asperity distance in (Swaminathan and Gilbert 2012), it is actually a

constant parameter in Eqs. 7. 3-6. In that study, the authors first assumed that such a constant could be a function of normal force; and then, their experimental outcomes proved their assumption, as they proposed Δ as a function of normal force.

$$\Delta = 844.46\, {F_N}^{-0.467} \tag{77.7}$$

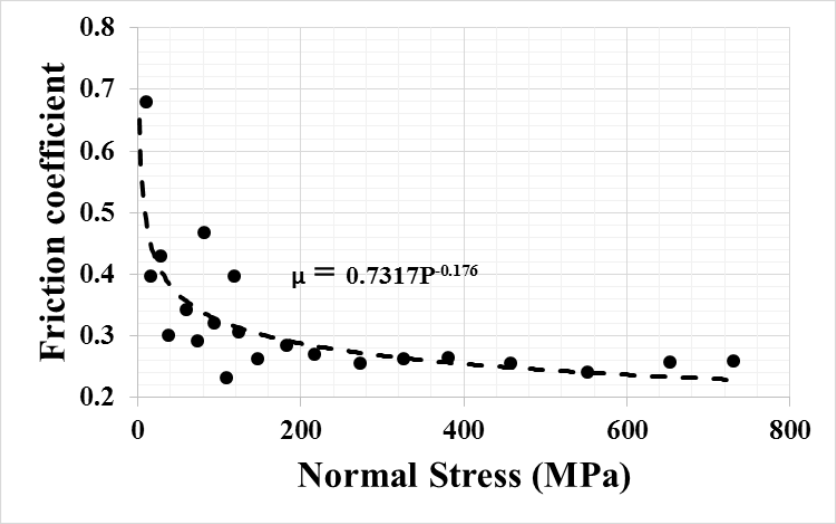

Figure 7.1– Coefficient of friction between CoCr and CoCr versus normal contact stress, data from (Swaminathan and Gilbert 2012).

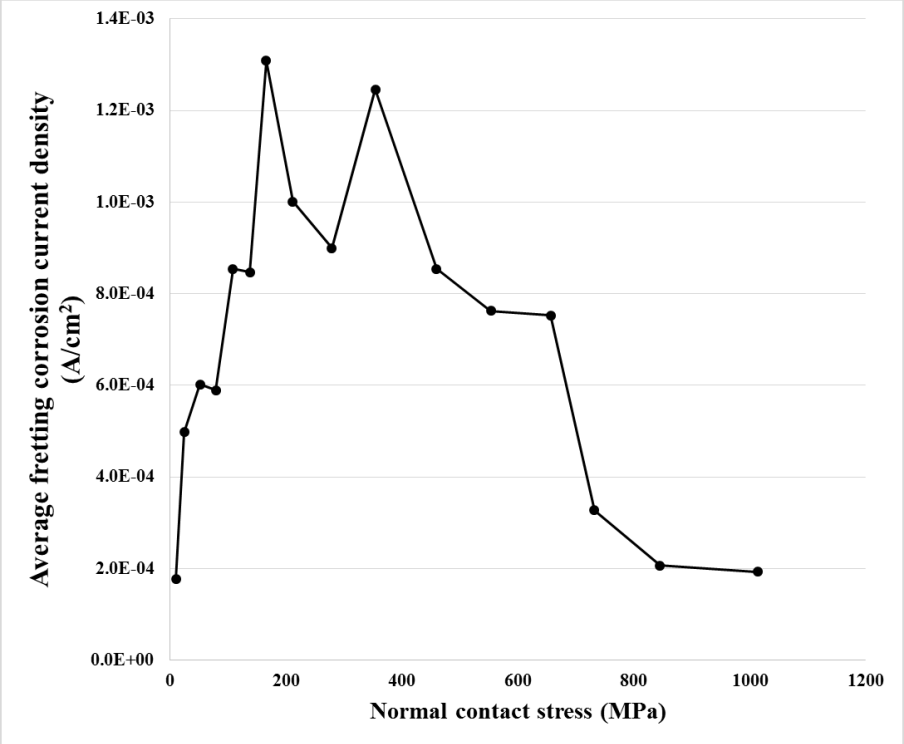

Figure 7.2– Average fretting corrosion current density versus normal contact stress for CoCr/CoCr combination, data from (Swaminathan and Gilbert 2012).

At each time increment, the normal contact stress (called CPRESS in ABAQUS), position and total displacement (called CSLIP in ABAQUS) of each surface node were retrieved from the ABAQUS/CAE analysis and transferred into the FORTRAN code. Using these data, this code was developed to calculate the reaction force applied to the surface and determine relative micro-motions between each pair of the closest contacting nodes (master and slave that were disc and pin, respectively). Having calculated the reaction force of the surface, Δ factor of the material surface was obtained using Equation. 7. 7. The FORTRAN code (UMESHMOTION

subroutin) reads the normal contact stresses from the ABAQUS CAE model and obtains the corresponding average fretting corrosion current densities from Figure 7.2. Having all the variables determined, the oxide layer thickness, *h*, for each node and at each time increment was then computed by Equation 7. 6. As reported in (Swaminathan and Gilbert 2012), during normal rates of fretting wear, the rate of repassivation is significantly greater than the rate of abrasion. Hence, during a half cycle of fretting wear, while the existing passive layer is being removed from the surface, a new oxide film will be generated instantly after the first half cycle. Thus, for the next half cycle, the new oxide layer will be removed from the surface. Figure 7.3 schematically shows the process of the fretting corrosion simulation employed in this study. At each time increment, the thickness of the oxide layer for each node was computed using Equation 7. 6. As mentioned above, in a CoCr/CoCr material combination, the oxide layer is Cr_2O_3 (Goldberg and Gilbert 1997). Having the thickness of the oxide layer for each node, the mass of the oxide layer for that node was computed (using the density of Cr_2O_3). As the mass percent of chromium in Cr_2O_3 is 68.4%, the mass of chromium can be defined. The mass percent of Cr in the substrate material, the mass of the removed material from the substrate (caused by repassivation of the oxide layer) was computed for each node (according to stoichiometry). Accordingly, the thickness of the material loss from the substrate caused by the oxide layer regeneration for each node was obtained using Eq. 7. 8:

$$h_{corr} = \frac{(0.684).h.\rho_{Cr2O3}}{(0.28).\rho_{Co-28Cr-6Mo}} \tag{77.8}$$

where h_{corr} is the thickness of the substrate removed by corrosion, ρ_{Cr2O3} is the density of Cr_2O_3, $\rho_{Co\text{-}28Cr\text{-}6Mo}$ is the density of Co-28Cr-6Mo alloy, and *h* is the thickness of the oxide layer.

As shown in Figure 7.3, at each time increment, the thickness of the regenerated/removed oxide layer is computed using Equation 7. 6. The material loss (h_{wear} plus h_{corr} for each node) of the substrate changes the geometry of the surface; and subsequently, the magnitude of the normal contact stress for each node. Hence, the values of $I_{Density}$, Δ and reaction force change. The code records the height of the removed oxide layer after each cycle to calculate the material loss

caused by mechanical fretting wear and corrosion for each node at each time increment. A PYTHON code together with a MATLAB code were then developed to compute the volume of the lost material and removed oxide layer at each time increment of the fretting corrosion simulation process.

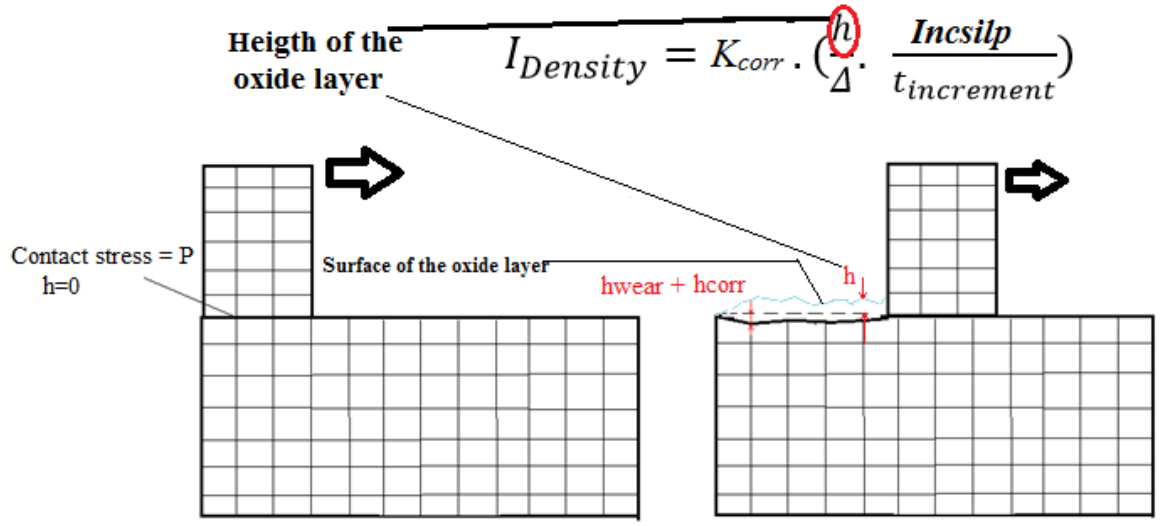

Figure 7.3– Schematic process of the fretting corrosion simulation used in this work.

7.2.2 Modelling of passive oxide layer

One cycle of a fretting wear sliding (two half cycles), as shown in Figure 7.4, was applied to the CoCr/CoCr pin-on-disc model while the pin was under a normal load. The amplitude of sliding was 50 µm which was the same as the sliding tests reported in (Swaminathan and Gilbert 2012). Normal loads of 10 N, 20 N, 44 N, 53 N, 70 N and 81 N were applied to evaluate the accuracy of the model in a wide range of normal loads. From the FE simulations, the height and volume of the oxide layer produced during one cycle (two half cycles) were obtained for several normal loads (or normal contact stresses). The predicted height of the oxide layer was then compared to the height of the oxide layer computed by Eq. 7. 3b, as presented in

Swaminathan's study (Swaminathan and Gilbert 2012)). For this purpose, the height of the oxide layer for each node, after each half a cycle, was obtained through the UMESHMOSHEN subroutine. The shape, volume and height of the oxide layer for each case of normal load were determined using MATLAB.

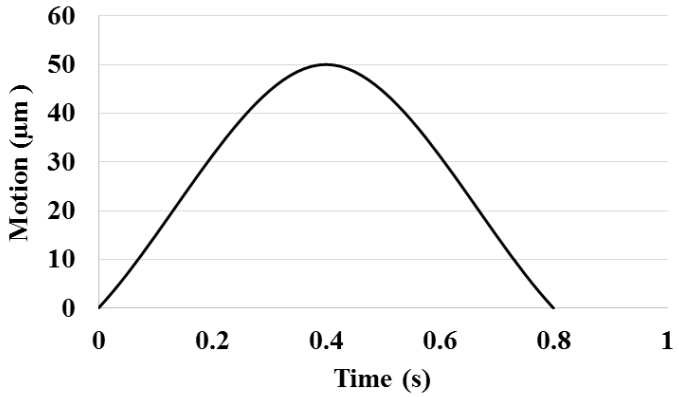

Figure 7.4– One cycle of the fretting wear sliding used to model the passive oxide layer removal and regeneration.

7.2.3 Simulation of fretting corrosion for 150 cycles of sliding

The developed FE model can be used to simulate fretting corrosion in a high cycle process of fretting wear with various sliding profiles. To do this, the model was used to simulate fretting corrosion for the same pin on disc system subjected to 150 cycles of sliding. This number of cycles is what was used in Swaminathan's work, for each determined normal load. One single cycle of the sliding profile for this simulation is shown in Figure 7.5 which is the same as the cycle used in the experimental tests (Swaminathan and Gilbert 2012). This simulation was developed for two normal contact stresses of 250 MPa and 500 MPa. According to Figure 7.5, for this simulation, the oxide layer was to be removed/generated four times in every cycle of sliding (as the sliding direction changes three times in one cycle).

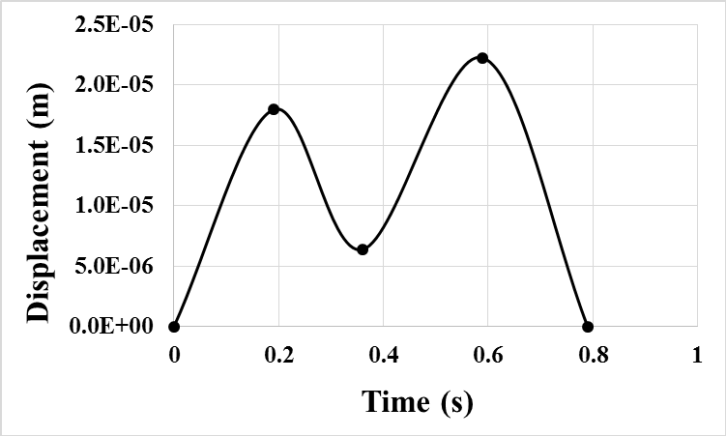

Figure 7.5– One cycle of the sliding profile which was repeated 150 times for the fretting corrosion simulation.

The algorithm of the FORTRAN code which was applied to the surface nodes, at each time increment, is given in Figure 7.6. In this algorithm, *X, Y* and *Z* define the position of each node in the coordination system. The "Master" variable determines whether a node belongs to the master component or the slave component (in this model disc was assumed as master and pin as slave). C_{slip} is the displacement of each node in the contacting plane and C_{press} is the normal contact stress of each node. *Incslip* is the relative displacement of each node in the contacting plane at each time increment. F_r is the reaction force for each node and $F_{r\text{-}TOT}$ is the total reaction force applied to the contact surface at each time increment. $h_{oxide\ layer}$ is the height of the oxide layer for each node at each time increment. h_{corr} and h_{wear} are the depths caused by corrosion and wear, respectively, for each node at each time increment. T_{cycle} is the time of each cycle. *Time(1)* is the total time of the simulation step. $T_{old\text{-}cycle}$ is the total time of the simulation step related to the previous cycle. N is the number of cycles. $h_{wear\text{-}tot\text{-}m}$, $h_{wear\text{-}tot\text{-}s}$, $h_{corr\text{-}tot\text{-}m}$ and $h_{corr\text{-}tot\text{-}s}$ are the total height of material loss in the master and slave components caused by mechanical wear and corrosion, respectively.

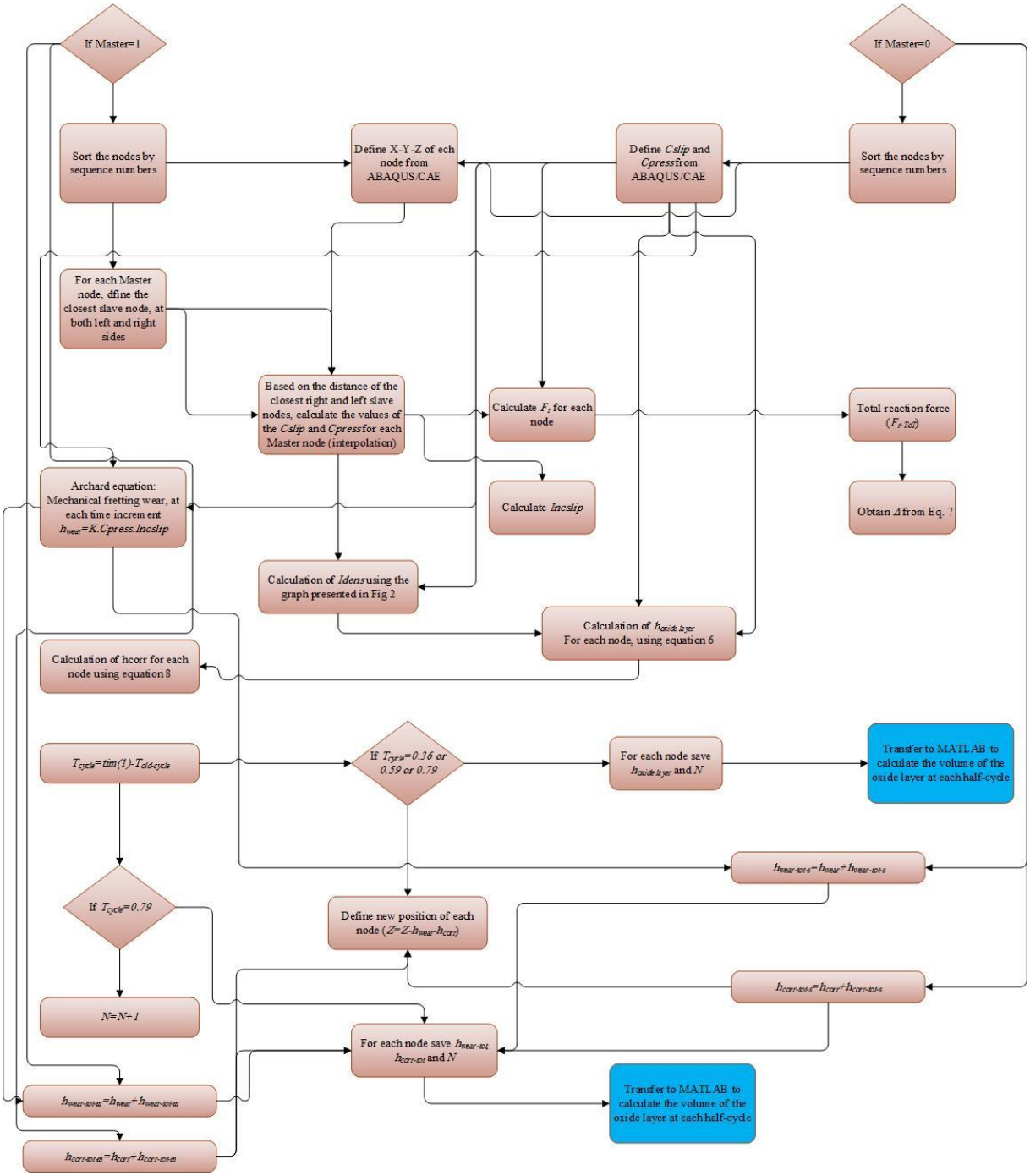
If Master=1
If Master=0
Sort the nodes by sequence numbers
Define X-Y-Z of ech node from ABAQUS/CAE
Define Cslip and Cpress from ABAQUS/CAE
Sort the nodes by sequence numbers
For each Master node, dfine the closest slave node, at both left and right sides
Based on the distance of the closest right and left slave nodes, calculate the values of the Cslip and Cpress for each Master node (interpolation)
Calculate F_t for each node
Total reaction force ($F_{t\text{-}Tot}$)
Archard equation: Mechanical fretting wear, at each time increment $h_{wear}=K.Cpress.Incslip$
Calculate Incslip
Obtain Δ from Eq. 7
Calculation of Idens using the graph presented in Fig 2
Calculation of $h_{oxide\ layer}$ For each node, using equation 6
Calculation of hcorr for each node using equation 8
$T_{cycle}=tim(1)-T_{old\text{-}cycle}$
If $T_{cycle}=0.36$ or 0.59 or 0.79
For each node save $h_{oxide\ layer}$ and N
Transfer to MATLAB to calculate the volume of the oxide layer at each half-cycle
$h_{wear\text{-}tot\text{-}s}=h_{wear}+h_{wear\text{-}tot\text{-}s}$
If $T_{cycle}=0.79$
Define new position of each node ($Z=Z\text{-}h_{wear}\text{-}h_{corr}$)
$h_{corr\text{-}tot\text{-}s}=h_{corr}+h_{corr\text{-}tot\text{-}s}$
$N=N+1$
For each node save $h_{wear\text{-}tot}$ $h_{corr\text{-}tot}$ and N
Transfer to MATLAB to calculate the volume of the oxide layer at each half-cycle
$h_{wear\text{-}tot\text{-}m}=h_{wear}+h_{wear\text{-}tot\text{-}m}$
$h_{corr\text{-}tot\text{-}m}=h_{corr}+h_{corr\text{-}tot\text{-}m}$

Figure 7.6– The algorithm of the FORTRAN code applied to the surface nodes of the CoCr pin and CoCr disc at each time increment.

7.3 Results

7.3.1 Verification: removal and formation of passive oxide layer during a single loading cycle

Figures 7.7 and 8 illustrate the distribution of the oxide layer on both the contacting surfaces under the applied normal loads for both the first and second half cycles. Table 1 presents the average height and volume of the oxide layer determined from the simulations and Eq. 7. 3b presented in (Swaminathan and Gilbert 2012). Good agreements were found between results of the simulation and those calculated by Eq. 7. 3b showing an average difference of 9% in the oxide layer height for all the normal loads. This successfully verified the fretting corrosion algorithm and simulations developed in this study. From the results of Table 1, it is apparent that for all the normal loads, the height of the oxide layer in the first and second half cycles are close. It can be also seen that with increasing the normal load, the height of the oxide layer reduces. For instance, with an increase from 10 N to 70 N, the total height of the oxide layer (first half cycle plus second half cycle) reduced by 84%.

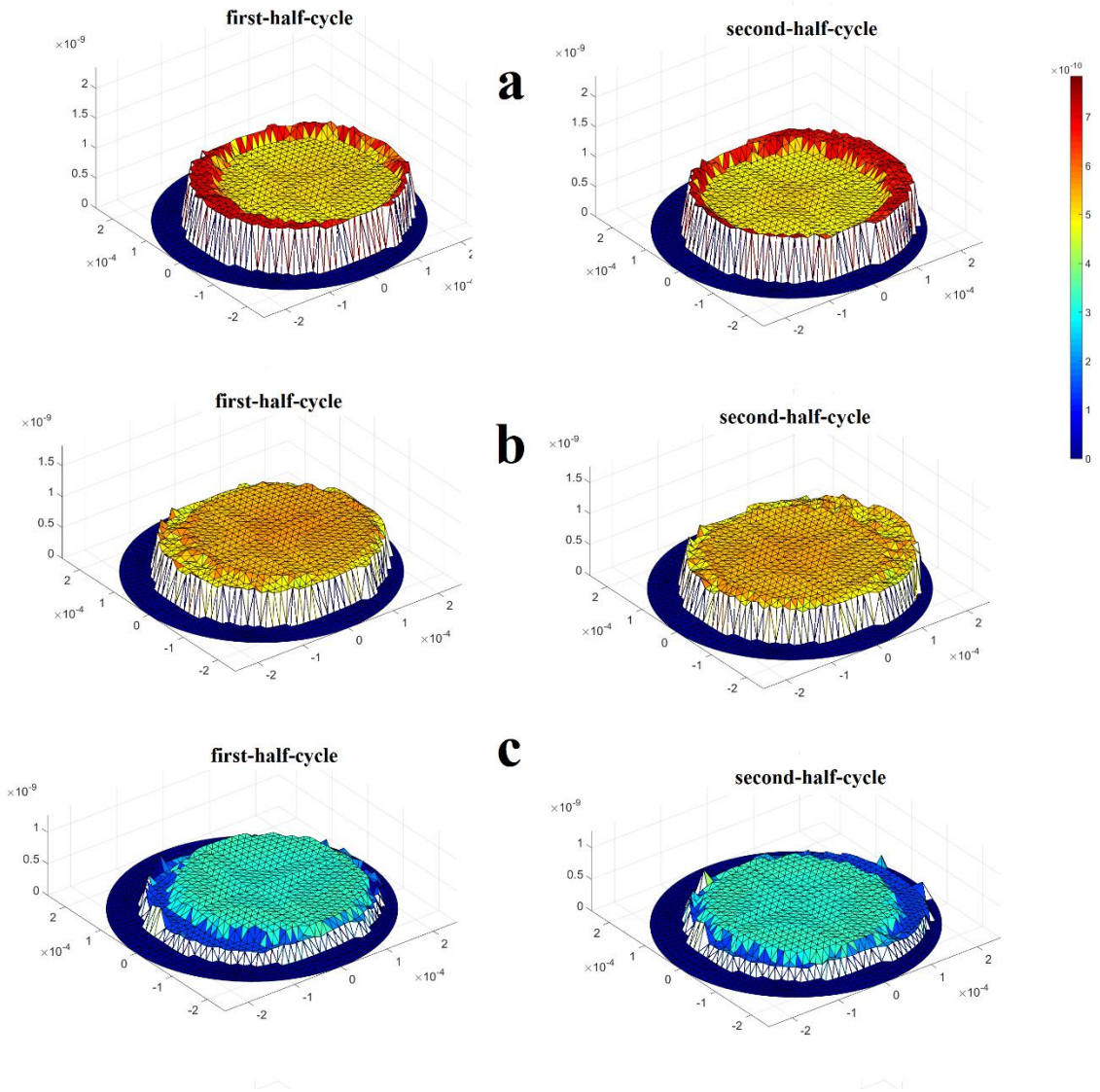

Figure 7.7– Passive oxide layer of Cr_2O_3 produced after each half cycle onto the CoCr disc surface under normal loads of: (a) 10 N, (b) 20 N, and (c) 44 N. All measures are in meters.

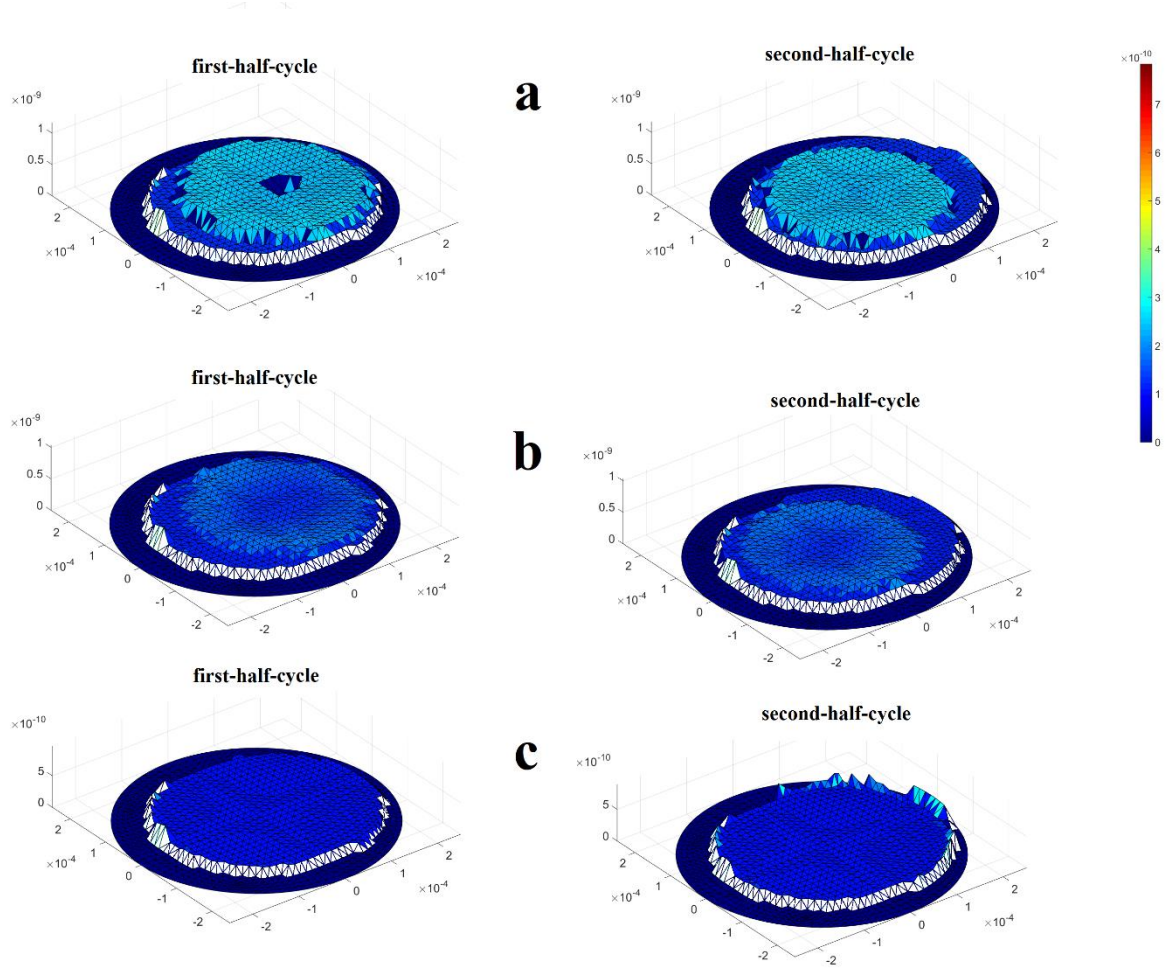

Figure 7.8– Passive oxide layer of Cr_2O_3 produced after each half cycle onto the CoCr disc surface under normal loads of: (a) 53 N, (b) 70 N, and (c) 81 N. All measures are in meters.

Table 7.1 Average height and volume of the passive oxide layer formed onto the CoCr disc surface under different normal loads of CoCr pin.

Normal Load and Nominal Normal Stress		**Fretting Corrosion Simulation Results**			**Using Equation 3b presented in (Swaminathan and Gilbert 2012)**
		First Half Cycle	Second Half Cycle	First half + Second half	First Half + Second Half
10 N (104 MPa)	Average Height (m)	5.30e-10	5.36e-10	10.66e-10	9.48e-10
	Volume (m^3)	7.84e-17	7.56e-17	15.40e-17	-
20 N (208 MPa)	Average Height (m)	3.43e-10	3.96e-10	7.39e-10	8.37e-10
	Volume (m^3)	6.12e-17	6.01e-17	12.3e-17	-
44 N (456 MPa)	Average Height (m)	2.71e-10	2.67e-10	5.38e-10	4.83e-10
	Volume (m^3)	3.41e-17	3.57e-17	6.98e-17	-
53 N (552 MPa)	Average Height (m)	2.01e-10	2.00e-10	4.01e-10	4.012e-10
	Volume (m^3)	2.64e-17	2.78e-17	5.42e-17	-
70 N (728 MPa)	Average Height (m)	0.86e-10	0.82e-10	1.68e-10	1.49e-10
	Volume (m^3)	1.05e-10	1.11e-10	2.16e-17	-
81 N	Average Height (m)	0.38e-10	0.36e-10	0.74e-10	0.69e-10

(844 MPa)	Volume (m^3)	0.48e-17	0.60e-17	1.08e-17	-

7.3.2 150 cycles of fretting corrosion

As mentioned in Section 2.4, the FE model was employed to simulate fretting corrosion for the same CoCr/CoCr pin on disc system under 150 cycles of sliding (with the sliding profile of Figure 7.5) and normal contact stresses of 250 MPa and 500 MPa in a corrosive environment of PBS. After applying the last cycle of fretting corrosion, the normal load (or the equivalent normal contact stress) was unloaded. Figure 7.9 shows the vertical displacement contours in both the disc and pin models. The displacements are normal to the contact surface which represent the total depth of material loss (due to both fretting wear and corrosion) from the outset surface. The displacements in the contours were scaled-up by a factor of 100 to better demonstrate the depth of material loss.

The maximum depth of the fretting corrosion material removal from the disc surface was 0.209 µm and 0.308 µm under 250 MPa and 500 MPa, respectively (Figure 7.9). There was 0.238 µm and 0.300 µm of material removal from the pin. It is obvious that the depth of the corroded surface in the pin is uniform, while in the disc the depth is not even over the corroded surface. This difference is because of the area of the disc and pin contact surfaces that were under normal loading. The whole area of the pin contact surface was continuously under the normal stress. However, the edge of the disc contact surface was not always subjected to the normal stress, according to the sliding regime (Figure 7.5).

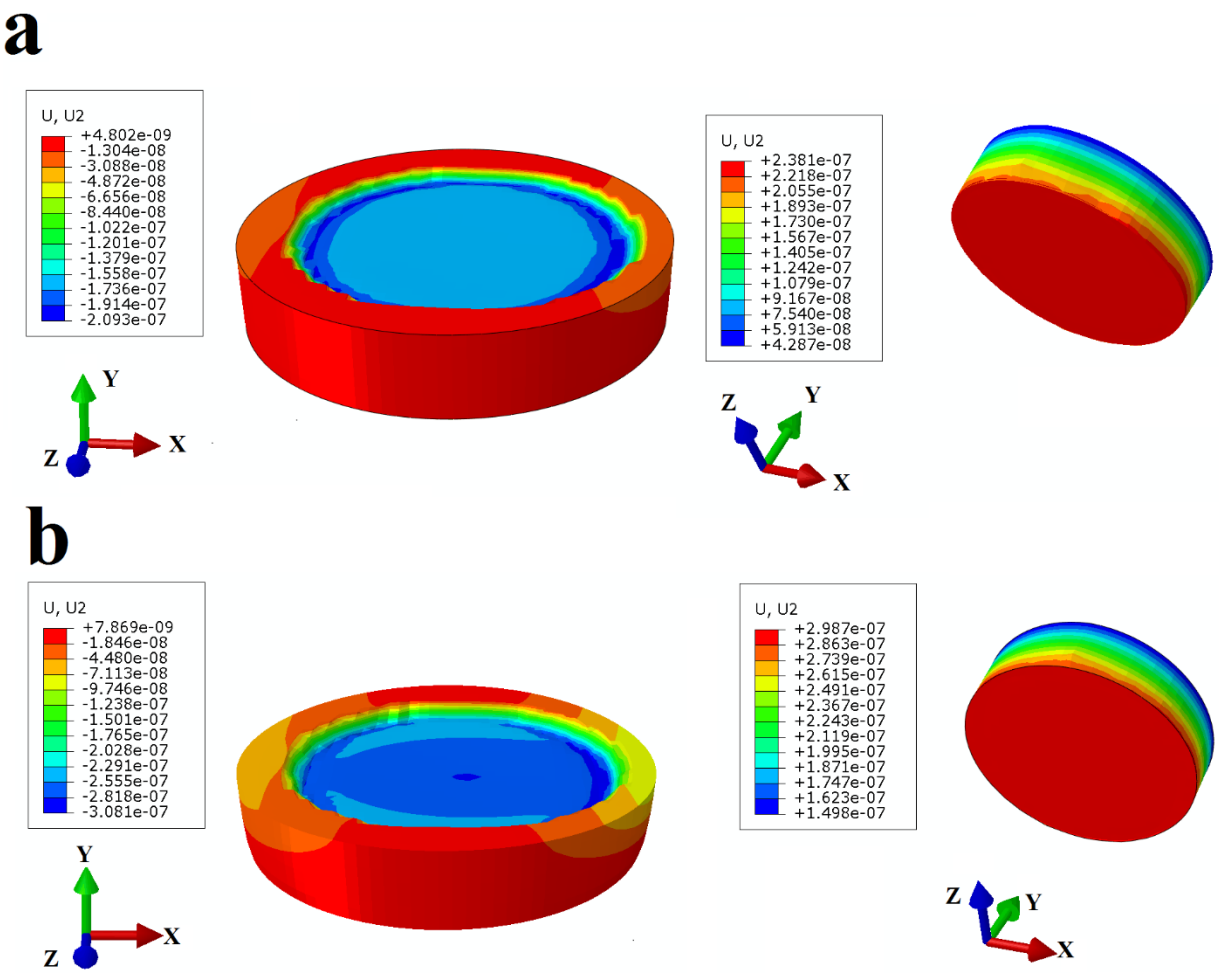

Figure 7.9– Contours of displacement in Y axis (normal to the contact surface) for both CoCr disc and CoCr pin after 150 cycles of fretting corrosion (with a sliding profile of Figure 7.5): (a) under normal stress of 250 MPa, and (b) under normal stress of 500 MPa. The displacements are in meters.

To determine the isolated contribution of mechanical fretting wear and electrochemical corrosion to the amount of material loss, the lost volume for each damaging component was

calculated separately (Table 2). Moreover, Figure 7.10 shows the lost volumes in the disc model (caused by fretting wear and corrosion separately) after 150 cycles of sliding with respect to the contact surface. From Table 2, it can be seen that the volume loss caused only by fretting wear is larger for the case of 500 MPa stress in both the disc and pin components. For instance, the worn volume in the disc increased from 9.07e-15 m^3 to 1.70e-14 m^3 when the normal contact stress was increased from 250 MPa to 500 MPa. This was, of course, because the wear depth is proportional to the normal contact stress, according to the Archard equation (Eq. 7. 2), resulting in a greater degree of volume loss under the greater normal stress. Table 2 however reveals that with increasing the normal stress, the material loss in both the disc and pin caused only by corrosion reduces. The corroded material detached from the disc reduced from 1.83e-14 m^3 to 9.15e-15 m^3 as a result of an increase in the normal stress from 250 MPa to 500 MPa. Table 2 also shows that the material loss caused by corrosion in the disc is greater than that of in the pin. For example, under 500 MPa, the material loss caused by corrosion in the disc and pin were 9.15e-15 m^3 and 6.07e-15 m^3, respectively. However, the material loss caused by wear is almost equal in both the pin and disc. It is also apparent that the volume of the removed oxide layer reduced by 36%, when the normal stress was increased from 250 MPa to 500 MPa.

Table 7.2 Material loss (in the form of volume) from the CoCr disc and CoCr pin surfaces as a result of fretting wear and corrosion, along with the volume of Cr_2O_3 oxide layer under normal contact stresses of 250 MPa and 500 MPa and after 150 cycles of sliding.

CoCr Disc		
	Normal Contact Stress = 250 MPa	Normal Contact Stress = 500 MPa
Material loss caused by fretting wear (m^3)	9.07e-15	1.70e-14
Material loss caused by electrochemical corrosion (m^3)	1.83e-14	9.15e-15
Total material loss (m^3)	2.74e-14	2.62e-14
CoCr Pin		
	Normal Contact Stress = 250 MPa	Normal Contact Stress = 500 MPa
Material loss caused by fretting wear (m^3)	9.04e-15	1.75e-14
Material loss caused by electrochemical corrosion (m^3)	9.11e-15	6.07e-15
Total material loss (m^3)	1.82e-14	2.36e-14
CoCr/CoCr Pin and Disc		
	Normal Contact Stress = 250 MPa	Normal Contact Stress = 500 MPa
Generated (removed) volume of Cr_2O_3oxide layer (m^3)	8.7e-15	5.6e-15

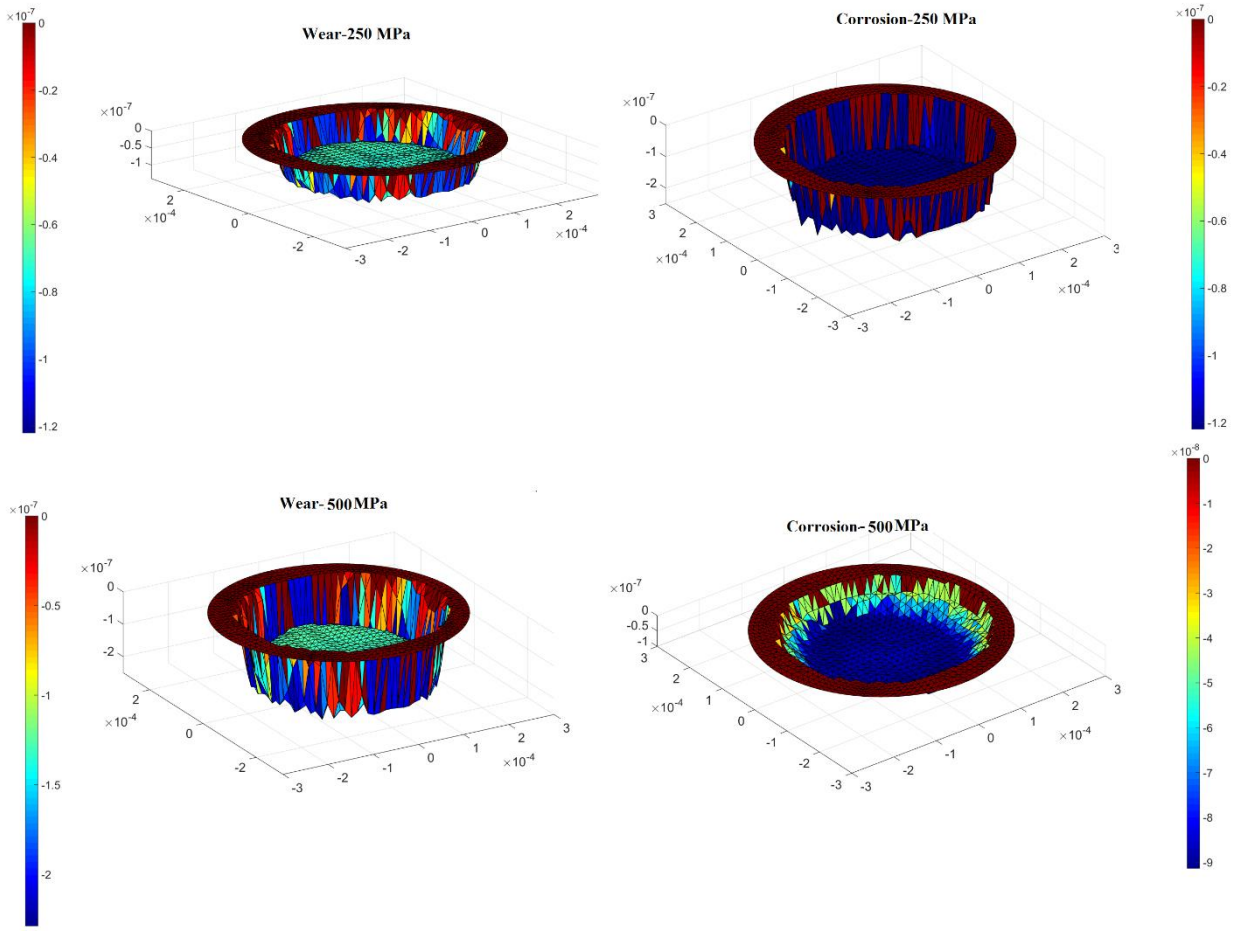

Figure 7.10– Lost material in the CoCr disc model due to the isolated effect of fretting wear and electrochemical corrosion after 150 cycles of sliding under normal contact stresses of 250 MPa and 500 MPa. All measures are in meters.

Figure 7.11 shows the material loss caused by fretting wear, electrochemical corrosion and total material loss versus number of cycles in disc, for both 250 MPa and 500 MPa normal stresses. As it can be seen in this figure the graphs have a linear trend over the process of fretting corrosion. However, it should be notified that this work is a displacement control case and accordingly the relative micro-motion, as an effective parameter on the magnitude of material loss, is constant, at each time increment. For a force control case, the relative micro-

motion for each time increment will not be constant and the trend of the graphs for a force-control case needs to be investigated.

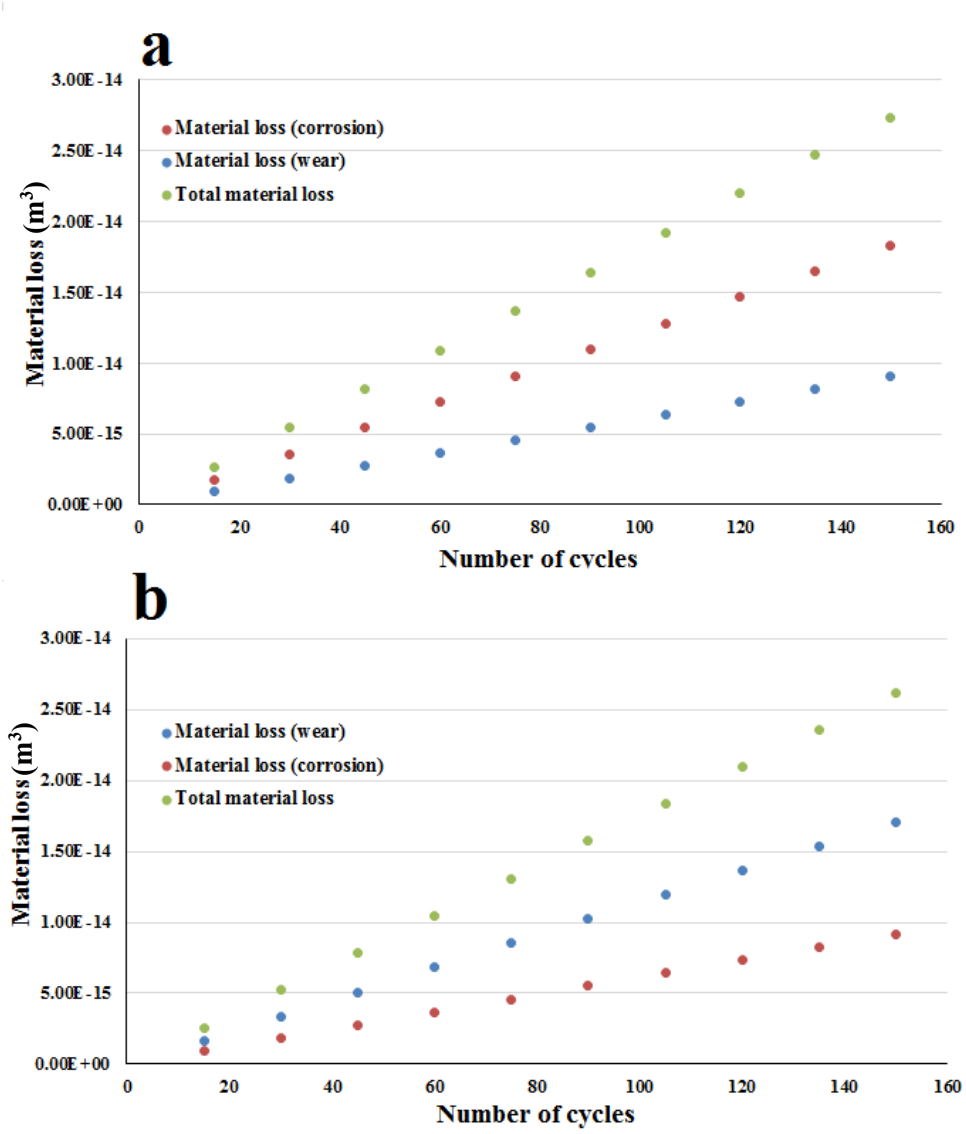

Figure 7.11– Lost material versus number of cycles (a) Normal stress 500 MPa (b) Normal stress 250 MPa

7.4 Discussion

From the Archard wear equation that was used to model fretting wear in this work, it is understood that with increasing the normal stress, the depth of material loss increases (Eq. 7. 2). Particularly in the simulations of this study, an increase in the normal contact stress from 250 MPa to 500 MPa resulted in an 87% increase in the volume loss from the CoCr disc. For corrosion, the variation in the material loss was found to be more complicated. With increasing the normal contact stress, the Δ factor decreases (Eq. 7. 7) which can reduce the depth of corroded surface (Eq. 7. 6). Moreover, $I_{Density}$ varies with normal stress (Figure 7.2). Although the behaviour of $I_{Density}$ is not a monotonic behaviour (as a function of normal stress), changing normal stress can significantly change the value of $I_{Density}$ and accordingly the depth of corroded surface (Eq. 7. 6). It should be noted that during the process of fretting corrosion, there is a continuous interaction between the mechanical fretting wear and electrochemical corrosion components. From the main applied equations, it is evident that the normal contact stress (which is dependent on the geometry of the contact surface) is the common parameter in both the mechanical and electrochemical components. Hence, at each time increment, material loss caused by each of these components can change the geometry of the contact surface; and consequently, the magnitude of the normal contact stress that in turn affects the material loss due to the both components. As a result, there can be no expectation for a linear behaviour of the fretting corrosion process as a function of normal stress and/or amplitude (profile) of sliding. The process appears to be highly dependent on the normal stress and sliding profile as well as the geometry of the contact surface and loading structure.

The FE model developed for the fretting corrosion process in this work has the ability to simulate the interactions between the mechanical fretting wear and electrochemical corrosion components. The formulations that were previously presented for fretting wear and electrochemical corrosion were adjusted so that they can be locally applied to elemental nodes of a finite element model. The developed code of the fretting corrosion algorithm (shown in Figure 7.6) is capable of simulating various profiles of fretting wear sliding, different contact

geometries, different material combinations and normal contact stresses. It is noted that the material loss results presented in this study are limited to the simulated fretting corrosion process at a CoCr/CoCr interface with its specified geometry and loading profiles. Some assumptions were made for the development of this model in accordance with the Swaminathan's equation, as detailed in the methodology section. Also, instead of the Archard wear model and Swaminathan's model (for electrochemical corrosion), alternative formulations of wear and corrosion can be incorporated in this algorithm provided that they can be applied directly to the nodes. This model can be a good platform for finite element modelling of fretting corrosion in various applications and future studies to further investigate surface damage to materials in fretting corrosion situations.

7.5 Summary

In this chapter, an adaptive finite element modelling method was successfully developed to simulate the fretting corrosion process at metallic interfaces. To do this, a computational code was developed in which the Archard wear equation and a previously established electrochemical equation were simultaneously employed. The algorithm of this code is able to determine the volume of passive oxide layers removed from the interface and/or re-generated onto the surface, material loss caused by fretting wear and material loss caused by corrosion, at each cycle of fretting wear in a corrosive environment. The fretting corrosion simulation method developed in this work was then used to simulate the fretting corrosion process for a CoCr/CoCr interface under a varying profile of fretting sliding and two different normal contact stresses of 250 MPa and 500 MPa. The results showed that with increasing the normal contact stress, material loss caused by fretting wear increases; however, it reduces the material loss caused by electrochemical corrosion and the volume of the removed oxide layer. This new model can be employed for various fretting corrosion situations with different material combinations, interface geometries and mechanical loading and sliding profiles.

Chapter 8 Conclusions

8.1 Conclusion remarks

In Chapter two, a three dimensional finite element model of an isolated femoral head–neck junction was developed. The model included real geometry of the head and neck components with a non-linear frictional contact and elastic–plastic properties of the mating materials. This model was well verified by a set of experimental results on assembling and disassembling processes. FE analyses of the assembling process revealed that CoCr/Ti head–neck junctions had a longer contact length compared to CoCr/CoCr junctions. Different torsional strengths in the two material combinations was found to be because of the lateral deformation of the neck under the application of the twist. The mismatch angle between the head and neck was found to play an important role in the integrity of the junction with both material combinations. The smaller the mismatch for a given assembly load, the firmer connection at the junction. This model can be further used for analysing stresses and micro-motions under real physical activity loadings with the aim of studying fretting wear behaviour of taper junctions in modular hip joint implants.

In Chapter three, the effects of realistic loads (level gait forces and frictional moments - F & M) of walking activity on the mechanical response of the head-neck interface in hip implants were studied. For understanding the level of contribution of the frictional moments to the mechanical response of the interface, two additional loading scenarios of gait forces only (F only) and frictional moments only (M only) were also studied. The 3D finite element model developed in the second chapter was used to run this investigation. The simulations were performed to obtain stress field, micro-motions and fretting work for this taper junction under a complex 6° of freedom loading during a gait cycle of walking. Normal contact stresses and micro-motions at the interface were mostly found in the ranges of 0–275 MPa and 0–38 μm, respectively. The frictional moments alone had a negligible effect in increasing the contacting area as only 0.27% of the non-contacting surface nodes were engaged in contact. F only made 8.43% of the non-contacting surface nodes to get in contact. Frictional moments were effective in the F & M case as the contacting nodes increased to 9.57% when compared to 8.43% in the

F only case. Superposition of the frictional moments and gait forces (F & M) in comparison with F only, also resulted in: a) Up to an approximately 100% increase in the maximum value of fretting work per unit area in the last three millimetres of the temporary extended contacting area (14–16 mm). b) An approximately 15% increase in the maximum magnitude of micro-motions. The results suggest that gait forces dominate the mechanical environment of the interface; however frictional moments when combined with the gait forces can have some considerable effects on increasing the fretting work and gradually increasing micro-motions in the contacting area. This may suggest that simplifying mechanical loads of daily activities to gait forces only in both finite element and in vitro studies needs acceptable justifications.

In Chapter four, an adaptive finite element simulation was developed to predict fretting wear in a head-neck taper junction of hip joint implant through a two dimensional (2D) model and based on the Archard wear equation. To this end, a UMESHMOTION code was developed that was verified by a set of numerical and experimental results of a pin-on-disc set-up reported by previous researchers. This model represents the most critical section of the head-neck junction which was identified from a 3D model of the junction subjected to one cycle of level gait loading which had been previously found in Chapter three. In order to reduce the computational cost, an adaptive wear simulation was used which assumes that the wear rate remains constant during a pre-determined number of cycles (ΔN). In this model, the ΔN factor was varied during the fretting process and the optimized values of the ΔN over the process of fretting wear was presented. This model developed for both dry and PBS conditions. The outcomes revealed that development of such a model in a dry condition is a major simplification.

In Chapter five, the fretting wear model produced in Chapter four was used to investigate the influence of the angular mismatch of the junction on the material loss and fretting wear process during 4,080,000 cycles of walking loading. To better understand the behaviour of the junction against fretting wear, contact stresses, relative micro-motions and contact lengths at the interface of the head and neck were evaluated over the loading cycles. Generally, it was understood that the contact pressure for junctions with an angular mismatch decreases with

increasing the number of cycles, while this parameter for the junction with a zero mismatch angle does not vary significantly over the neck length. For all the studied cases, the relative micro-motions increase from the proximal side to the distal side. The proximal contact with the larger mismatch angle (0.124°) had the largest micro-motion. Lost area, as a parameter which can be a good representative of material loss, in each case was computed over 4,080,000 cycles. The lowest lost area for both the head and neck was found in the distally contacting junction with the smaller mismatch angle (0.024°) followed by the proximal contact with 0.024°. The highest worn areas occurred in the larger mismatch angle (0.124°) junctions, less in distal and more in proximal. It was therefore understood that taper junctions with distal angular mismatches are more resistant to fretting wear when compared to their proximal counterparts.

In Chapter six, the main research objective was to evaluate the effect of assembly force on the material loss and fretting wear process. It was concluded that high assembly forces reduce the relative micro-motions between the head and neck at the taper junction. However, they can also increase the contact pressures and the contact region at the interface which in turn intensify the fretting wear process and consequently increased material removal. The results of this chapter showed that the effect of the last two parameters (contact pressure and contact length) was more dominant in wearing out the surface of the studied CoCr/CoCr junction with a taper angle mismatch of 0.01°. Hence, with increasing the assembly force, the degree of material loss increased for this particular design and material combination of the junction studied in this work.

In Chapter seven, a new adaptive finite element model (using ABAQUS UMESHMOTION subroutine) was successfully developed to simulate the process of fretting corrosion in metal-on-metal contacts with the aim to capture the material surface damage due to both mechanical fretting wear and electrochemical corrosion simultaneously. This model is able to calculate the removed/re-generated passive oxide layer, and material loss caused by fretting wear and corrosion. The model was verified with a mechanical-electrochemical formulation established

previously for a series of pin-on-disc fretting corrosion experiments. The FE model was then used to simulate material loss of a CoCr/CoCr pin on disc system under a complex sliding profile and two normal stresses repeating for 150 cycles. The results showed that with increasing the normal contact stress, the corroded material detached from the disc (due to corrosion only) reduced from 1.83e-14 m^3 to 9.15e-15 m^3 as a result of an increase in the normal stress from 250 MPa to 500 MPa. It was also revealed that the volume of the removed oxide layer reduced by 36% when the normal stress was increased from 250 MPa to 500 MPa. This model is capable of simulating fretting corrosion for any complex fretting sliding regime, different material combinations and various geometries for high number of cycles. Other valid equations of the mechanical and electrochemical surface damage related to wear and corrosion could be incorporated in this model provided they can be adjusted to apply to the model elemental nodes.

References

(!!! INVALID CITATION !!! (Donaldson, Coburn et al. 2014)).

Ambrose, J. R. (1983). "Repassivation Kinetics." Treatise on Materials Science and Technology **23**: 175-204.

Archard, J. (1953). "Contact and rubbing of flat surfaces." Journal of applied physics **24**(8): 981-988.

Archard, J. and W. Hirst (1956). The wear of metals under unlubricated conditions. Proceedings of the Royal Society of London A: Mathematical, Physical and Engineering Sciences, The Royal Society.

Archard, J. F. (1953). "Contact and Rubbing of Flat Surfaces." Journal of Applied Physics **24**(8): 981-988.

Ashkanfar, A., D. J. Langton and T. J. Joyce (2017). "Does a micro-grooved trunnion stem surface finish improve fixation and reduce fretting wear at the taper junction of total hip replacements? A finite element evaluation." Journal of Biomechanics.

Balamurugan, A., S. Rajeswari, G. Balossier, A. H. S. Rebelo and J. M. F. Ferreira (2008). "Corrosion aspects of metallic implants — An overview." Materials and Corrosion **59**(11): 855-869.

Barwell, F. T. (1958). "Wear of metals." Wear **1**(4): 317-332.

Bergmann, G., G. Deuretzbacher, M. Heller, F. Graichen, A. Rohlmann, J. Strauss and G. N. Duda (2001). "Hip contact forces and gait patterns from routine activities." J Biomech **34**(7): 859-871.

Bergmann, G., G. Deuretzbacher, M. Heller, F. Graichen, A. Rohlmann, J. Strauss and G. N. Duda (2001). "Hip contact forces and gait patterns from routine activities." Journal of Biomechanics **34**(7): 859-871.

Bergmann, G., F. Graichen and A. Rohlmann (2004). "Hip joint contact forces during stumbling." Langenbeck's Archives of Surgery **389**(1): 53-59.

Berthier, Y., L. Vincent and M. Godet (1989). "Fretting fatigue and fretting wear." Tribology International **22**(4): 235-242.

Bill, R. C. (1978). "FRETTING OF AISI 9310 STEEL AND SELECTED FRETTING-RESISTANT SURFACE TREATMENTS." ASLE Trans **21**(3): 236-242.

Billi, F. and P. Campbell (2010). "Nanotoxicology of metal wear particles in total joint arthroplasty: a review of current concepts." J Appl Biomater Biomech **8**(1): 1-6.

Bisseling, P., T. Tan, Z. Lu, P. A. Campbell and J. L. C. van Susante (2013). "The absence of a metal-on-metal bearing does not preclude the formation of a destructive pseudotumor in the hip—a case report." Acta Orthopaedica **84**(4): 437-441.

Bitounis, D., J. Pourchez, V. Forest, D. Boudard, M. Cottier and J. P. Klein (2016). "Detection and analysis of nanoparticles in patients: A critical review of the status quo of clinical nanotoxicology." Biomaterials **76**: 302-312.

Bitter, T., I. Khan, T. Marriott, E. Lovelady, N. Verdonschot and D. Janssen (2017). "A combined experimental and finite element approach to analyse the fretting mechanism of the head–stem taper junction in total hip replacement." Proceedings of the Institution of Mechanical Engineers, Part H: Journal of Engineering in Medicine **231**(9): 862-870.

Brown, S. R., W. A. Davies, D. H. DeHeer and A. B. Swanson (2002). "Long-Term Survival of McKee-Farrar Total Hip Prostheses." Clinical Orthopaedics and Related Research **402**: 157-163.

Chana, R., C. Esposito, P. A. Campbell, W. K. Walter and W. L. Walter (2012). "Mixing and matching causing taper wear: corrosion associated with pseudotumour formation." J Bone Joint Surg Br **94**(2): 281-286.

Charnley, J. (1961). "ARTHROPLASTY OF THE HIP: A New Operation." The Lancet **277**(7187): 1129-1132.

Chu, Y.-H., J. J. Elias, G. N. Duda, F. J. Frassica and E. Y. S. Chao (2000). "Stress and micromotion in the taper lock joint of a modular segmental bone replacement prosthesis." Journal of Biomechanics **33**(9): 1175-1179.

Chu, Y., J. J. Elias, G. N. Duda, F. J. Frassica and E. Y. Chao (2000). "Stress and micromotion in the taper lock joint of a modular segmental bone replacement prosthesis." J Biomech **33**(9): 1175-1179.

Cobb, A. G. and T. P. Schmalzreid (2006). "The clinical significance of metal ion release from cobalt-chromium metal-on-metal hip joint arthroplasty." Proc Inst Mech Eng H **220**(2): 385-398.

Collin, J. A. and S. M. Macro (1964). "The effect of stress direction during fretting on subsequent fatigue life." Proceeding American Society for Testing and Materials **64**: 547-560.

Collire, J. P., V. A. Surprenant, R. E. Jensen and M. B. Mayor (1991). "Corrosion at the Interface of Cobalt-Alloy Heads on Titanium-Alloy Stems." Clinical Orthopaedics and Related Research **271**: 305.

D'Silva, S. and S. Jain (2014). "Design of a modified leaf spring with an integrated damping system for added comfort and longer life." International Journal of Research in Engineering and Technology **3**(1): 30-34.

Davis, J. R. (2000). ASM Specialty Handbook: Nickel, Cobalt, and Their Alloys, ASM International.

Del Balso, C., M. G. Teeter, S. C. Tan, B. A. Lanting and J. L. Howard (2015). "Taperosis: Does head length affect fretting and corrosion in total hip arthroplasty?" Bone Joint J **97-b**(7): 911-916.

Dimah, M. K., F. Devesa Albeza, V. Amigó Borrás and A. Igual Muñoz (2012). "Study of the biotribocorrosion behaviour of titanium biomedical alloys in simulated body fluids by electrochemical techniques." Wear **294–295**(0): 409-418.

Ding, J., S. B. Leen and I. R. McColl (2004). "The effect of slip regime on fretting wear-induced stress evolution." International Journal of Fatigue **26**(5): 521-531.

Documentation, A. ABAQUS Documentation. USA, Dassault Systèmes.

Donaldson, F. E., J. C. Coburn and K. L. Siegel (2014). "Total hip arthroplasty head-neck contact mechanics: a stochastic investigation of key parameters." J Biomech **47**(7): 1634-1641.

Doorn, P. F., P. A. Campbell, J. Worrall, P. D. Benya, H. A. McKellop and H. C. Amstutz (1998). "Metal wear particle characterization from metal on metal total hip replacements: transmission electron microscopy study of periprosthetic tissues and isolated particles." J Biomed Mater Res **42**(1): 103-111.

Duisabeau, L., P. Combrade and B. Forest (2004). "Environmental effect on fretting of metallic materials for orthopaedic implants." Wear **256**(7–8): 805-816.

Duisabeau, L., P. Combrade and B. Forest (2004). "Environmental effect on fretting of metallic materials for orthopaedic implants." Wear **256**.

Dyrkacz, R. M. R., J. M. Brandt, J. B. Morrison, S. T. O' Brien, O. A. Ojo, T. R. Turgeon and U. P. Wyss "Finite element analysis of the head–neck taper interface of modular hip prostheses." Tribology International(0).

Dyrkacz, R. M. R., J. M. Brandt, J. B. Morrison, S. T. O' Brien, O. A. Ojo, T. R. Turgeon and U. P. Wyss (2015). "Finite element analysis of the head–neck taper interface of modular hip prostheses." Tribology International **91**: 206-213.

Dyrkacz, R. M. R., J. M. Brandt, O. A. Ojo, T. R. Turgeon and U. P. Wyss (2013). "The influence of head size on corrosion and fretting behaviour at the head-neck interface of artificial hip joints." Journal of Arthroplasty **28**(6): 1036-1040.

Elkins, J. M., J. J. Callaghan and T. D. Brown (2014). "Stability and trunnion wear potential in large-diameter metal-on-metal total hips: a finite element analysis." Clin Orthop Relat Res **472**(2): 529-542.

English, R., A. Ashkanfar and G. Rothwell (2015). "A computational approach to fretting wear prediction at the head–stem taper junction of total hip replacements." Wear **338**(Supplement C): 210-220.

English, R., A. Ashkanfar and G. Rothwell (2015). "A computational approach to fretting wear prediction at the head–stem taper junction of total hip replacements." Wear **338–339**: 210-220.

English, R., A. Ashkanfar and G. Rothwell (2016). "The effect of different assembly loads on taper junction fretting wear in total hip replacements." Tribology International **95**: 199-210.

Eschweiler, J., L. Fieten, J. Dell'Anna, K. Kabir, S. Gravius, M. Tingart and K. Radermacher (2012). "Application and evaluation of biomechanical models and scores for the planning of total hip arthroplasty." Proc Inst Mech Eng H **226**(12): 955-967.

Farhoudi, H., K. Fallahnezhad, R. H. Oskouei and M. Taylor (2017). "A finite element study on the mechanical response of the head-neck interface of hip implants under realistic forces and moments of daily activities: Part 1, level walking." Journal of the Mechanical Behavior of Biomedical Materials.

Farhoudi, H., R. H. Oskouei, C. F. Jones and M. Taylor (2015). "A novel analytical approach for determining the frictional moments and torques acting on modular femoral components in total hip replacements." Journal of Biomechanics **48**(6): 976-983.

Farhoudi, H., R. H. Oskouei, C. F. Jones and M. Taylor (2015). "A novel analytical approach for determining the frictional moments and torques acting on modular femoral components in total hip replacements." J Biomech **48**(6): 976-983.

Farhoudi, H., R. H. Oskouei, A. A. Pasha Zanoosi, C. F. Jones and M. Taylor (2016). "An Analytical Calculation of Frictional and Bending Moments at the Head-Neck Interface of Hip Joint Implants during Different Physiological Activities." Materials **9**(12): 982.

Feng, I. M. and H. H. Uhilg (1954). Journal of Applied Mechanics **21**: 395.

Fouvry, S. (2001). "Shakedown analysis and fretting wear response under gross slip condition." Wear **251**(1–12): 1320-1331.

Fouvry, S., P. Kapsa and L. Vincent (1996). "Quantification of fretting damage." Wear **200**(1–2): 186-205.

Fricka, K. B., H. Ho, W. J. Peace and C. A. Engh Jr (2012). "Metal-on-Metal Local Tissue Reaction Is Associated With Corrosion of the Head Taper Junction." The Journal of Arthroplasty **27**(8, Supplement): 26-31.e21.

Georgiou, G., A. Siapkara, A. Dimitrakopoulou, S. Provelengios and E. Dounis (2006). "Dissociation of bipolar hemiarthroplasty of the hip after dislocation." Injury **37**(2): 162-168.

Geringer, J., B. Forest and P. Combrade (2005). "Fretting-corrosion of materials used as orthopaedic implants." Wear **259**(7): 943-951.

Gill, I. P., J. Webb, K. Sloan and R. J. Beaver (2012). "Corrosion at the neck-stem junction as a cause of metal ion release and pseudotumour formation." J Bone Joint Surg Br **94**(7): 895-900.

Glascott, J., F. H. Stott and G. C. Wood (1984). "The transition from severe to mild sliding wear for Fe-12%Cr-base alloys at low temperatures." Wear **97**(2): 155-178.

Glyn-Jones, S., A. J. R. Palmer, R. Agricola, A. J. Price, T. L. Vincent, H. Weinans and A. J. Carr (2015). "Osteoarthritis." The Lancet **386**(9991): 376-387.

Godfrey, D. and E. E. Bisson (1952). Lubr. ENG **8**: 241.

Goldberg, J. R. and J. L. Gilbert (1997). "Electrochemical response of CoCrMo to high-speed fracture of its metal oxide using an electrochemical scratch test method." J Biomed Mater Res **37**(3): 421-431.

Goldberg, J. R., J. L. Gilbert, J. J. Jacobs, T. W. Bauer, W. Paprosky and S. Leurgans (2002). "A multicenter retrieval study of the taper interfaces of modular hip prostheses." Clin Orthop Relat Res(401): 149-161.

Goldberg, J. R., J. L. Gilbert, J. J. Jacobs, T. W. Bauer, W. Paprosky and S. Leurgans (2002). "A multicenter retrieval study of the taper interfaces of modular hip prostheses." Clinical orthopaedics and related research **401**: 149-161.

Goldring, M. B. and S. R. Goldring (2010). "Articular cartilage and subchondral bone in the pathogenesis of osteoarthritis." Annals of the New York Academy of Sciences **1192**(1): 230-237.

Goryacheva, I. G., P. T. Rajeev and T. N. Farris (2000). "Wear in Partial Slip Contact." Journal of Tribology **123**(4): 848-856.

Grupp, T. M., T. Weik, W. Bloemer and H.-P. Knaebel (2010). "Modular titanium alloy neck adapter failures in hip replacement - failure mode analysis and influence of implant material." BMC Musculoskeletal Disorders **11**(1): 3.

Grupp, T. M., T. Weik, W. Bloemer and H. P. Knaebel (2010). "Modular titanium alloy neck adapter failures in hip replacement--failure mode analysis and influence of implant material." BMC Musculoskelet Disord **11**: 3.

Gührs, J., M. Körner, M. Bechstedt, A. Krull and M. M. Morlock (2017). "Stem taper mismatch has a critical effect on ceramic head fracture risk in modular hip arthroplasty." Clinical Biomechanics **41**: 106-110.

Harris, S. J., M. P. Overs and A. J. Gould (1985). "The use of coatings to control fretting wear at ambient and elevated temperatures." Wear **106**(1–3): 35-52.

Heiney, J. P., S. Battula, G. A. Vrabec, A. Parikh, R. Blice, A. J. Schoenfeld and G. O. Njus (2009). "Impact magnitudes applied by surgeons and their importance when applying the femoral head onto the Morse taper for total hip arthroplasty." Arch Orthop Trauma Surg **129**(6): 793-796.

Heinz, R. (1989). "Fretting wear - examples, test methods and prevative measures." **20**: 14-20.

Hernigou, P., S. Queinnec and C. H. Flouzat Lachaniette (2013). "One hundred and fifty years of history of the Morse taper: from Stephen A. Morse in 1864 to complications related to modularity in hip arthroplasty." International Orthopaedics **37**(10): 2081-2088.

Higgs, G. B., J. A. Hanzlik, D. W. MacDonald, J. L. Gilbert, C. M. Rimnac, S. M. Kurtz and C. the Implant Research Center Writing (2013). "Is Increased Modularity Associated With Increased Fretting and Corrosion Damage in Metal-On-Metal Total Hip Arthroplasty Devices?: A Retrieval Study." The Journal of arthroplasty **28**(8 0): 2-6.

Hills, D. A. and D. Nowell (1994). "Mechanics of fretting fatigue." Kluwer academic publishers.

Hothi, H. S., A. P. Eskelinen, R. Berber, O. S. Lainiala, T. P. Moilanen, J. A. Skinner and A. J. Hart (2017). "Factors associated with trunnionosis in the metal-on-metal Pinnacle hip." The Journal of arthroplasty **32**(1): 286-290.

Hurricks, P. L. (1970). "The mechanism of fretting — A review." Wear **15**(6): 389-409.

Hussenbocus, S., D. Kosuge, L. B. Solomon, D. W. Howie and R. H. Oskouei (2015). "Head-Neck Taper Corrosion in Hip Arthroplasty." BioMed Research International **2015**: 9.

Iwabuchi, A. (1991). "The role of oxide particles in the fretting wear of mild steel." Wear **151**(2): 301-311.

Jauch, S. Y., L. G. Coles, L. V. Ng, A. W. Miles and H. S. Gill (2014). "Low torque levels can initiate a removal of the passivation layer and cause fretting in modular hip stems." Med Eng Phys **36**(9): 1140-1146.

Jauch, S. Y., G. Huber, E. Hoenig, M. Baxmann, T. M. Grupp and M. M. Morlock (2011). "Influence of material coupling and assembly condition on the magnitude of micromotion at the stem–neck interface of a modular hip endoprosthesis." Journal of Biomechanics **44**(9): 1747-1751.

Johansson, L. (1994). "Numerical Simulation of Contact Pressure Evolution in Fretting." Journal of Tribology **116**(2): 247-254.

John Cooper, H., C. J. Della Valle, R. A. Berger, M. Tetreault, W. G. Paprosky, S. M. Sporer and J. J. Jacobs (2012). "Corrosion at the Head-Neck Taper as a Cause for Adverse Local Tissue Reactions After Total Hip Arthroplasty." The Journal of Bone and Joint Surgery. American volume **94**(18): 1655-1661.

Johnson, K. L. (1985). "Contact Mechanics." Cambridge University Press, Cambridge.

Johnson, K. L. (1995). "Contact mechanics and the wear of metals." Wear **190**(2): 162-170.

Johnson, K. L. and K. L. Johnson (1987). Contact Mechanics, Cambridge University Press.

Kapoor, A. (1997). "Wear by plastic ratchetting." Wear **212**(1): 119-130.

Knight, S. R., R. Aujla and S. P. Biswas (2011). "Total Hip Arthroplasty - over 100 years of operative history." Orthopedic Reviews **3**(2): e16.

Kocagöz, S. B., R. J. Underwood, S. Sivan, J. L. Gilbert, D. W. MacDonald, J. S. Day and S. M. Kurtz (2013). "Does Taper Angle Clearance Influence Fretting and Corrosion Damage at the Head-Stem Interface? A Matched Cohort Retrieval Study." Seminars in arthroplasty **24**(4): 246-254.

Lai, J. and K. Stadler (2016). "Investigation on the mechanisms of white etching crack (WEC) formation in rolling contact fatigue and identification of a root cause for bearing premature failure." Wear **364–365**: 244-256.

Langton, D. J., R. Sidaginamale, J. K. Lord, A. V. F. Nargol and T. J. Joyce (2012). "Taper junction failure in large-diameter metal-on-metal bearings." Bone & Joint Research **1**(4): 56-63.

Learmonth, I. D., C. Young and C. Rorabeck "The operation of the century: total hip replacement." The Lancet **370**(9597): 1508-1519.

Lieberman, J. R., C. M. Rimnac, K. L. Garvin, R. W. Klein and E. A. Salvati (1994). "An analysis of the head-neck taper interface in retrieved hip prostheses." Clin Orthop Relat Res(300): 162-167.

Loeser, R. F. (2006). "Molecular Mechanisms of Cartilage Destruction: Mechanics, Inflammatory Mediators, and Aging Collide." Arthritis and rheumatism **54**(5): 1357-1360.

Mali, S. A. (2016). "Mechanically assisted crevice corrosion in metallic biomaterials: a review." Materials Technology **31**(12): 732-739.

Maruyama, N., H. Kawasaki, A. Yamamoto, S. Hiromoto, H. Imai and T. Hanawa (2005). "Friction-Wear Properties of Nickel-Free Co–Cr–Mo Alloy in a Simulated Body Fluid." MATERIALS TRANSACTIONS **46**(7): 1588-1592.

Mathew, M. T., P. Srinivasa Pai, R. Pourzal, A. Fischer and M. A. Wimmer (2009). "Significance of Tribocorrosion in Biomedical Applications: Overview and Current Status." Advances in Tribology **2009**: 12.

McColl, I. R., J. Ding and S. B. Leen (2004). "Finite element simulation and experimental validation of fretting wear." Wear **256**(11–12): 1114-1127.

Meng, H. C. and K. C. Ludema (1995). "Wear models and predictive equations: their form and content." Wear **181–183, Part 2**(0): 443-457.

Mitchell, R. G. (1983). "An airline view of the corrosion problem." Industry Corrosion: 11.

Molent, L. (2015). "Alternative methods for derivation of safe life limits for a 7050-T7451 aluminium alloy structure." International Journal of Fatigue **74**: 55-64.

Mroczkowski, M. L., J. S. Hertzler, S. M. Humphrey, T. Johnson and C. R. Blanchard (2006). "Effect of impact assembly on the fretting corrosion of modular hip tapers." J Orthop Res **24**(2): 271-279.

Nassutt, R., I. Mollenhauer, K. Klingbeil, O. Henning and H. Grundei (2006). "[Relevance of the insertion force for the taper lock reliability of a hip stem and a ceramic femoral head]." Biomedizinische Technik. Biomedical engineering **51**(2): 103-109.

Oskouei, R. H., K. Fallahnezhad and S. Kuppusami (2016). "An Investigation on the Wear Resistance and Fatigue Behaviour of Ti-6Al-4V Notched Members Coated with Hydroxyapatite Coatings." Materials **9**(2): 111.

Pennock, A. T., A. H. Schmidt and C. A. Bourgeault (2002). "Morse-type tapers: factors that may influence taper strength during total hip arthroplasty." J Arthroplasty **17**(6): 773-778.

Ponter, A. R. S., A. D. Hearle and K. L. Johnson (1985). "Application of the kinematical shakedown theorem to rolling and sliding point contacts." Journal of the Mechanics and Physics of Solids **33**(4): 339-362.

Pourzal, R., D. J. Hall, N. Q. Ha, R. M. Urban, B. R. Levine, J. J. Jacobs and H. J. Lundberg (2016). "Does surface topography play a role in taper damage in head-neck modular junctions?" Clinical orthopaedics and related research **474**(10): 2232-2242.

Ramoutar, D. N., E. A. Crosnier, F. Shivji, A. W. Miles and H. S. Gill (2017). "Assessment of Head Displacement and Disassembly Force With Increasing Assembly Load at the

Head/Trunnion Junction of a Total Hip Arthroplasty Prosthesis." The Journal of Arthroplasty **32**(5): 1675-1678.

Rehmer, A., N. E. Bishop and M. M. Morlock (2012). "Influence of assembly procedure and material combination on the strength of the taper connection at the head-neck junction of modular hip endoprostheses." Clin Biomech (Bristol, Avon) **27**(1): 77-83.

Rehmer, A., N. E. Bishop and M. M. Morlock (2012). "Influence of assembly procedure and material combination on the strength of the taper connection at the head–neck junction of modular hip endoprostheses." Clinical Biomechanics **27**(1): 77-83.

Rodrigues, D. C., R. M. Urban, J. J. Jacobs and J. L. Gilbert (2009). "IN VIVO SEVERE CORROSION AND HYDROGEN EMBRITTLEMENT OF RETRIEVED MODULAR BODY TITANIUM ALLOY HIP-IMPLANTS." Journal of biomedical materials research. Part B, Applied biomaterials **88**(1): 206-219.

Sackfield, A. and D. A. Hills (1983). "Some useful results in the tangentially loaded hertzian contact problem." The Journal of Strain Analysis for Engineering Design **18**(2): 107-110.

Sansone, V., D. Pagani and M. Melato (2013). "The effects on bone cells of metal ions released from orthopaedic implants. A review." Clinical Cases in Mineral and Bone Metabolism **10**(1): 34-40.

Sato, J., M. Shima, T. Sugawara and A. Tahara (1988). "Effect of lubricants on fretting wear of steel." Wear **125**(1–2): 83-95.

Scholl, L., J. Longaray, L. Raja, R. Lee, A. Faizan, L. Herrera, M. Thakore and J. Nevelos (2015). "Friction in modern total hip arthroplasty bearings: Effect of material, design, and test methodology." Proceedings of the Institution of Mechanical Engineers, Part H: Journal of Engineering in Medicine **230**(1): 50-57.

Sivakumar, B., S. Kumar and T. S. N. Sankara Narayanan (2011). "Fretting corrosion behaviour of Ti–6Al–4V alloy in artificial saliva containing varying concentrations of fluoride ions." Wear **270**(3–4): 317-324.

Soderberg, S. and O. Vingsbo (1987). "Wear of materials." ASEM: 885-894.

Srinivasan, A., E. Jung and B. R. Levine (2012). "Modularity of the femoral component in total hip arthroplasty." Journal of the American Academy of Orthopaedic Surgeons **20**(4): 214-222.

Swaminathan, V. and J. L. Gilbert (2012). "Fretting corrosion of CoCrMo and Ti6Al4V interfaces." Biomaterials **33**(22): 5487-5503.

Swaminathan, V. and J. L. Gilbert (2012). "Fretting corrosion of CoCrMo and Ti6Al4V interfaces." Biomaterials **33**(22): 5487-5503.

Uhling, H. H. (1954). "Mechanism of fretting corrosion." Journal of applied Mechanics **21**: 401.

Urban, R. M., J. J. Jacobs, M. J. Tomlinson, J. Gavrilovic, J. Black and M. Peoc'h (2000). "Dissemination of wear particles to the liver, spleen, and abdominal lymph nodes of patients with hip or knee replacement." J Bone Joint Surg Am **82**(4): 457-476.

Viceconti, M., M. Baleani, S. Squarzoni and A. Tonil (1997). "Fretting wear in a modular neck hip prosthesis." Journal of Biomedical Materials Research **35**(2): 207-216.

Viceconti, M., O. Ruggeri, A. Toni and A. Giunti (1996). "Design-related fretting wear in modular neck hip prosthesis." J Biomed Mater Res **30**(2): 181-186.

Vingsbo, O. and S. Söderberg (1988). "On fretting maps." Wear **126**(2): 131-147.

Walter, L. R., E. Marel, R. Harbury and J. Wearne (2008). "Distribution of chromium and cobalt ions in various blood fractions after resurfacing hip arthroplasty." J Arthroplasty **23**(6): 814-821.

Waterhouse, R. B. (1972). "Fretting corrosion." Pergamon Press.

Waterhouse, R. B. (1992). "Fretting wear." ASM handbook **18**: 242-256.

Waterhouse, R. B. and D. E. Taylor (1974). "Fretting debris and the delamination theory of wear." Wear **29**(3): 337-344.

Watrehouse, R. B. (1985). "Introduction to fretting wear seminar, Nottingham." Seminar, Nottingham

106: 3.

Wessinghage, D. (1991). "Themistocles Gluck." Z Orthop Unfall **129**(05): 383-388.

Xushou, Z., Z. Chuenhe and Z. Chailu (1989). "Slip amplitude effects and microstructural characteristics of surface layers in fretting wear of carbon steel." Wear **134**(2): 297-309.

Zhang, T., N. M. Harrison, P. F. McDonnell, P. E. McHugh and S. B. Leen (2013). "A finite element methodology for wear–fatigue analysis for modular hip implants." Tribology International **65**: 113-127.

Zhang, T., N. M. Harrison, P. F. McDonnell, P. E. McHugh and S. B. Leen (2014). "Micro-macro wear-fatigue of modular hip implant taper-lock coupling." Journal of Strain Analysis for Engineering Design **49**(1): 2-18.

Zhu, M. H., Z. B. Cai, W. Li, H. Y. Yu and Z. R. Zhou (2009). "Fretting in prosthetic devices related to human body." Tribology International **42**(9): 1360-1364.

Zhu, M. H. and Z. R. Zhou (2011). "On the mechanisms of various fretting wear modes." Tribology International **44**(11): 1378-1388.

Appendix A FORTRAN code to simulate Fretting wear in the head-neck junction

```
      SUBROUTINE UMESHMOTION(UREF,ULOCAL,NODE,NNDOF,
       LNODETYPE,ALOCAL,NDIM,TIME,DTIME,PNEWDT,
       KSTEP,KINC,KMESHSWEEP,JMATYP,JGVBLOCK)
      INCLUDE 'ABA_PARAM.INC'
      DIMENSION ULOCAL(NDIM),JELEMLIST(100000)
      DIMENSION ALOCAL(NDIM,100000),TIME(2)
      DIMENSION JMATYP(100000),JGVBLOCK(100000)

      INTEGER:: control1, control2


      INTEGER::master
      REAL::CPRESS,CSHEAR,CSLIP,COPEN,XCOORD,YCOORD,INCSLIP
      REAL::RIGHT-CP,LEFT-CP,RIGHT-SLIPINC,LEFT-SLIPINC,Right-Slope,Left-
Slope,W_TOTT,W_TOTT_m
      DIMENSION ARRAY(15)
      INTEGER::LOCNUM,NELEMMAX
      CHARACTER*120 PARTNAME
       REAL::Wear

      REAL::Horiz-Er, Vert-Er
      common/wear/
       Final-node1,
       Final-node12,
       Slave-Node-Num,
       Master-Node-Num,
       Master-Node(30000),
       Slave-Node(30000),
       Prev-Slide(30000),
       Pres-Slide(30000),
```

```
 Pressure-Slave(30000),
 X-Slave(30000),
 Y-Slave(30000),
 motion-Slave(30000),
 W_TOT(30000),
 W_TOT_old(30000),
 W_TOT_m(30000),
 W_TOT_old_m(30000),

 End-Node-Slave(100000),
 End-Node-Master(100000)
control2=0
control1=1

master=0

LEFT-CP=0
RIGHT-CP=0
LEFT-SLIPINC=0
RIGHT-SLIPINC=0
LEFT-X=1.001*XCOORD
RIGHT-X=0.999*XCOORD

Warning=0.1

NELEMMAX = 500
NELEMS = NELEMMAX

OPEN(unit=19,file='c:\Temp\fretting\head neck wearing\1a.txt',status='unknown')

Final-node1=NODE
CALL GETNODETOELEMCONN(NODE,NELEMS,JELEMLIST,JELEMTYPE,
 JRCD,JGVBLOCK)
LOCNUM = 0
JRCD = 0
PARTNAME = ' '
```

```
CALL GETVRMAVGATNODE(NODE,JTYP,'CSTRESS',ARRAY,JRCD,
 JELEMLIST,NELEMS,JMATYP,JGVBLOCK)
CPRESS = ARRAY(1)
CSHEAR = ARRAY(2)


CALL GETVRMAVGATNODE(NODE,0,'CDISP',ARRAY,JRCD,
 JELEMLIST,NELEMS,JMATYP,JGVBLOCK)
CSLIP = ARRAY(2)
COPEN = ARRAY(1)
CALL GETPARTINFO(NODE,0,PARTNAME,LOCNUM,JRCD)


CALL GETVRN(NODE,'COORD',ARRAY,JRCD,JGVBLOCK,LTRN)
XCOORD=ARRAY(1)
YCOORD=ARRAY(2)
control2=0


IF(PARTNAME=='PART-2-1')THEN
          master=1
  IF(End-Node-Master(NODE)==0)THEN
      WRITE(18,*)'found a new master',NODE
      Master-Node-Num=Master-Node-Num+1
      Slave-Node(Master-Node-Num)=NODE
      End-Node-Master(NODE)=Master-Node-Num

  END IF

ELSE
  IF(End-Node-Slave(NODE)==0)THEN
      Slave-Node-Num=Slave-Node-Num+1
      Master-Node(Slave-Node-Num)=NODE
      End-Node-Slave(NODE)=Slave-Node-Num
  END IF
```

```
        Pressure-Slave(End-Node-Slave(NODE))=CPRESS
        X-Slave(End-Node-Slave(NODE))=XCOORD
        Y-Slave(End-Node-Slave(NODE))=YCOORD

        Pres-Slide(End-Node-Slave(NODE))=CSLIP
        INCSLIP=CSLIP-Prev-Slide(End-Node-Slave(NODE))

      END IF
      Horiz-Er_R=0.00005
      Horiz-Er_L=0.00005
      Left-control=0
      Right-control=0

      IF(master==1)THEN

        DO control1=1,Slave-Node-Num
            IF(X-Slave(control1).GT.XCOORD)THEN
                IF(SQRT(((XCOORD-X-Slave(control1))**2)+((YCOORD-Y-
Slave(control1))**2))<Horiz-Er_R)THEN
                    RIGHT-CP=Pressure-Slave(control1)

                    RIGHT-SLIPINC=Pres-Slide(control1)-Prev-Slide(control1)
                    RIGHT-X=X-Slave(control1)

                    Horiz-Er_R=SQRT(((XCOORD-X-Slave(control1))**2)+((YCOORD-Y-
Slave(control1))**2))

                    Right-control=1

                END IF
            ELSE
                IF(SQRT(((XCOORD-X-Slave(control1))**2)+((YCOORD-Y-
Slave(control1))**2))<Horiz-Er_L)THEN
                    LEFT-CP=Pressure-Slave(control1)
                    LEFT-SLIPINC=Pres-Slide(control1)-Prev-Slide(control1)
                    LEFT-X=X-Slave(control1)
                    Horiz-Er_L=SQRT(((XCOORD-X-Slave(control1))**2)+((YCOORD-Y-
Slave(control1))**2))
```

```
                                    Left-control=1

          END IF
        END IF
    END DO

    IF(Right-control==0)THEN

        CPRESS=LEFT-CP
        INCSLIP=LEFT-SLIPINC

    END IF
    IF(Left-control==0)THEN
                    CPRESS=RIGHT-CP
        INCSLIP=RIGHT-SLIPINC
    END IF

    IF(Left-control==0.AND.Right-control==0)THEN

        CPRESS=0
        INCSLIP=0
    END IF

    IF(Left-control==1.AND.Right-control==1)THEN

    Right-Slope=(RIGHT-CP-LEFT-CP)/(RIGHT-X-LEFT-X)
    CPRESS=LEFT-CP+Right-Slope*(XCOORD-LEFT-X)
    Left-Slope=(RIGHT-SLIPINC-LEFT-SLIPINC)/(RIGHT-X-LEFT-X)
    INCSLIP=LEFT-SLIPINC+Left-Slope*(XCOORD-LEFT-X)
    END IF
END IF
Wear=(CPRESS)*ABS(INCSLIP)*0.17e-14*50
IF(master==0)THEN

W_TOTT=Wear+W_TOT_old(End-Node-Slave(NODE))
W_TOT(End-Node-Slave(NODE))=W_TOTT
END IF
```

```
IF(master==1)THEN
W_TOTT_m=Wear+W_TOT_old_m(End-Node-Master(NODE))
W_TOT_m(End-Node-Master(NODE))=W_TOTT_m
END IF

IF(KSTEP==1)THEN
  Wear=0
END IF



ULOCAL(2)=ULOCAL(2)-Wear

WRITE (19,*) node,master,Wear,W_TOTT_m,W_TOTT
IF(master==0)THEN

 WRITE(18,1000),NODE,CPRESS,CSHEAR,master,Prev-Slide(End-Node-Slave(NODE)),
 INCSLIP,Wear,XCOORD,YCOORD
ELSE IF(master==1)THEN

 WRITE(16,1000),NODE,CPRESS,CSHEAR,master,Prev-Slide(End-Node-Slave(NODE)),
 INCSLIP,Wear,XCOORD,YCOORD
END IF

IF(KINC==1)THEN
  IF(Master-Node(1)==NODE)THEN
      WRITE(17,*),'LOADSTEP',KSTEP
  END IF
  WRITE(17,*),'0 ','0',XCOORD,YCOORD
END IF

IF(NODE==3377)THEN

  DO control1=1,Slave-Node-Num
      Prev-Slide(control1)=Pres-Slide(control1)
  END DO
```

```
  DO control1=1,Slave-Node-Num
      W_TOT_old(control1)=W_TOT(control1)
  END DO
  DO control1=1,Master-Node-Num
      W_TOT_old_m(control1)=W_TOT_m(control1)
  END DO

  IF(master==1)THEN
  END IF
END IF


  Final-node12=NODE
END
```

Appendix B FORTRAN code to simulate Fretting corrosion in the head-neck junction

```
            SUBROUTINE UMESHMOTION(UREF,ULOCAL,NODE,NNDOF,
       LNODETYPE,ALOCAL,NDIM,TIME,DTIME,PNEWDT,
       KSTEP,KINC,KMESHSWEEP,JMATYP,JGVBLOCK)
C
      INCLUDE 'ABA_PARAM.INC'
C

      DIMENSION ULOCAL(NDIM),JELEMLIST(100000)
      DIMENSION ALOCAL(NDIM,100000),TIME(2)
      DIMENSION JMATYP(100000),JGVBLOCK(100000)
      INTEGER::control2,control1
      INTEGER::master
      REAL::CPRESS,CSHEAR,CSLIP,COPEN,XCOORD,YCOORD,INCSLIP,U1,U2,U3,uum,sum
            REAL::RIGHT-CP,LEFT-CP,RIGHT-SLIPINC,LEFT-SLIPINC,Right-Slope,Left-
Slope,W_TOTT,W_TOTT_m,forcetot,
      DIMENSION ARRAY(15)
            INTEGER::LOCNUM,NELEMMAX
      CHARACTER*80 PARTNAME
       REAL::Wear,Idens,h0,hf,hn,delta,force,ss,dd,hcorr

      real*4 :: tt
      REAL::Horiz-Er, Vert-Er
      common/wear/
       Final-node1,
       Final-node12,
       Slave-Node-Num,
       Master-Node-Num,
       Master-Node(30000),
       Slave-Node(30000),
```

```
 Prev-Slide(30000),
 Pres-Slide(30000),
 Pressure-Slave(30000),
 X-Slave(30000),
 uu(30000),
 Y-Slave(30000),
 szcrd(30000),
 motion-Slave(30000),
 W_TOT(30000),
 W_TOT_old(30000),
 W_TOT_m(30000),
 W_TOT_old_m(30000),
 h_TOT(30000),
 h_TOT_old(30000),
 h_TOT_m(30000),
 h_TOT_old_m(30000),
 hm(30000),
 hs(30000),
 hsold(30000),
 forcem(30000),
 f1(30000),
 told(30000),
 toldm(30000),
 tir(30000),
 tts(30000),
 sim(30000),
 tolds(30000),
 toldms(30000),
 tirs(30000),
 ttss(30000),
 hmold(30000),

 End-Node-Slave(100000),
 End-Node-Master(100000)

control2=0
control1=1
```

```
forcetot=0

master=0
LEFT-CP=0
RIGHT-CP=0
LEFT-SLIPINC=0
RIGHT-SLIPINC=0
LEFT-X=1.001*XCOORD
RIGHT-X=0.999*XCOORD

Warning=0.1

NELEMMAX = 500
NELEMS = NELEMMAX

OPEN(unit=19,file='c:\Temp\corrosion\1000w2.txt',status='unknown')
OPEN(unit=20,file='c:\Temp\corrosion\1000ww.txt',status='unknown')
 OPEN(unit=21,file='c:\Temp\corrosion\sum1000w.txt',status='unknown')

Final-node1=NODE
CALL GETNODETOELEMCONN(NODE,NELEMS,JELEMLIST,JELEMTYPE,
 JRCD,JGVBLOCK)
LOCNUM = 0
JRCD = 0
PARTNAME = ' '

CALL GETVRMAVGATNODE(NODE,JTYP,'CSTRESS',ARRAY,JRCD,
 JELEMLIST,NELEMS,JMATYP,JGVBLOCK)
CPRESS = ARRAY(1)
CSHEAR = ARRAY(2)

CALL GETVRMAVGATNODE(NODE,0,'CDISP',ARRAY,JRCD,
 JELEMLIST,NELEMS,JMATYP,JGVBLOCK)
CSLIP = ARRAY(2)
COPEN = ARRAY(1)
CALL GETPARTINFO(NODE,0,PARTNAME,LOCNUM,JRCD)
```

```
CALL GETVRN(NODE,'COORD',ARRAY,JRCD,JGVBLOCK,LTRN)
XCOORD=ARRAY(1)
YCOORD=ARRAY(2)
ZCOORD=ARRAY(3)
CALL GETVRN(NODE,'U',ARRAY,JRCD,JGVBLOCK,LTRN)
U1=ARRAY(1)
U2=ARRAY(2)
U3=ARRAY(3)
control2=0
IF(PARTNAME=='PART-1-1')THEN
  master=1
  IF(End-Node-Master(NODE)==0)THEN
      WRITE(18,*)'found a new master',NODE
      Master-Node-Num=Master-Node-Num+1
      Slave-Node(Master-Node-Num)=NODE

      End-Node-Master(NODE)=Master-Node-Num

  END IF

ELSE
  IF(End-Node-Slave(NODE)==0)THEN
      Slave-Node-Num=Slave-Node-Num+1
      Master-Node(Slave-Node-Num)=NODE

      End-Node-Slave(NODE)=Slave-Node-Num

  END IF


  Pressure-Slave(End-Node-Slave(NODE))=CPRESS
  X-Slave(End-Node-Slave(NODE))=XCOORD
  Y-Slave(End-Node-Slave(NODE))=YCOORD
  szcrd(End-Node-Slave(NODE))=ZCOORD
  Pres-Slide(End-Node-Slave(NODE))=CSLIP
  INCSLIP=CSLIP-Prev-Slide(End-Node-Slave(NODE))
```

```
         uu(End-Node-Slave(NODE))=U1
        END IF


      Horiz-Er_R=1.5e-5
      Horiz-Er_L=1.5e-5
      Left-control=0
      Right-control=0

      IF(master==1)THEN


        DO control1=1,Slave-Node-Num

            IF(X-Slave(control1).GT.XCOORD)THEN

                IF(SQRT(((XCOORD-X-Slave(control1))**2)+((ZCOORD-
szcrd(control1))**2))<Horiz-Er_R)THEN

                    RIGHT-CP=Pressure-Slave(control1)

                    RIGHT-SLIPINC=Pres-Slide(control1)-Prev-Slide(control1)
                    RIGHT-X=X-Slave(control1)

                    Horiz-Er_R=SQRT(((XCOORD-X-Slave(control1))**2)+((ZCOORD-
szcrd(control1))**2))

                    Right-control=1

                END IF
            ELSE
                IF(SQRT(((XCOORD-X-Slave(control1))**2)+((ZCOORD-
szcrd(control1))**2))<Horiz-Er_L)THEN

                    LEFT-CP=Pressure-Slave(control1)

                    LEFT-SLIPINC=Pres-Slide(control1)-Prev-Slide(control1)
```

```
                    LEFT-X=X-Slave(control1)

                    Horiz-Er_L=SQRT(((XCOORD-X-Slave(control1))**2)+((ZCOORD-
szcrd(control1))**2))

                    Left-control=1

                END IF
            END IF
        END DO


        IF(Right-control==0)THEN
            CPRESS=LEFT-CP
            INCSLIP=LEFT-SLIPINC

        END IF
        IF(Left-control==0)THEN

            CPRESS=RIGHT-CP
            INCSLIP=RIGHT-SLIPINC
        END IF
        IF(Left-control==0.AND.Right-control==0)THEN

            CPRESS=0
            INCSLIP=0
        END IF
        IF(Left-control==1.AND.Right-control==1)THEN

        Right-Slope=(RIGHT-CP-LEFT-CP)/(RIGHT-X-LEFT-X)
        CPRESS=LEFT-CP+Right-Slope*(XCOORD-LEFT-X)
        Left-Slope=(RIGHT-SLIPINC-LEFT-SLIPINC)/(RIGHT-X-LEFT-X)
        INCSLIP=LEFT-SLIPINC+Left-Slope*(XCOORD-LEFT-X)
        END IF
        END IF

      IF(master==1)THEN
```

```
    force=(CPRESS*(1.71e-10))
    forcem(End-Node-Master(NODE))=force
    DO control1=1,Master-Node-Num
     forcetot=forcetot+forcem(control1)
     sim(control1)=forcetot
     end do

end if
uum=uu(End-Node-Slave(9278))



IF(master==0)THEN
    forcetot=sim(End-Node-Master(3304))
    end if


delta=((844.46e-6)*((forcetot)**(-0.467)))



 if (CPRESS.LT.6e6) then
     Idens=0
 END if
 if ((CPRESS.GE.6e6).AND.(CPRESS.LT.174e6)) then
     Idens=((5.98e-12)*CPRESS+4.15e-4)*(1e4)
 END if
 if ((CPRESS.GE.174e6).AND.(CPRESS.LT.271e6)) then
     Idens=((-3.43e-12)*CPRESS+2.06e-3)*(1e4)
 END if
 if ((CPRESS.GE.271e6).AND.(CPRESS.LT.349e6)) then
     Idens=((4.49e-12)*CPRESS-9.12e-5)*(1e4)
 END if
 if ((CPRESS.GE.349e6).AND.(CPRESS.LT.548e6)) then
```

```
      Idens=((-2.34e-12)*CPRESS+2.3e-3)*(1e4)
 END if
 if ((CPRESS.GE.548e6).AND.(CPRESS.LT.651e6)) then
      Idens=(7.5e-4)*(1e4)
 END if
 if ((CPRESS.GE.651e6).AND.(CPRESS.LT.733e6)) then
      Idens=((-5.03e-12)*CPRESS+4.27e-3)*(1e4)
 END if
 if (CPRESS.GE.733e6) then
      Idens=(5.84e-4)*(1e4)
 END if

 if(master==0) then
  hn=hsold(End-Node-Slave(NODE))
 if (CPRESS.GT.0.and.ABS(INCSLIP).GT.0) then
      h0=(Idens*delta*(6e-13))/((ABS(INCSLIP)))

      if (h0.GT.0) then
      hn=h0
      end if
      hs(End-Node-Slave(NODE))=hn
 end if

 tt=time(1)-toldm(End-Node-Master(3292))


  if (tt==0.or.tt==0.2.or.tt==0.4.or.tt==0.6.or.tt==0.8) then

    hm(End-Node-Slave(NODE))=0
hn=0
 end if
 END if

 IF(master==1)THEN


 hn=hmold(End-Node-Master(NODE))
```

```
 if (CPRESS.GT.0.and.ABS(INCSLIP).GT.0) then
     h0=(Idens*delta*(6e-13))/((ABS(INCSLIP)))

     if (h0.GT.0) then
     hn=h0
     end if
     hm(End-Node-Master(NODE))=hn

 END if

tir(End-Node-Master(NODE))=time(1)
tt=time(1)-toldm(End-Node-Master(3292))

tts(End-Node-Master(NODE))=tt

 if (tt==0.or.tt==0.2.or.tt==0.4.or.tt==0.6.or.tt==0.8) then
     DO control1=1,Master-Node-Num

     sum=sum+hm(control1)
     end do
    hm(End-Node-Master(NODE))=0
hn=0
 end if

  END if

  if (tt==0.1.or.tt==0.3.or.tt==0.5.or.tt==0.7) then
  hcorr=0.75*hn
  end if
Wear=(CPRESS)*ABS(INCSLIP)*2.8e-14

IF(master==0)THEN
    if (time(1).GT.0.1) then
h_TOTT=hcorr+h_TOT_old(End-Node-Slave(NODE))
h_TOT(End-Node-Slave(NODE))=h_TOTT
end if
END IF
```

```
IF(master==1)THEN
h_TOTT_m=hcorr+h_TOT_old_m(End-Node-Master(NODE))
h_TOT_m(End-Node-Master(NODE))=h_TOTT_m

END IF

IF(master==0)THEN
W_TOTT=Wear+W_TOT_old(End-Node-Slave(NODE))
W_TOT(End-Node-Slave(NODE))=W_TOTT
END IF
IF(master==1)THEN
W_TOTT_m=Wear+W_TOT_old_m(End-Node-Master(NODE))
W_TOT_m(End-Node-Master(NODE))=W_TOTT_m
END IF

IF(KSTEP==1)THEN
  Wear=0
END IF

if (time(1).GT.0.1) then
ULOCAL(3)=ULOCAL(3)-Wear-hcorr
end if

WRITE (20,*) node,master,Wear,W_TOTT_m,W_TOTT
WRITE (19,*) node,master,hcorr,h_TOTT_m,h_TOTT
WRITE (21,*) node,master,tt,uum,sum

IF(master==0)THEN
 WRITE(18,1000),NODE,CPRESS,CSHEAR,master,Prev-Slide(End-Node-Slave(NODE)),
 INCSLIP,Wear,XCOORD,YCOORD
ELSE IF(master==1)THEN
 WRITE(16,1000),NODE,CPRESS,CSHEAR,master,Prev-Slide(End-Node-Slave(NODE)),
 INCSLIP,Wear,XCOORD,YCOORD
END IF

IF(KINC==1)THEN
```

```
  IF(Master-Node(1)==NODE)THEN
      WRITE(17,*),'LOADSTEP',KSTEP
  END IF
  WRITE(17,*),'0 ','0',XCOORD,YCOORD
END IF



IF(NODE==3304)THEN


  DO control1=1,Slave-Node-Num
      Prev-Slide(control1)=Pres-Slide(control1)
  END DO

  DO control1=1,Slave-Node-Num
      W_TOT_old(control1)=W_TOT(control1)
  END DO
  DO control1=1,Master-Node-Num
      W_TOT_old_m(control1)=W_TOT_m(control1)
  END DO

  DO control1=1,Slave-Node-Num
      h_TOT_old(control1)=h_TOT(control1)
  END DO
  DO control1=1,Master-Node-Num
      h_TOT_old_m(control1)=h_TOT_m(control1)
  END DO

  DO control1=1,Master-Node-Num
      if (hm(control1).GT.0) then
          hmold(control1)=hm(control1)
      end if
  END DO
  DO control1=1,Slave-Node-Num
      if (hs(control1).GT.0) then
          hsold(control1)=hs(control1)
```

```
        end if
      END DO

      DO control1=1,Master-Node-Num
         if (tts(control1)==0.8) then
             told(control1)=tir(control1)
         end if
         if (tts(control1).LT.0.8) then
             told(control1)=0
         end if
         if (told(control1).GT.toldm(control1)) then
             toldm(control1)=told(control1)
         end if

      END DO


    END
```